SEACRAS

Development of a methodology for monitoring marine environment pollution by analyzing satellite imagery as part of the implementation of the WASTEREDUCE project - INTERREG VI-A ITALY - CROATIA 2021-2027.

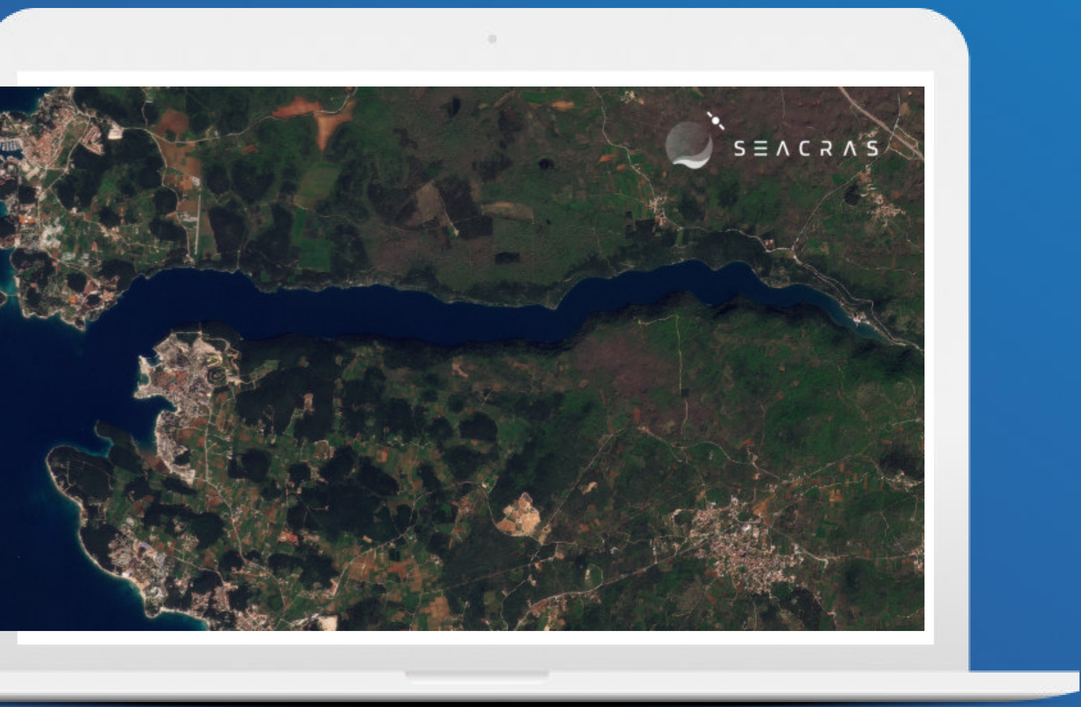

Interreg

Co-funded by the European Union

Italy – Croatia

WASTEREDUCE

NATURA HISTRICA

SEACRAS.COM

Usluga: *Izrada metodologije praćenja onečišćenja morskog okoliša analizom satelitskih snimaka za potrebe JU Natura Histrica, u sklopu provedbe projekta WASTEREDUCE - INTERREG VI-A ITALIJA - HRVATSKA 2021.-2027.*
Klasa ugovora: 406-01/25-01/1
URBROJ ugovora: 09/2025
WASTEREDUCE - INTERREG IT-CRO
EBN: 15/2025/JN

Naručitelj: Javna ustanova za upravljanje zaštićenim dijelovima prirode istarske županije "Natura Histrica"
Riva 8,
52100 Pula, Croatia
OIB: 45370781471

Contractor: SEA CRAS d.o.o. Avenija Dubrovnik 15, Zagreb,
OIB: 70844303390

SEA CRAS d.o.o.

Director:
Dr. Mario Špadina

Voditelj izrade Dr Mario Špadina

Stručni suradnici Robert Šulc, mag. georg.

Josip Karadža, mag.georg.

Recommended Citation

Špadina M., Šulc R., Karadža J. (2025): *Methodology for monitoring marine environment pollution by analyzing satellite imagery,*, as part of the implementation of the WASTEREDUCE project - INTERREG VI-A ITALY - CROATIA 2021-2027.

Commissioned by: Public Institution for the Management of Protected Areas of Istria County “Natura Histrica”

Development of a methodology for monitoring marine environment pollution by analyzing satellite imagery as part of the implementation of the WASTEREDUCE project - INTERREG VI-A ITALY - CROATIA 2021-2027.

Av. Dubrovnik 15, Zagreb, Croatia +385 91 193 08 75 info@seacras.com

Table of contents

Introduction

Project WASTEREDUCE – Integrated Strategies and Solutions for Waste Reduction in Protected and Natura 2000 Areas, Cross-Border Cooperation Programme under the European Territorial Cooperation INTERREG VI-A Italy – Croatia 2021–2027
Specific Objective 2.2 Strengthening the protection and preservation of nature, biodiversity, and green infrastructure, including in urban areas, and reducing all forms of pollution:

- Project title: WASTEREDUCE – Integrated Strategies and Solutions for Waste Reduction in Protected and Natura 2000 Areas
- Project acronym: WASTEREDUCE
- Duration: 30 months (01 February 2024 – 31 July 2026)
- Main Objective: The project aims to improve waste management in protected areas and Natura 2000 sites through the implementation of concrete and joint actions to address the waste phenomenon using various approaches and intervention methods. The emphasis is on improving waste management strategies and developing innovative digital solutions.

The cross-border challenge is to reduce the impact of waste on green and blue areas and improve waste management in protected and Natura 2000 areas. The focus is on aquatic and coastal zones, particularly vulnerable areas affected by anthropogenic waste. WASTEREDUCE brings together eight key public and private partners from Italy and Croatia. By sharing knowledge, experience, and transferring expertise on this topic, the partnership will act synergistically to combat pollution, namely to reduce the environmental impact of waste in protected and Natura 2000 areas, and thereby indirectly preserve their ecosystems.

Technology description

General Protocol for Very High Spatial Resolution (VHR) Optical Satellite Data Processing

Objective: To transform raw or pre-processed VHR optical satellite imagery into analysis-ready data (ARD) or specific end products, suitable for fine-grained analysis and precise object-level machine learning.

Relevant VHR Sensors (Examples):

- Maxar: WorldView-1/2/3/4, GeoEye-1, Legion (next-gen)
- Airbus: Pleiades, Pleiades Neo, SPOT (high-res end)
- Planet: SkySat (and increasingly enhanced PlanetScope)
- BlackSky: Global (rapid revisit)
- Other Commercial: SuperView, Gaofen, Kompsat (various nations)

Data processing description

Methodology for very high spatial resolution (VHR) satellite data processing for marine monitoring

Workflow stages:

1. Data acquisition & retrieval (with scheduler)
2. Pre-processing (sensor & scene correction)
3. Core processing (ML image recognition & matching)
4. Post-processing & quality control
5. Storage & export

Stage 1: Data acquisition & retrieval (with scheduler)

Goal: Securely and efficiently obtain the necessary VHR satellite imagery, often through tasking or accessing archives.

Steps:

1. Define area of interest (AOI) & time of interest (TOI) with precision:
    - Increased granularity: For VHR, AOIs are often smaller (e.g., individual buildings, specific construction sites, small urban blocks). TOI might be for very specific dates or even within-day revisits.
    - Tasking: VHR often requires "tasking" a satellite (requesting a new acquisition over your AOI at a specific time) rather than just querying an archive. This is common for Maxar, Pleiades, SkySat.
2. Sensor selection & prioritization (VHR Focus):
    - Prioritize based on Ground Sample Distance (GSD) (e.g., < 0.5m), revisit capabilities (intraday for SkySat), and specific spectral bands.

- Commercial APIs: access is almost exclusively via proprietary APIs (e.g., Maxar GBDX/Platform APIs, Planet Tasking API, SkySat API).
- Scheduler: as before, cloud schedulers or event-driven triggers are used for automated ingestion.

3. Data filtering (enhanced precision):
    - Cloud Cover: even more critical. A small cloud can obscure key objects. Often requires *per-pixel* cloud masks or very low overall cloud cover thresholds.
    - Off-nadir angle: extremely important for VHR. Higher off-nadir angles introduce significant geometric distortions (e.g., building lean) and larger shadows, which can severely impact object recognition. Filter for angles typically < 20-30 degrees.
    - Sun elevation angle: for consistent object illumination and shadow analysis, filter for specific sun elevation ranges, especially for 3D reconstruction.
    - Quality flags: detailed vendor-provided quality flags are essential.
4. Download & data level:
    - VHR providers typically offer highly processed data levels:
        - Pansharpened: combining high-resolution panchromatic band with lower-resolution multispectral bands to create a high-resolution color image.
        - Orthorectified: geometrically corrected and aligned to a precise map projection, often using precise DEMs.
        - Analytic/surface reflectance: radiometrically and atmospherically corrected.
    - Typical VHR data is already level-2 or higher.

Stage 2: Pre-processing (Sensor & Scene Correction)

Goal: Further refine VHR data for optimal ML input, addressing subtle distortions and ensuring extreme precision.

General steps (apply as needed, depending on vendor data level):

1. Radiometric correction:
   - Typically handled by VHR vendors. Verify the data level (TOA or BOA) and radiometric bit depth (e.g., 11-bit, 16-bit) which is usually higher, providing richer color depth.
2. Atmospheric correction:
   - BOA reflectance is king: for quantitative analysis, especially time series or spectral indexing (e.g., NDVI for specific objects), ensure BOA surface reflectance. Many VHR providers offer this directly.
3. Geometric correction & orthorectification:
   - Sub-pixel accuracy: for VHR, sub-pixel co-registration accuracy is often required for ML tasks like change detection or precise feature extraction. Vendor orthorectification is usually excellent, but for multi-temporal analysis, additional co-registration tools may be needed.
   - Building lean/perspective distortion: even with orthorectification, tall objects can still exhibit significant "lean" (relief displacement) in off-nadir images. If 3D object reconstruction or precise footprinting is a goal, specialized processing (e.g., 3D restitution from stereo pairs, building height models) is needed, or these distortions must be accounted for by the ML model.
4. Image co-registration (critical for VHR):
   - Automated & robust: essential for accurate ML on time series. Tools must handle small shifts and rotations across VHR scenes.
5. Cloud, cloud shadow, and snow masking (enhanced detail):

- Precision masking: masks need to be highly accurate at the pixel level to avoid tiny cloud/shadow artifacts affecting small objects. Automated methods (often ML-based) are critical.
- Haze/thin cloud: VHR data is still affected by haze. Dedicated atmospheric compensation or haze removal algorithms might be beneficial.

6. Pansharpening (if not provided):
    - If you receive separate panchromatic and multispectral bands, this step is crucial to combine them into a single, high-resolution color product. Techniques like Gram-Schmidt, PCA, or more advanced ML-based pansharpening can be used.
7. Data tiling/patching (even more critical):
    - Smaller patches: due to the higher resolution and larger overall image dimensions (in pixels), you'll often need to cut images into smaller patches for ML model input to fit into GPU memory. Overlapping patches are vital to prevent edge effects.

Stage 3: Core processing (ML image recognition & matching)

Goal: Apply state-of-the-art machine learning models to extract fine-grained information and perform precise object recognition.

Steps:

1. Data Preparation for ML (VHR specific):
    - Micro-level annotation: ML model training for VHR often requires incredibly detailed and precise annotations of tiny objects (e.g., individual cars, windows, small infrastructure). This is a *major* effort.

- Complex class hierarchies: VHR enables more detailed classification (e.g., not just "building" but "single-family home," "apartment building," "warehouse").

2. ML model selection & adaptation:
    - Architecture choice: deeper and more complex CNNs (e.g., U-Net, Mask R-CNN, YOLO, Vision Transformers) are often required to capture the intricate details in VHR imagery.
    - Transfer learning: fine-tuning pre-trained models on VHR-specific datasets is common due to the high cost of VHR data and annotation.
    - Scale invariance: models need to be robust to objects appearing at different scales due to perspective or actual size variations.
    - Contextual information: VHR allows for better use of contextual information (e.g., "cars are on roads or in parking lots").
3. GPU utilization (maximum impact):
    - More GPU power: processing VHR data, especially for training or inference of complex models, will demand significantly more powerful GPUs (e.g., A100, H100) or more GPUs in parallel, due to larger pixel counts per area and model complexity.
    - Distributed processing: for large AOIs, distributed computing frameworks (e.g., Dask, Spark, Ray) across multiple GPUs/CPUs are essential.
4. Result Generation (Enhanced Detail):
    - Outputs are typically highly precise vector features (polygons for buildings, lines for roads, points for trees) with associated attributes and confidence scores.

Stage 4: Post-processing & quality control

Goal: Refine VHR ML outputs to meet high accuracy requirements, often involving human-in-the-loop validation.

Steps:

1. Topological refinement:
   - Automated and manual cleanup of vector outputs (e.g., snapping lines, removing self-intersections, ensuring polygon closure for tiny features).
2. Accuracy assessment & validation (higher standard):
   - Ground truth: requires extremely precise ground truth data (e.g., field surveys, high-accuracy drone data, manual expert annotation of VHR images).
   - Metrics: focus on fine-grained metrics like centroid distance for points, IoU for polygons, and pixel accuracy for segmentation.
   - Human-in-the-loop: manual review and correction by GIS experts are often integrated into the workflow to achieve the required accuracy for commercial VHR products.
3. Metadata generation/update:
   - Detailed metadata including precise acquisition parameters (off-nadir angle, sun angle), processing history, and specific accuracy metrics.

Stage 5: Storage & export

Goal: Efficiently store vast amounts of VHR data and its derivatives, making it accessible for high-performance applications.

Steps:

1. Storage into bucket (volume & organization):

- Massive data volumes: even small AOIs can generate large VHR datasets due to high resolution. efficient storage strategies (e.g., COGs, Zarr for array data) are vital.
- Partitioning: organize data by geographic tiling scheme (e.g., MGRS grid, custom grid) for efficient access.
- Data retention: same 2-year policy, but the sheer volume of raw VHR data might push more aggressively towards colder tiers faster, or require careful selection of what raw data to retain.

2. Data export/delivery (optimized for VHR):
    - Streaming services: for interactive applications, data needs to be streamable (e.g., via WMS/WMTS for tiles, vector tiles for features).
    - APIs: geospatial APIs (STAC, OGC API Features/Coverages) are crucial for accessing specific VHR products.
    - Condensed output (100 MB): your 100 MB daily output will likely be in vector format (e.g., GeoJSON, Shapefile) representing detected objects, or a very compressed raster map.

Summary of key differences: VHR vs. Medium resolution

Feature	Medium resolution (e.g., Sentinel-2, Landsat)	Very High Resolution (e.g., Maxar, Pleiades, SkySat)
Spatial Resolution	10m - 30m (pixel represents a larger area)	0.3m - 5m (pixel represents fine detail, individual objects)
Data Volume	Moderate (e.g., 500MB - 1GB per scene)	Significantly higher (e.g., several GB per scene for a similar ground area), much more pixels.
Data Acquisition	Primarily archival query (free/open access) or broad-area subscriptions.	Often requires tasking (new acquisition), commercial subscriptions.
Cost	Generally free/low cost.	Significantly Higher Cost per unit area.
Revisit Time	Varies (e.g., 5 days for Sentinel-2 at equator, global coverage common).	Higher frequency often available (e.g., intraday for SkySat), but usually for specific AOIs.
Geometric	Good, but VHR requires additional	Exceptional vendor-provided orthorectification,

Av. Dubrovnik 15, Zagreb, Croatia +385 91 193 08 75 info@seacras.com

Accuracy	fine-tuning.	but still requires co-registration for time series.
Atmospheric Correction	Often a necessary user step (L1C to L2A).	Often provided as a pre-corrected product (Analytic/Surface Reflectance).
Shadows/Perspective	Less pronounced impact.	Significant impact on object recognition due to building lean and large shadows.
Cloud Masking	Important for general analysis.	Critical and requires pixel-perfect accuracy for small object visibility.
ML Processing	Can use lighter models, less GPU memory. Focus on land cover, broad change.	Requires deeper, more complex ML models (CNNs, Transformers) for fine features.
GPU Requirements	Moderate, often able to run on mid-range GPUs.	Demands high-end GPUs (A100, H100) and/or distributed processing.
Data Preparation for ML	Larger patches, coarser annotations.	Smaller, overlapping patches; incredibly precise, fine-grained annotations.
Accuracy Assessment	Broader accuracy metrics.	Requires very high-precision ground truth; human-in-the-loop QA common.
Storage & I/O	Manageable for single scenes.	Challenges in I/O due to massive file sizes in pixels, necessitating efficient formats (COG, Zarr).

Waterbodies classification based on the spectral description

In oceanography and remote sensing of aquatic environments, "Case 1" and "Case 2" waters are a classification scheme based on the optical properties of the water and the relative contributions of different substances that interact with light. This classification is crucial because it dictates which algorithms and models are appropriate for retrieving information (like chlorophyll concentration) from ocean color satellite data.

The original concept was proposed by Morel and Prieur in 1977, and the definitions have evolved, but the core distinction remains.

Case 1 Waters

Short Description: Case 1 waters are those whose optical properties (how light is absorbed and scattered) are primarily determined by phytoplankton (and their associated co-varying organic matter).

Key characteristics:

- Dominant optically active constituent: phytoplankton and their degradation products (e.g., chlorophyll-a, detritus, and colored dissolved organic matter - CDOM - that *co-varies* directly with phytoplankton).
- Location: typically found in open ocean, oligotrophic (nutrient-poor) waters, far from terrestrial influence.These waters are often characterized by their deep blue to blue-green color.
- Relationship between constituents: in Case 1 waters, the concentrations of other optically active substances (like CDOM and non-algal particles) are assumed to co-vary directly and predictably with the concentration of chlorophyll-a (a proxy for phytoplankton biomass). This means if you know the chlorophyll concentration, you can reasonably estimate the contribution of other constituents to the water's optical signal.
- Modeling simplification: This predictable relationship allows for simpler bio-optical models to be used to retrieve chlorophyll-a concentrations from satellite ocean color data. These models often rely on ratios of remote-sensing reflectance in different blue-green wavelengths.
- Example: the vast expanses of the central gyres in the Atlantic or Pacific Ocean are classic examples of Case 1 waters.

Case 2 Waters

Short description: Case 2 waters are those whose optical properties are influenced not only by phytoplankton but also by other substances that do not necessarily co-vary with phytoplankton. These waters are optically much more complex.

Key characteristics:

- Dominant optically active constituent(s): In addition to phytoplankton, Case 2 waters have significant and independent concentrations of other optically active constituents. These include:
  - Colored Dissolved Organic Matter (CDOM): often referred to as "yellow substance," derived from terrestrial runoff (e.g., from rivers, wetlands), sewage, or resuspension of sediments. Its concentration does not directly correlate with phytoplankton.
  - Non-Algal Particles (NAP) / Total Suspended Solids (TSS): inorganic mineral particles (e.g., clay, silt, sand) from riverine input, coastal erosion, sediment resuspension from the bottom (e.g., by currents or dredging), or aeolian (wind-blown) dust.
  - Bottom reflectance: In shallow Case 2 waters, light reflected from the seafloor can also significantly influence the optical signal reaching the surface.
- Location: typically found in coastal waters, estuaries, bays, inland lakes, and sometimes turbid open ocean regions influenced by river plumes or upwelling of sediments. These waters often have a green, yellow, brown, or even reddish appearance due to the diverse constituents.
- Relationship between constituents: The concentrations of CDOM, NAP, and phytoplankton can vary independently of each other. This means knowing the

chlorophyll concentration alone is insufficient to accurately model the water's optical properties.

- Modeling complexity: Retrieving water constituent concentrations from Case 2 waters is much more challenging. It requires more sophisticated and often site-specific bio-optical models that can decouple the independent contributions of multiple optically active constituents. Algorithms often need to use more spectral bands, sometimes extending into the red and near-infrared, and might rely on iterative or inverse modeling approaches.
- Example: the Baltic Sea, the mouth of the Amazon River, highly turbid estuaries, or many freshwater lakes are typical examples of Case 2 waters.

Feature	Case 1 Waters	Case 2 Waters
Primary Influence	Phytoplankton & co-varying organic matter	Phytoplankton + Independent contributions from CDOM, Non-Algal Particles, and potentially bottom reflectance
Relationship of Constituents	Co-vary predictably with chlorophyll-a	Vary independently of chlorophyll-a
Typical Location	Open ocean, oligotrophic waters	Coastal waters, estuaries, lakes, turbid zones
Typical Color	Deep blue to blue-green	Green, yellow, brown, red (more turbid/colored)
Remote Sensing Models	Simpler, often empirical, chlorophyll-centric algorithms	More complex, often semi-analytical or site-specific algorithms needed to separate multiple components

Bathymetry influence on optical satellite data processing for water quality parameters derivation

This matrix details how water depth (specifically relative to a 25m threshold) and optical water type (Case 1 vs. Case 2) fundamentally influence the derivation of water quality parameters from optical satellite data.

Key concepts:

- WQ parameters: water quality parameters (e.g., Chlorophyll-a (Chl-a), Total Suspended Solids (TSS), Colored Dissolved Organic Matter (CDOM), secchi disk depth, turbidity, euphotic zone depth).
- Bottom influence: how light reflected from the seafloor impacts the optical signal measured by the satellite.
- Algorithms: types of bio-optical models/algorithms suitable for water quality parameter retrieval.
- Complexity: overall difficulty and uncertainty of retrieval.

Water depth / water type	Case 1 Waters (open ocean, oligotrophic)	Case 2 Waters (coastal, estuarine, turbid, inland)
I. Water depth > 25m	1. Deep Case 1 Waters	2. Deep Case 2 Waters
Bottom influence	None. Light doesn't reach/return from bottom.	None (or negligible). Bottom light attenuated before reaching surface.
Light penetration	High (clear water). Light penetrates deep.	Moderate to low (turbid/colored water). Light penetration limited by constituents.
WQ parameters derivable	Primary: Chl-a, CDOM (some types), K_d (light attenuation). Primarily for inherent optical	Primary: Chl-a, TSS/Turbidity, CDOM. Key challenge: decoupling independent contributions of multiple optically active constituents.

Av. Dubrovnik 15, Zagreb, Croatia +385 91 193 08 75 info@seacras.com

	properties (IOPs) of water itself.	
Algorithm types	Standard ocean color algorithms: empirical or semi-analytical algorithms relying on blue-green band ratios (e.g., OC4, OC3). Simple, robust.	Advanced Case 2 algorithms: - semi-analytical/analytical: model-based, try to invert reflectance to constituent concentrations (e.g., GSM, Carder, QAA). - Neural networks/machine learning: trained on diverse Case 2 datasets. - Inversion models: often iterative. Require more spectral bands (red, NIR).
Complexity & uncertainty	Relatively low complexity. High confidence in Chl-a retrieval.	High complexity. Significant challenges in accurate retrieval due to multiple independent variables. Algorithms must separate signals. Higher uncertainty.
Applications	Large-scale phytoplankton blooms, ocean productivity, carbon cycling, climate monitoring.	Tracking large river plumes, estuarine dynamics, regional pollution, harmful algal blooms, sediment transport.
General remote sensing approach	Standard broad-area, lower-to-moderate spatial resolution sensors (e.g., MODIS, VIIRS, Sentinel-3) are well-suited.	Requires sensors with more spectral bands (including red/NIR) and often moderate to high spatial resolution (e.g., Sentinel-2, Landsat, some commercial VHR).
II. Water depth le 25m	3. Shallow Case 1 Waters	4. Shallow Case 2 Waters
Bottom influence	Significant. Light reaches and reflects from the bottom, heavily influencing the water-leaving radiance.	Potentially significant. Even in turbid water, if light penetrates to bottom and substrate is highly reflective (e.g., sand), it can still influence signal. More complex to separate from water column.
Light penetration	Very high. Clear water, light almost	Moderate to Low. Bottom influence depends heavily on water clarity and bottom type. Might be minimal in very turbid waters.

	always reaches bottom.	
WQ parameters derivable	Extremely challenging for WQ. Bottom signal often overwhelms or biases water column signal. Primary focus:bathymetry, bottom mapping (coral, seagrass), not water quality.	Extremely challenging for WQ. Bottom influence, high WQ constituent variability, and spatial heterogeneity compound complexity. Primary focus: often bathymetry, bottom mapping, or qualitative turbidity assessment rather than precise WQ values.
Algorithm types	Rarely direct WQ algorithms. Often require algorithms that simultaneously retrieve bathymetry, bottom type, and water column properties. - Analytical inversion models: attempt to decouple water column and bottom signals. - Hyperspectral sensors: offer more spectral detail to aid separation.	Highly advanced/experimental: Requires very sophisticated multi-spectral/hyperspectral algorithms capable of separating complex water column signals from potentially confounding bottom reflectance. Often site-specific. - Machine Learning (ML): Can be trained on extensive ground truth.
Complexity & uncertainty	Very high complexity & uncertainty for WQ. Bottom reflectance is the dominant signal; difficult to isolate and quantify subtle WQ changes.	Highest complexity & uncertainty for WQ. All challenges of deep Case 2, plus confounding bottom signal. Often results in high uncertainty or inability to retrieve precise WQ.
Applications	Bathymetry mapping in clear waters, coral reef and seagrass bed	Bathymetry mapping in shallow turbid areas (more difficult), qualitative assessment of very turbid plumes over shallow banks, broad habitat mapping.

	mapping/health monitoring.	
General remote sensing approach	Requires high spatial resolution sensors (e.g., WorldView, Pleiades, SkySat, Sentinel-2) to resolve bottom features. Often uses specific wavelengths (e.g., blue, green) and analytical models.	Requires very high spatial resolution (0.3m-5m) and potentially hyperspectral sensors. Heavy reliance on robust, often ML-based, inversion methods, and extensive in-situ data.

Reliability and accuracy of the technology in the context of determining marine status descriptors

Overview of most common water quality parameters derived from satellite data

Satellite remote sensing primarily measures the optically active constituents (OACs) in the water column, meaning those substances that absorb and scatter light. Other optically inactive parameters can sometimes be inferred indirectly if they have a strong, predictable correlation with an OAC.

I. Optically Active Constituents (Directly Measurable by Satellite):

1. Chlorophyll-a (Chl-a) Concentration:
    - Description: The primary photosynthetic pigment in phytoplankton. It's a key indicator of algal biomass, primary productivity, and trophic status (eutrophication).

- Why it's derived: Phytoplankton strongly absorb blue and red light and reflect green and near-infrared (NIR) light. These spectral features allow for its retrieval.
- Common Algorithms:
  - Empirical/Semi-empirical: Often based on band ratios (e.g., blue-to-green ratios like OCx algorithms: OC3, OC4 for Case 1 waters; or red-NIR algorithms for turbid/Case 2 waters like normalized difference chlorophyll index - NDCI, 3-band algorithms).
  - Semi-analytical/Analytical: Inversion models based on radiative transfer principles.
  - Machine Learning (ML): Can be trained on large datasets to find complex relationships.
- Calibration Needs: Critical. Algorithms are tuned using coincident in situ Chl-a measurements and satellite-derived remote sensing reflectance (Rrs). This involves regression analysis to establish the relationship between spectral ratios/features and actual Chl-a values. Different water types or regions often require regional algorithm tuning or re-calibration.

2. Total Suspended Solids (TSS) / Turbidity / Suspended Particulate Matter (SPM):
   - Description: The concentration of all particulate matter suspended in the water column (both organic and inorganic). Turbidity is an optical property (light scattering), while TSS/SPM is a mass concentration. They are highly correlated. Indicators of erosion, runoff, dredging, and water clarity.
   - Why it's derived: Suspended particles primarily increase the backscattering of light, especially in the red and near-infrared (NIR) wavelengths, where water absorption is high but particle scattering can still be strong.
   - Common Algorithms:

        - Empirical: Single-band or band-ratio algorithms (e.g., using red or NIR bands, or ratios of red/NIR to green).
        - Semi-analytical: Models based on relationships between backscattering coefficients (derived from satellite data) and TSS concentration.
        - Machine Learning: Increasingly used for complex, highly variable turbid waters.
    - Calibration Needs: Essential. In situ TSS (gravimetric methods) or Turbidity (nephelometric turbidity units - NTU) measurements are matched with satellite reflectance to develop or validate algorithms. Regional calibration is very common due to varying particle types (mineral, organic) and sizes, which have different optical properties.

3. Colored Dissolved Organic Matter (CDOM) / Dissolved Organic Carbon (DOC):
    - Description: Dissolved organic matter that absorbs light, particularly in the blue and ultraviolet (UV) regions. Often referred to as "yellow substance." Derived from terrestrial runoff (e.g., tannins from wetlands), algal decay, or pollution. Impacts light penetration and UV protection.
    - Why it's derived: CDOM strongly absorbs light in the blue-UV spectral range, leading to a characteristic decrease in blue reflectance from the water.
    - Common Algorithms:
        - Empirical: Often use blue band absorption features or ratios involving blue and green/red bands.
        - Semi-analytical: Inversion models that try to separate CDOM absorption from other constituents' absorption.
    - Calibration Needs: Crucial. In situ CDOM absorption coefficients (e.g., aCDOM at 440 nm) are measured using spectrophotometry and correlated with

satellite data. Challenges arise from spectral overlap with Chl-a absorption in the blue.

4. Sea Surface Temperature (SST) / Lake Surface Water Temperature (LSWT):
    - Description: The temperature of the uppermost layer of the water body. Influences biological processes (algal growth, fish migration), physical processes (mixing, stratification), and climate.
    - Why it's derived: Water emits thermal radiation, which can be detected by satellite thermal infrared (TIR) sensors.
    - Common Algorithms: Radiative transfer models that correct for atmospheric effects (absorption and emission by water vapor, CO_2) using multiple thermal bands (e.g., split-window algorithms).
    - Calibration Needs: High accuracy. In situ temperature measurements (thermometers, CTDs, buoys) are used to calibrate and validate the satellite-derived temperature products. Global standard products are highly accurate (e.g., 0.5°C).

II. Optically Inactive or Indirectly Derivable Parameters:

Parameters like salinity, dissolved oxygen (DO), pH, total phosphorus (TP), and total nitrogen (TN) are not directly measured by current optical satellites as they do not have unique spectral signatures in the visible or infrared range that can be clearly detected from space.

- Indirect Derivation: These can sometimes be inferred indirectly through:
    - Statistical Correlations: If they have a strong, consistent statistical relationship with an optically active parameter (e.g., high TP often correlates with high Chl-a in eutrophic systems). These relationships are highly site-specific and less robust.

    - Data Fusion/Modeling: Combining satellite-derived OACs with in situ measurements, hydrological models, or ecological models.
- Calibration Needs: Extremely high. Any indirect derivation requires extensive and robust in situ datasets to establish and validate the statistical relationships, which are often not globally transferable.

The role of ground truth (in situ) data in calibration

Calibration with in situ data is the cornerstone of quantitative water quality remote sensing. It involves a systematic process:

1. Coincident Data Collection:
    - Timing: In situ measurements must be collected as close as possible in time to the satellite overpass (ideally within ± 3 hours, sometimes ± 1 hour for rapidly changing systems).
    - Location: In situ sampling points must be precisely georeferenced and ideally located within homogeneous water pixels to avoid spatial mismatch.
    - Measurements: Direct, accurate measurements of the water quality parameters of interest (e.g., Chl-a via filtration and spectrophotometry, TSS via gravimetric analysis, CDOM via absorption spectroscopy, temperature via calibrated thermometers) are taken.
    - Radiometric Measurements: For algorithm development, in situ measurements of water-leaving radiance or remote sensing reflectance (using a spectroradiometer) are often collected simultaneously with the water quality parameters to establish direct spectral relationships.
2. Atmospheric Correction Validation:

- Before water quality parameters can be derived, the satellite signal must be corrected for atmospheric effects to retrieve accurate water-leaving radiance or remote sensing reflectance.
- In situ radiometric measurements are also used to validate the atmospheric correction algorithms applied to the satellite imagery.

3. Algorithm Development & Tuning:
   - Empirical/Statistical: In situ data are used to derive regression equations or train machine learning models that link satellite-derived spectral information (e.g., band ratios, spectral shape features) to the actual in situ water quality concentrations. This often involves trial-and-error with different band combinations and statistical models.
   - Semi-analytical/Analytical: While these algorithms are based on physics, they often require "tuning" of specific parameters (e.g., inherent optical properties of local water constituents) using in situ measurements to optimize their performance for a particular water body or region.
4. Validation & Accuracy Assessment:
   - After an algorithm is developed, an independent set of in situ data (not used in development) is used to validate its performance.
   - Statistical metrics like Root Mean Square Error (RMSE), Mean Absolute Percentage Error (MAPE), R-squared (R2), and bias are calculated to quantify the accuracy and precision of the satellite-derived products against ground truth.
5. Long-term Monitoring & Recalibration:
   - Water bodies are dynamic. Over time, changes in constituent properties (e.g., different algal species, sediment composition) or sensor degradation can necessitate recalibration of algorithms using new in situ data. Regular,

consistent in situ monitoring programs are therefore vital for sustaining long-term, accurate satellite-based water quality monitoring.

Assessment of technology implementation resources

General protocol for cloud resource estimation (optical satellite data processing)

Objective: To systematically identify and quantify the cloud resources required for processing optical satellite data, enabling cost estimation and infrastructure planning.

Core Principles:

- Decomposition: Break down the overall workflow into distinct, measurable stages.
- Parameterization: For each stage, identify key metrics and variables that drive resource consumption.
- Scalability: Consider how resource needs will change with increasing data volume or processing complexity.
- Optimization: Identify opportunities to reduce resource consumption (and thus cost).

Protocol Stages:

1. Define Workflow & Data Characteristics
2. Estimate Storage Requirements
3. Estimate Processing (Compute) Requirements
4. Estimate Network (Egress/Ingress) Requirements
5. Identify Ancillary Service Requirements
6. Consolidate & Optimize

Stage 1: Define Workflow & Data Characteristics

Goal: Clearly understand the processing pipeline and the nature of the data.

Key Questions/Information Needed:

1. Daily Data Ingest Volume: What is the average daily volume of raw satellite data (e.g., in GB, TB)?
   - *Examples:* "X GB of medium-resolution data," "Y GB of VHR data."
2. Data Source & Resolution: What type of optical satellite data (e.g., Sentinel-2, PlanetScope, Maxar WorldView, Pleiades)? What is its typical spatial resolution?
   - *Impact:* Directly affects file size (pixels per unit area), preprocessing needs, and GPU requirements.
3. Exact Processing Steps: Outline the full processing pipeline from raw input to final output.
   - *Examples:* Retrieval, Pre-processing (radiometric, atmospheric, geometric), ML Inference, Data Fusion, Post-processing, etc.
4. Output Data Volume & Type: What is the daily volume of the final, condensed output (e.g., 100 MB of vector data, 5 GB of processed raster)?
5. Data Retention Policy: How long must raw, intermediate, and final processed data be stored, and in what tiers (e.g., hot, warm, cold/archive)?
6. Processing Frequency: Is processing daily, weekly, on-demand, or real-time?
7. Performance Requirements: What is the acceptable latency for processing (e.g., within 24 hours, real-time results)?

Stage 2: Estimate Storage Requirements

Goal: Quantify storage capacity and access patterns.

Key Parameters to Estimate:

1. Total Raw Data Storage:
   - `Daily Ingest Volume * Number of Days to Retain Raw Data`
2. Total Processed/Intermediate Data Storage:
   - `Average Daily Intermediate Data Volume * Number of Days to Retain Intermediate Data`
   - `Average Daily Final Output Volume * Number of Days to Retain Final Output`
   -
3. Storage Access Patterns:
   - How frequently is data accessed from each tier (e.g., frequently read for processing, rarely read for archive)?
   - Estimate the number of read/write operations (API calls) for buckets.

Calculation Focus: Total GB/month per storage tier (e.g., "X GB Hot Storage," "Y GB Cold Storage").

Stage 3: Estimate Processing (Compute) Requirements

Goal: Determine the necessary compute power for all processing steps, especially ML.

Key Parameters to Estimate:

1. Compute Instance Type:

  - For CPU-bound tasks (e.g., scheduling, lighter pre-processing): Number of vCPUs and amount of RAM.
  - For GPU-bound tasks (e.g., ML inference): Type of GPU (e.g., T4, A10, A100), number of GPUs, and associated vCPUs/RAM.
  - *Impact:* Directly affects hourly cost.
2. Processing Time per Data Unit:
  - How long does it take for a specific unit of data (e.g., 1 GB of raw data, one image scene) to go through the GPU-intensive ML stage?
  - *This is often the most critical and hardest to estimate without benchmarking.*
3. Daily/Monthly Compute Hours:
  - `Daily Data Ingest Volume / Data Unit Size * Processing Time per Data Unit = Total Daily Compute Hours`
  - `Total Daily Compute Hours * 30 Days = Total Monthly Compute Hours`
4. Scaling Strategy:
  - Will compute instances be always-on, shut down when idle, or use serverless/burst functions?
  - Consider using spot/preemptible instances for cost savings on interruptible workloads.
  - *Impact:* Drives effective hourly cost.
5. Orchestration/Scheduler Compute:
  - Small VM or serverless function usage for scheduling and workflow management. This is typically minor but should be acknowledged.

Calculation Focus: Total compute hours per instance type per month (e.g., "X hours of `g4dn.xlarge` instance," "Y hours of Lambda function").

Stage 4: Estimate Network (Egress/Ingress) Requirements

Goal: Quantify data transfer costs.

Key Parameters to Estimate:

1. Data Egress (Downloads from Cloud):
   - `Daily Output Data Volume Downloaded by Users * 30 Days = Total Monthly Egress`
   - `Any other data downloaded from cloud storage (e.g., for external applications)`
   - *Impact:* Egress is typically the most expensive network cost.
2. Data Ingress (Uploads to Cloud):
   - `Daily Raw Data Ingest Volume * 30 Days = Total Monthly Ingress`
   - *Note:* Ingress is generally free or very low cost on major cloud providers.
3. Internal Data Transfer:
   - Data transfer *between* cloud services *within the same region* (e.g., storage to compute) is usually free or very low cost.
   - Data transfer *between different regions* within the cloud is charged and can be significant. Assume single-region for initial estimates unless specified.

Calculation Focus: Total GB/month for egress (e.g., "Z GB Egress").

Stage 5: Identify Ancillary Service Requirements

Goal: Account for supporting services that incur costs.

Examples of Services:

- Database: If ML results or metadata are stored in a managed database (e.g., PostgreSQL, NoSQL DB).
- Monitoring & Logging: Services like CloudWatch, Stackdriver, Azure Monitor.
- Container Registry: For Docker images of ML models.
- Managed ML Services: If using higher-level platforms (e.g., SageMaker, Vertex AI) beyond raw GPU instances.
- Networking Services: Load balancers, VPNs, specialized network configurations.
- Security Services: WAFs, DDoS protection.

Calculation Focus: Estimate costs based on usage patterns or fixed rates for these services (e.g., "X hours/GB for monitoring," "Y database instance-hours").

Stage 6: Consolidate & Optimize

Goal: Aggregate all estimated costs and identify strategies for cost reduction.

Steps:

1. Sum All Estimated Costs: Add up costs from Storage, Compute, Network, and Ancillary Services for a total monthly estimate.
2. Apply Free Tiers: Deduct any free tier allowances (especially for new accounts) from the total.
3. Explore Optimization Strategies:
    - Reserved Instances/Savings Plans: For predictable, long-running compute.
    - Spot/Preemptible Instances: For fault-tolerant, interruptible workloads.
    - Data Lifecycle Management: Aggressively move data to colder storage tiers.

- Auto-scaling: Scale compute resources up and down with demand.
- Right-Sizing: Ensure instances are not over-provisioned.
- Efficient Code/Models: Optimize ML models for faster inference.
- Processing In-Cloud: Minimize data egress by doing all heavy processing within the cloud.

4. Refine Estimates: Based on optimization strategies, revise the initial cost figures.
5. Use Cloud Provider Calculators: Always input your refined parameters into the official AWS, Google Cloud, or Azure pricing calculators for the most accurate current figures.

Feature/Metric	PlanetScope (1 image: 25 MB)	Maxar WorldView Legion (1 image: 76 MB)	Pleiades Neo (1 image: 390 MB)	SkySat (1 image: 760 MB)	Aggregate (Daily Total)
Data Type	RGB+TOA+BOA + Metadata	BOA + Metadata	BOA + Metadata	RGB (240MB) + BOA (520MB) + Metadata	Varied VHR (0.3m-1m) & Medium-Res (3-5m), all pre-processed.
Spatial Resolution (Typical)	~3-5m (SuperDove)	~0.3-0.5m	~0.3m	~0.5-0.8m	Blended resolutions, requiring robust ML models.
Daily Ingest Volume	25 MB	76 MB	390 MB	760 MB	~1.25 GB/day
Annual Ingest Volume	9.125 GB	27.74 GB	142.35 GB	277.4 GB	~456.25 GB/year
2-Year Raw Data Volume	18.25 GB	55.48 GB	284.7 GB	554.8 GB	~912.5 GB (~0.91 TB) (This is the total raw data stored for 2 years)
Primary GPU Type for ML	NVIDIA T4 (efficient for smaller images)	NVIDIA A10 (good balance for VHR)	NVIDIA A10	NVIDIA A10	Single NVIDIA A10 instance (optimized for sequential processing).
Estimated	~15 seconds	~30 seconds	~2 minutes	~4 minutes	~6.75 minutes active GPU

Processing Time per Image (on A10)			(120 seconds)	(240 seconds)	time daily (Total sum of individual processing times)
Estimated Daily Billed GPU Time	Part of the shared 30 mins/day for all images	Part of the shared 30 mins/day for all images	Part of the shared 30 mins/day for all images	Part of the shared 30 mins/day for all images	30 minutes (0.5 hours) (Accounts for startup, overhead, min. billing increment)
Estimated Monthly GPU Compute Cost	N/A (covered by shared cost)	N/A (covered by shared cost)	N/A (covered by shared cost)	N/A (covered by shared cost)	$18.00 (0.5 hrs/day * 30 days/month * $1.20/hr for A10 GPU instance including VM base)
Estimated Monthly Storage Cost	N/A (covered by shared cost)	N/A (covered by shared cost)	N/A (covered by shared cost)	N/A (covered by shared cost)	$5.94 (Breakdown: Hot: $2.81, Cold: $2.40, Processed Output: $0.73)
Estimated Monthly Egress Cost	N/A (covered by shared cost)	N/A (covered by shared cost)	N/A (covered by shared cost)	N/A (covered by shared cost)	$0.27 (for 3 GB/month of 100MB daily condensed output)
Estimated Monthly Scheduler Cost	N/A (covered by shared cost)	N/A (covered by shared cost)	N/A (covered by shared cost)	N/A (covered by shared cost)	$5.00 (flat monthly)
TOTAL ESTIMATED MONTHLY CLOUD COST	N/A (covered by total)	N/A (covered by total)	N/A (covered by total)	N/A (covered by total)	~$29.21 (This is the aggregated cost for managing all these data sources in one system)

Technology maintenance

In addition to the financial aspects, the practicalities of maintaining such a satellite data processing system in the cloud are crucial for its long-term success. Here's a short description of the key maintenance areas:

Maintenance of a Cloud-Based Satellite Data Processing System

Maintaining a cloud-based system for processing daily satellite data, especially with diverse VHR sources and ML components, involves several ongoing activities to ensure its reliability, efficiency, and accuracy. Key areas include:

1. System Monitoring & Alerting:
    - Purpose: Continuously observe the health and performance of all components.
    - Activities: Setting up dashboards and alerts for compute resource utilization (CPU, GPU, RAM), storage capacity, network traffic, processing job status (success/failure, duration), and API call limits for data providers. Anomalies trigger immediate notifications to operators.
2. Data Pipeline Health Checks:
    - Purpose: Verify that data flows smoothly from acquisition to final output.
    - Activities: Regularly checking scheduler logs for failed triggers, API responses from data providers for errors, successful data downloads to staging buckets, and the integrity of data transfers between processing stages. This includes verifying cloud cover filtering and other initial data quality checks.
3. ML Model Monitoring & Retraining:
    - Purpose: Ensure the ML models maintain performance and adapt to changing conditions.
    - Activities: Monitoring model inference accuracy, drift detection (identifying if model performance degrades over time due to changes in input data characteristics like new sensors or environmental shifts), and data quality of model outputs. Periodically, models may require retraining with new, annotated data to maintain or improve accuracy. This involves managing training data sets and MLOps pipelines.
4. Software & Dependency Management:

- Purpose: Keep processing software, libraries, and container images up-to-date.
- Activities: Patching operating systems, updating Python libraries (e.g., geospatial libraries like GDAL, Rasterio, ML frameworks like TensorFlow/PyTorch), and ensuring compatibility between different software versions within containerized environments. This also includes managing GPU drivers.

5. Data Lifecycle Management & Storage Optimization:
   - Purpose: Efficiently manage data across storage tiers and ensure data integrity.
   - Activities: Regularly reviewing and enforcing data lifecycle policies to transition data from hot to cold/archive storage to optimize costs. This includes verifying data checksums and backup strategies for critical processed outputs.
6. Security Updates & Compliance:
   - Purpose: Protect the system from vulnerabilities and adhere to security best practices.
   - Activities: Applying security patches to cloud infrastructure and software, managing access controls (IAM roles, user permissions), and regularly auditing configurations to ensure compliance with relevant data privacy or industry standards.
7. Cost Optimization & Resource Right-Sizing:
   - Purpose: Continuously seek ways to reduce cloud expenditure.
   - Activities: Reviewing cloud bills, identifying underutilized resources, optimizing compute instance types and scaling configurations (e.g., using spot instances where appropriate), and fine-tuning data lifecycle policies. This is an ongoing process of balancing performance and cost.

8. Documentation & Knowledge Transfer:
    - Purpose: Maintain clear records of the system's architecture, configurations, and operational procedures.
    - Activities: Updating runbooks, architecture diagrams, and troubleshooting guides. Ensuring that knowledge is shared across the team to enable effective incident response and future development.

Detailed description of the technology used

Satellite monitoring results were obtained using the Coastal Intelligence software solution developed by Sea Cras d.o.o. The software is based on a proprietary artificial intelligence algorithm for processing very high-resolution (VHR) satellite imagery. Within this study, it was employed to quantify chlorophyll-a concentration (descriptor D5), total suspended matter (descriptor D7), and marine litter (descriptor D10). The software has been validated and successfully applied in multiple projects for public institutions in the Republic of Croatia and the European Union.

Satellite monitoring was conducted based on the current conditions on a given day, i.e., detection at a single observation time. A total of 58 VHR satellite images were collected, of which 46 were included in the analysis as they met the meteorological conditions required for successful processing. Although the project originally planned weekly monitoring of chlorophyll-a and total suspended matter concentrations, the analysis encompassed all available dates from May to September 2024 for which high-quality satellite imagery satisfied the meteorological criteria. This approach provided a higher temporal resolution than the minimum required, thereby enhancing the reliability of detecting seasonal and spatially dependent patterns.

For the analysis of descriptors D5, D7, and D10, satellite data from Maxar WorldView Legion, Pléiades Neo, Planet SkySat, and Planet Dove constellations were used. Their high spatial resolution enabled precise detection of small-scale phenomena and floating objects.

Analysis of descriptors D5 and D7 was conducted using four virtual measurement stations, labeled Locations 1–4, positioned to represent varying degrees of sea openness and enclosure (Figure 1). For each station, values were averaged over a 3×3 pixel neighborhood to obtain more stable and representative estimates of chlorophyll-a and total suspended matter concentrations. This approach provided a detailed view of spatial variability and its correlation with external factors, including meteorological conditions and anthropogenic influences.

To improve interpretation of satellite data, relevant meteorological data were collected for the monitoring period from the nearest Croatian Meteorological and Hydrological Service (DHMZ) station – Rovinj. Daily measurements of precipitation, wind direction and speed, and air temperature at 14:00 were analyzed. The 14:00 time was selected because it most closely corresponds to the satellite overpass, typically between 11:00 and 12:30, making it more representative for comparison than, for example, 07:00 morning measurements.

In addition to atmospheric data, sea surface temperature was obtained from the nearest DHMZ marine meteorological station – Sv. Ivan na Pučini – serving as an additional reference for interpreting thermal and biogeochemical processes within the Lim Bay water body.

Figure 1. Locations of virtual measurement stations within the satellite monitoring area of the Lim Bay

Note: The thematic data layers were overlaid on the base satellite imagery (base map, foundational layer, basemap). The base layer (basemap) was used as a reference map for the entire high-resolution study area.

Monitoring area

Lim Bay is a submerged canyon valley in karst terrain, located on the western coast of Istria, between Rovinj and Vrsar. The bay is approximately 10 km long, with an average width of 600 m and steep canyon walls reaching up to 150 meters in height. Together with

its natural continuation – the Lim Channel – it forms a unique landscape and hydrological unit. Due to its natural value and preservation, Lim Bay was declared a significant landscape in 1964, with a total protected area of 8.828 km²
(source: https://www.natura-histrica.hr/hr/zasticena-područja).

The area covered by this study refers exclusively to the marine surface, with an emphasis on the inner part of Lim Bay and the extended marine waters toward the west, partially extending beyond the boundaries of the officially protected area (Figure 2)

Figure 2. Thematic map of the satellite monitoring area of the Lim Bay

The total area of the analyzed marine zone is 6.85 km², in accordance with project requirements. This spatial coverage was selected to ensure representative monitoring of relevant biogeochemical processes and to achieve higher spatial sensitivity in tracking eutrophication, hydrographic changes, and marine litter.

This defined area allows monitoring of:

- The inner, more enclosed part of the bay, where changes are most pronounced.
- The more open western part, where transitional processes between the bay and the open water-like marine system are observed.

Monitoring period and timing

Very high-resolution satellite imagery was used to calculate chlorophyll-a concentration (descriptor D5), total suspended matter (descriptor D7), and marine litter (D10). The images were acquired via satellites, with metadata—including overpass time over the monitoring area—corresponding to the period between 11:00 and 12:30 hours.

The satellite imagery was analyzed within the defined study area. Only images collected between May 1 and September 30, 2024, that met the meteorological criteria necessary for successful analysis, were included in the study[1].

Meteorological and oceanographic data

Meteorological and oceanographic data were collected for all days included in the satellite analysis, aiming to support the interpretation of results related to biochemical descriptors D5 (eutrophication) and D7 (hydrographic changes). Meteorological data, including precipitation, wind direction and speed, and air temperature at 14:00 h loca time,, were

[1] Glavni kriterij bio je odsutnost naoblake iznad i oko definiranog područja monitoringa.

obtained from the Rovinj station (DHMZ), while sea temperature data were collected from the Sv. Ivan na Pučini marine station.

Monthly graphs for May, June, July, August, and September 2024 are presented below, covering all days of each month and illustrating changes in atmospheric conditions during the observation period. For selected dates included in the satellite image analysis, an additional table was prepared that also includes air and sea temperature data. This combined dataset enables comparison of meteorological conditions with daily changes in biochemical parameters within a broader seasonal context.

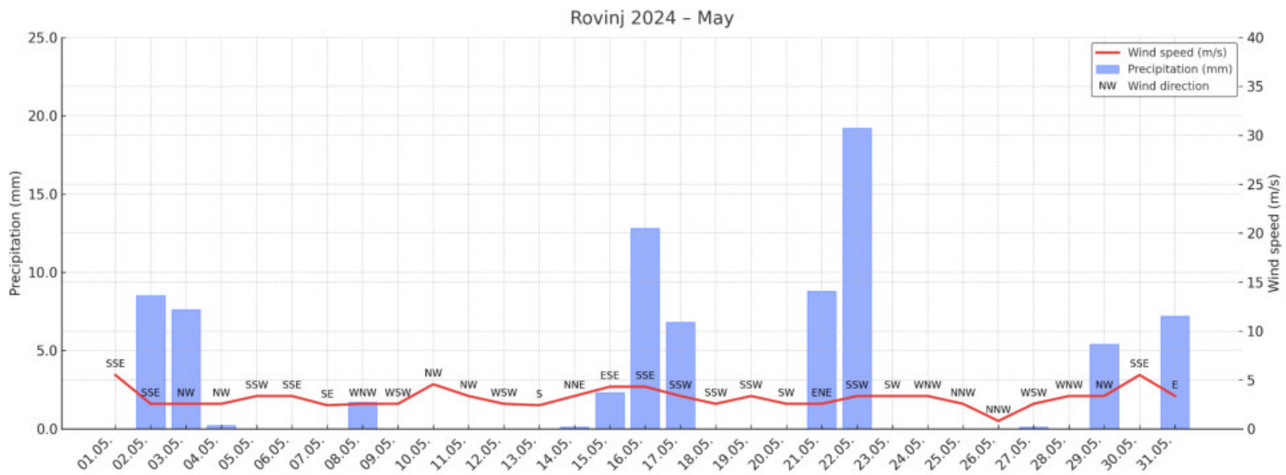

Figure 3. Meteorological data on precipitation, wind speed, and wind direction for May 2024 – Rovinj station (DHMZ)

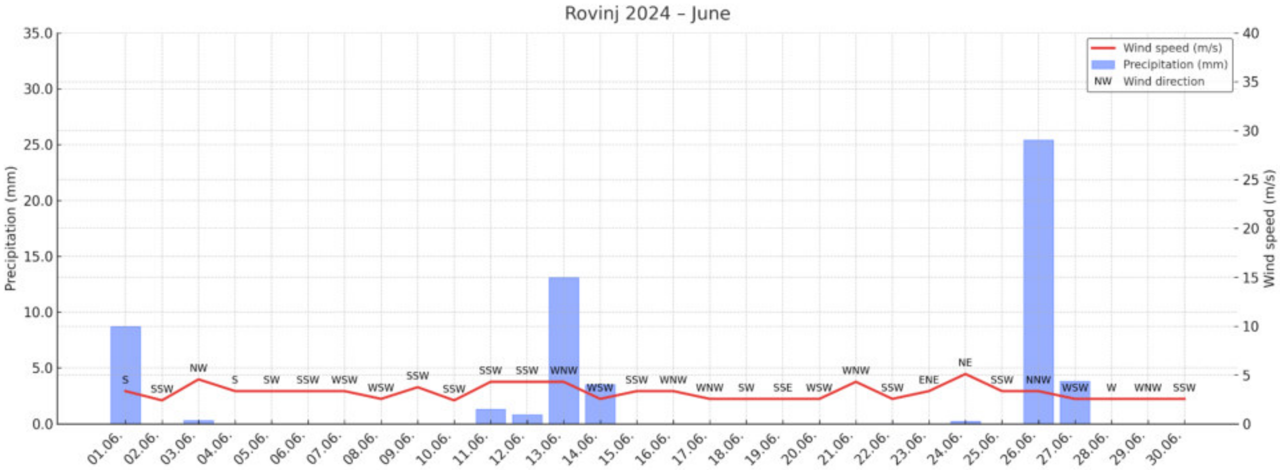

Figure 4. Meteorological data on precipitation, wind speed, and wind direction for June 2024 – Rovinj station (DHMZ)

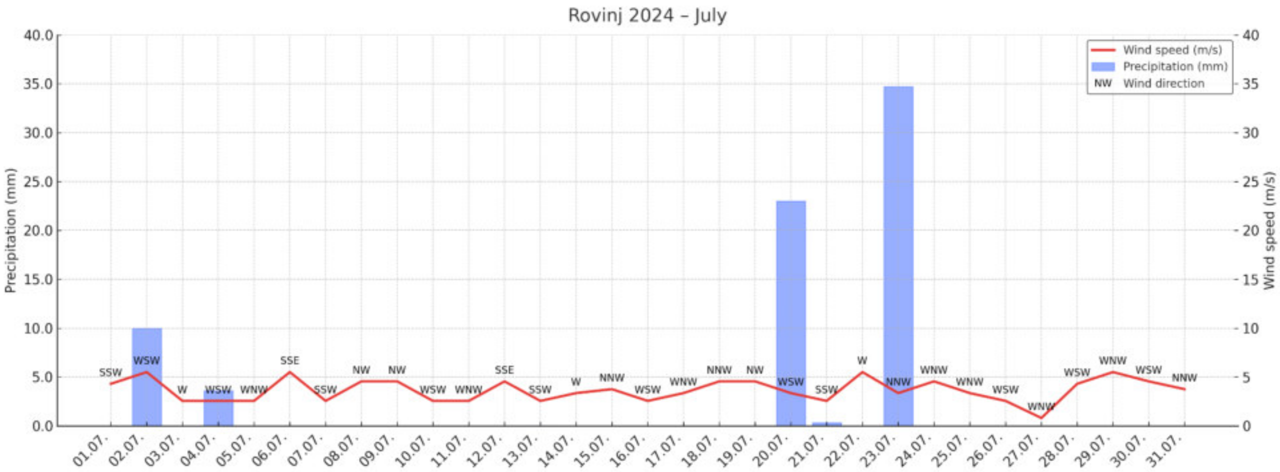

Figure 5. Meteorological data on precipitation, wind speed, and wind direction for July 2024 – Rovinj station (DHMZ)

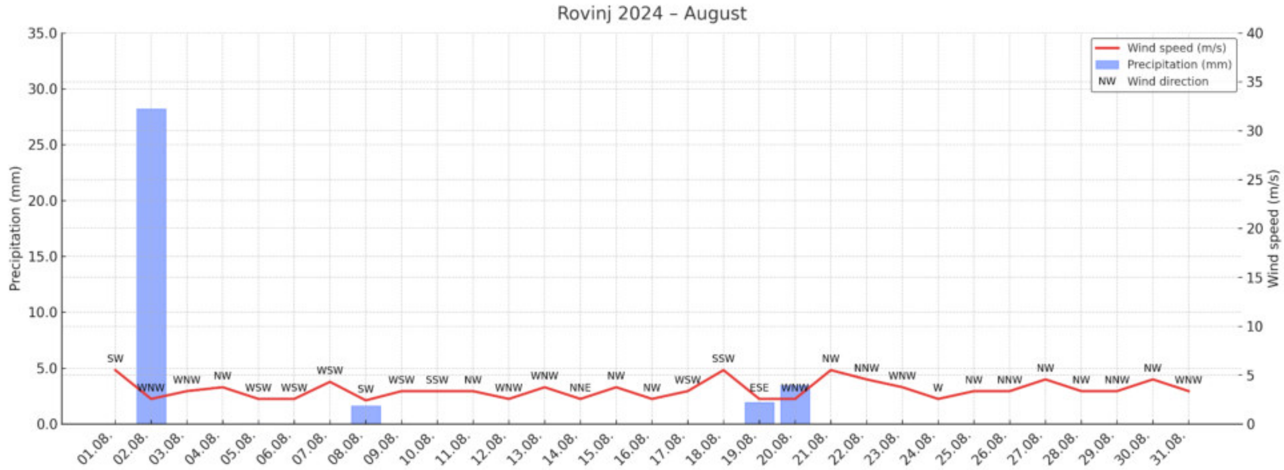

Figure 6. Meteorological data on precipitation, wind speed, and wind direction for August 2024 – Rovinj station (DHMZ)

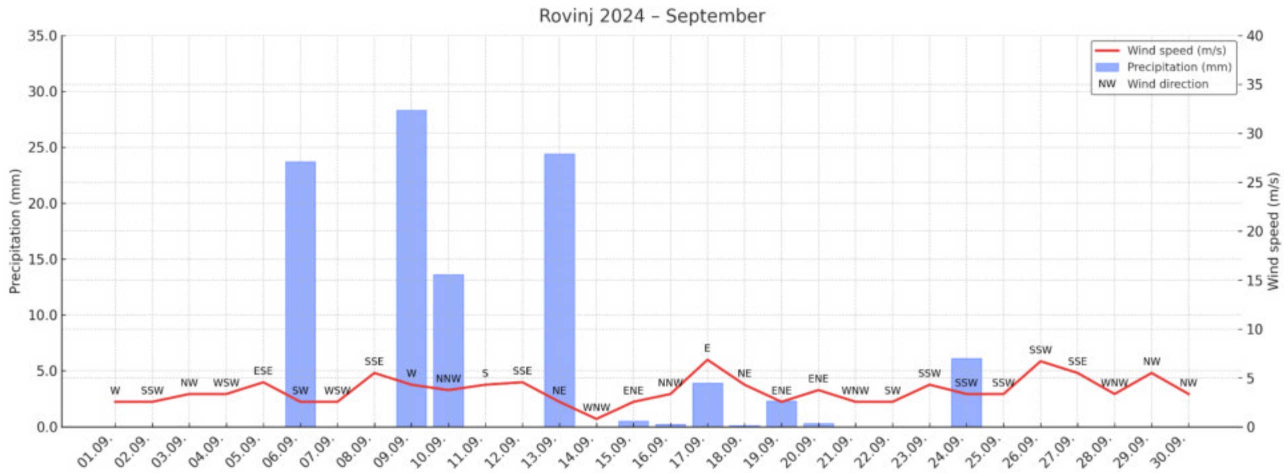

Figure 7. Meteorological data on precipitation, wind speed, and wind direction for September 2024 – Rovinj station (DHMZ)

Table 1. Meteorological and oceanographic data for the dates included in the analysis (May - September 2024)

Date	Precipitation (mm)	Wind speed (km/h)	Wind direction	Air temperature (°C)	Sea temperature (°C)
01.05.2024.	0	24,12	SSE	19,2	16,3
05.05.2024.	0	15,48	SSW	16,2	16,0

08.05.2024.	1,7	15,48	WNW	16	16,4
10.05.2024.	0	24,12	NW	17,4	16,3
17.05.2024.	6,8	15,48	SSW	18	17,5
18.05.2024.	0	15,48	SSW	18	17,7
22.05.2024.	19,2	15,48	SSW	18,8	18,3
23.05.2024.	0	15,48	SW	18,7	18,5
24.05.2024.	0	15,48	WNW	18,1	19,0
25.05.2024.	0	15,48	NNW	18,8	19,2
26.05.2024.	0	2,88	NNW	19	19,2
28.05.2024.	0	15,48	WNW	19,6	21,1
03.06.2024.	0,3	24,12	NW	18,2	21,2
12.06.2024.	0,8	15,48	SSW	20,4	24,4
15.06.2024.	0	15,48	SSW	21,6	24,0
23.06.2024.	0	15,48	ENE	24,8	24,5
30.06.2024.	0	15,48	SSW	26,3	24,3
05.07.2024.	0	15,48	WNW	22,8	24,0
06.07.2024.	0	24,12	SSE	24,3	24,2
08.07.2024.	0	24,12	NW	26,1	25,3
10.07.2024.	0	15,48	WSW	28	25,6
15.07.2024.	0	24,12	NNW	28,3	27,5
17.07.2024.	0	15,48	WNW	28,5	28,0
18.07.2024.	0	24,12	NNW	28,7	28,0
19.07.2024.	0	24,12	NW	29,6	28,0
21.07.2024.	0,3	15,48	SSW	25,5	27,8
22.07.2024.	0	24,12	W	26	27,6
27.07.2024.	0	2,88	WNW	26,1	27,9
29.07.2024.	0	24,12	WNW	26,6	28,2
30.07.2024.	0	24,12	WSW	25,5	28,0
31.07.2024.	0	24,12	NNW	26,3	27,5
02.08.2024.	28,2	15,48	WNW	24,6	28,0
06.08.2024.	0	15,48	WSW	25,5	26,8
07.08.2024.	0	15,48	WSW	26,6	28,1
09.08.2024.	0	15,48	WSW	26,1	28,8
10.08.2024.	0	15,48	SSW	27	28,7

11.08.2024.	0	15,48	NW	27,6	28,9
13.08.2024.	0	24,12	WNW	28	28,9
15.08.2024.	0	24,12	NW	27	28,9
16.08.2024.	0	15,48	NW	26,4	28,5
18.08.2024.	0	15,48	SSW	27,2	28,5
28.08.2024.	0	15,48	NW	26,3	27,3
04.09.2024.	0	15,48	WSW	24,8	26,0
10.09.2024.	13,6	24,12	NNW	20,4	26,1
21.09.2024.	0	15,48	WNW	17,8	22,7
23.09.2024.	0	15,48	SSW	19,8	22,5

During the period from May to September 2024, pronounced weather variations were recorded that could have influenced biochemical processes in the sea. May and August were characterized by heavier precipitation events, while July experienced lower rainfall but stronger winds. Air temperature increased, reaching its peak in July and August. These conditions provide important context for understanding changes in descriptors D5 and D7, as discussed below.

Demonstration of technology at the client's pilot site

Monitoring of chlorophyll-a concentration (Descriptor D5)

As part of the satellite monitoring, an analysis of chlorophyll-a concentration was conducted as a key indicator of eutrophication (Descriptor D5). Eutrophication is the process of increased biological productivity due to elevated nutrient concentrations, often associated with anthropogenic impacts and hydrographically confined areas.

Table 2 presents the daily mean values of chlorophyll-a concentration for the four virtual stations on days when the satellite images met quality criteria and were included in the analysis. This presentation enables a comparison of spatial and temporal dynamics within the monitored period (May – September 2024).

Table 2. Concentration of chlorophyll-a (mg/m^3) by virtual measurement stations for the analyzed dates in Lim Bay

Date	Location 1	Location 2	Location 3	Location 4
01.05.2024.	0,31	0,23	0,27	0,42
05.05.2024.	0,36	0,38	0,38	0,59
08.05.2024.	/*	0,33	0,32	/*
10.05.2024.	0,40	0,32	0,32	0,65

17.05.2024.	0,46	0,35	0,33	0,68
18.05.2024.	/	/	0,37	0,42
22.05.2024.	0,66	0,42	0,38	0,48
23.05.2024.	0,49	0,32	0,32	0,68
24.05.2024.	0,53	0,31	0,37	0,67
25.05.2024.	/*	0,32	0,33	0,61
26.05.2024.	0,34	0,32	0,28	0,82
28.05.2024.	0,28	0,21	/*	/*
03.06.2024.	0,31	0,26	0,35	0,63
12.06.2024.	/*	/*	0,37	0,99
15.06.2024.	0,51	0,49	0,37	0,69
23.06.2024.	0,32	0,29	0,23	0,71
30.06.2024.	0,24	0,19	0,24	0,44
05.07.2024.	0,30	0,29	0,44	0,81
06.07.2024.	/*	0,34	0,31	0,54
08.07.2024.	0,45	0,20	0,26	0,44
10.07.2024.	0,45	0,29	0,34	0,59
15.07.2024.	0,36	0,29	0,40	0,76
17.07.2024.	0,35	0,31	0,33	0,79
18.07.2024.	0,19	0,24	0,24	0,48
19.07.2024.	0,23	0,27	0,31	/*
21.07.2024.	0,36	0,24	0,23	0,49
22.07.2024.	/*	0,30	0,31	0,55
27.07.2024.	0,31	0,32	0,35	0,63
29.07.2024.	0,27	0,35	0,38	1,00
30.07.2024.	0,30	0,34	0,23	0,86
31.07.2024.	0,20	0,28	0,36	0,62
02.08.2024.	0,34	0,31	0,34	0,96
06.08.2024.	0,31	0,31	0,33	0,71
07.08.2024.	0,38	0,23	0,33	0,72
09.08.2024.	0,41	0,33	0,34	0,85

10.08.2024.	0,33	0,34	/*	/*
11.08.2024.	0,67	0,51	0,36	0,80
13.08.2024.	0,44	0,29	0,28	0,58
15.08.2024.	0,29	0,36	0,33	0,58
16.08.2024.	0,22	0,24	0,31	0,60
18.08.2024.	0,26	0,20	/*	/*
28.08.2024.	0,25	0,26	0,31	0,69
04.09.2024.	0,24	0,24	0,29	0,48
10.09.2024.	0,51	0,34	0,36	0,94
21.09.2024.	0,25	0,25	0,30	0,84
23.09.2024.	0,29	0,27	0,34	/*

*No data due to unfavorable atmospheric conditions over the observed area at the time of the satellite's pass

A visual representation of chlorophyll-a concentrations by virtual stations and dates is shown in Figure 8, facilitating easier comparison of dynamics between different locations over the observed period.

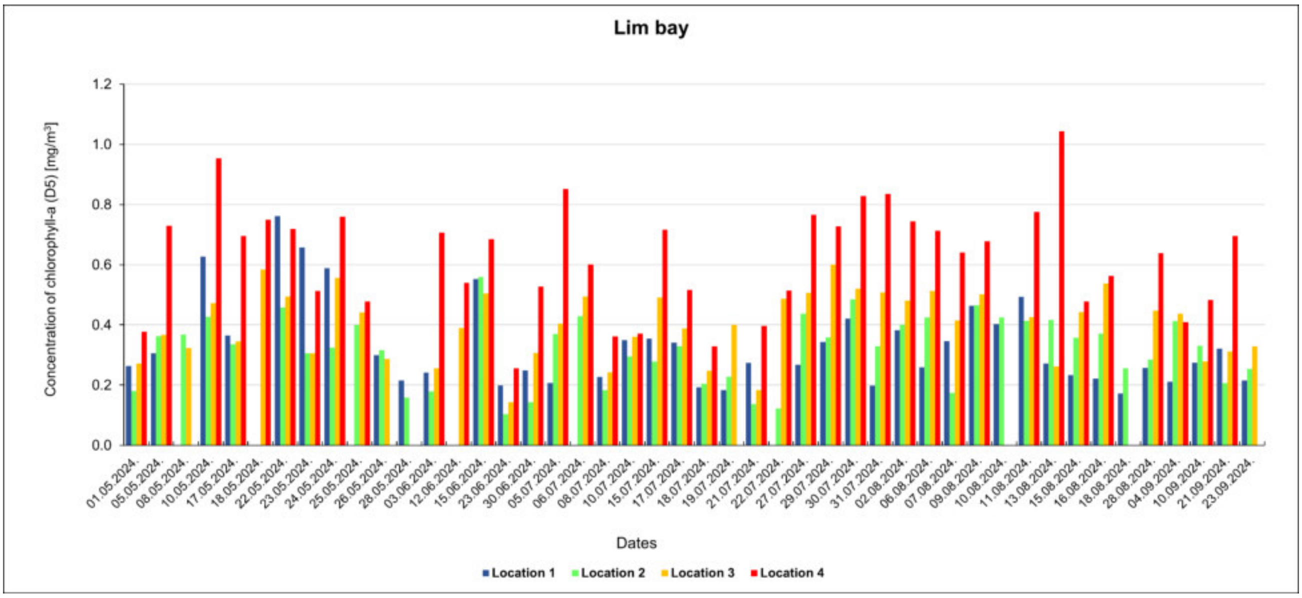

Figure 8. Graph of the spatial and temporal distribution of chlorophyll-a concentration by virtual measurement stations (May – September 2024)

Detailed analysis of chlorophyll-a concentration by virtual station

The following bar charts show chlorophyll-a concentrations for each individual virtual monitoring station, organized by month. This presentation provides a clearer insight into the dynamics of changes at each location and the local variations.

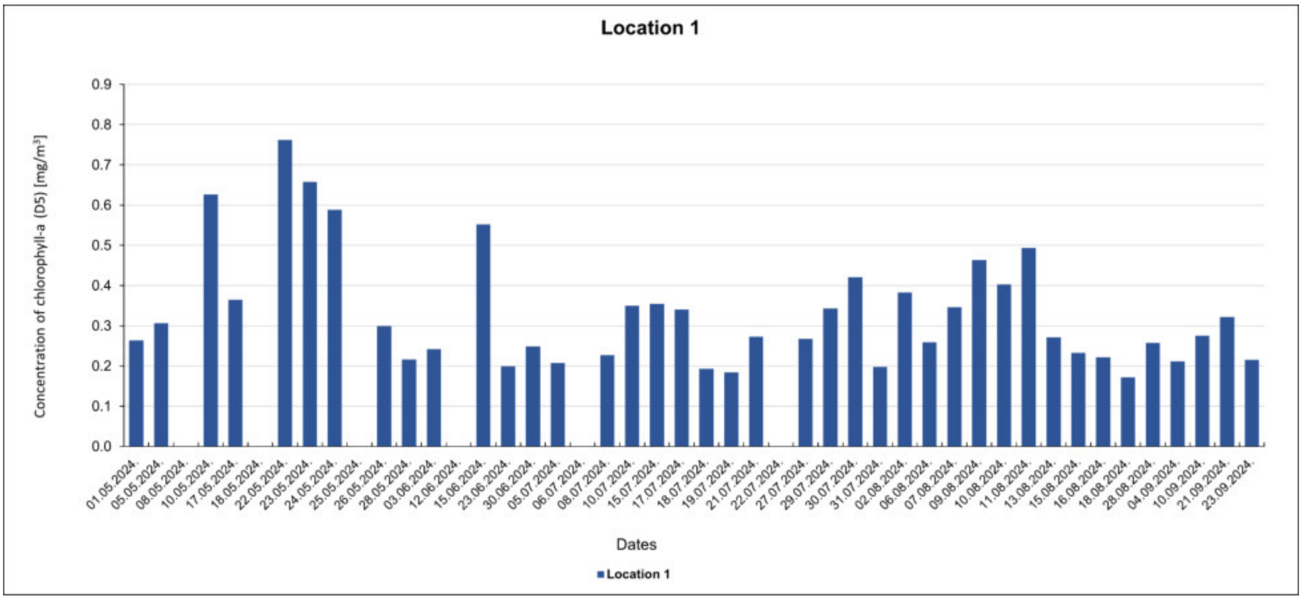

Figure 9. Graph of chlorophyll-a concentration variation at Location 1 (May–September 2024)

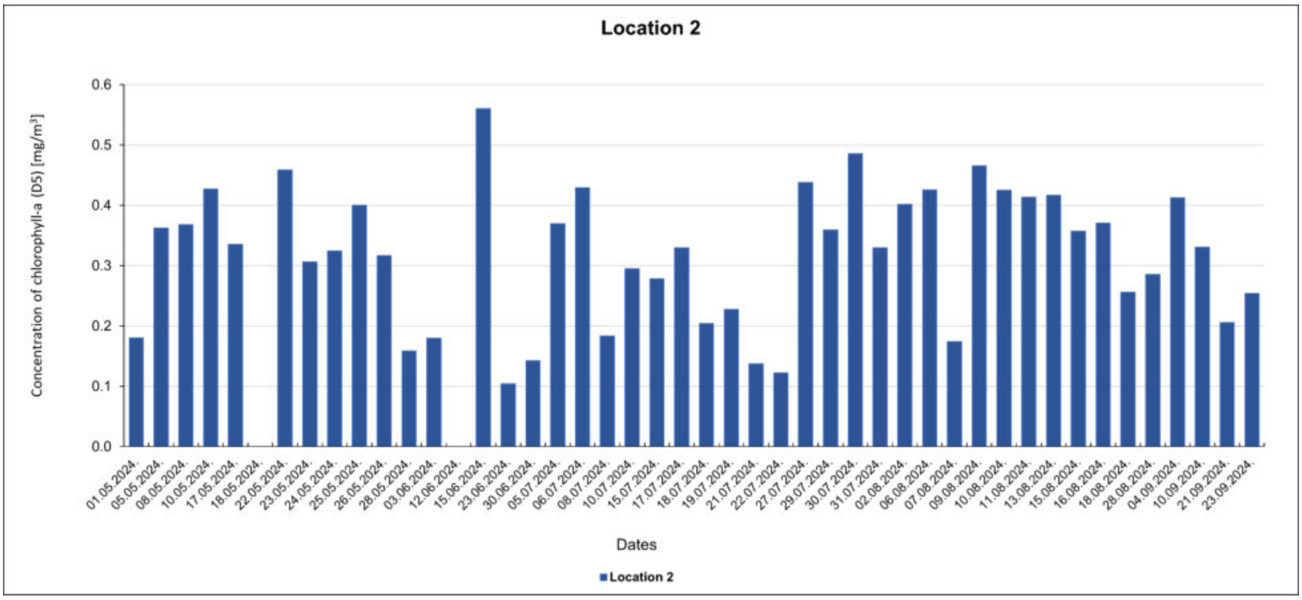

Figure 10. Graph of chlorophyll-a concentration variation at Location 2 (May–September 2024)

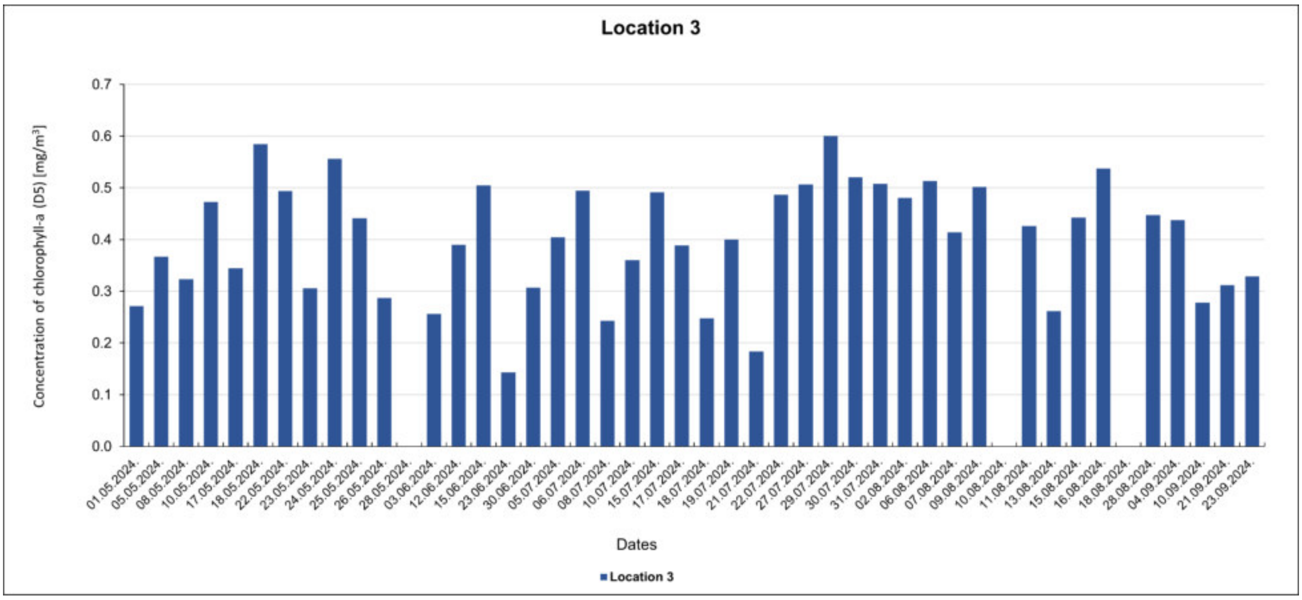

Figure 11. Graph of chlorophyll-a concentration variation at Location 3 (May–September 2024)

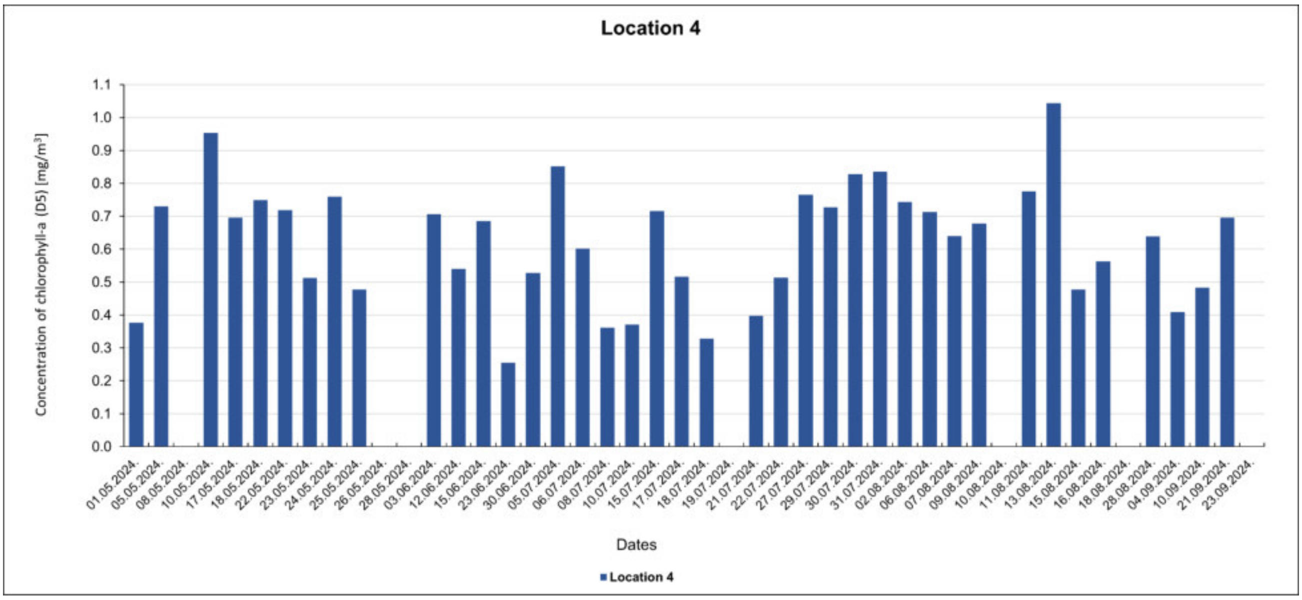

Figure 12. Graph of chlorophyll-a concentration variation at Location 4 (May–September 2024)

Visualization of the spatial distribution of chlorophyll-a for selected dates

As a visual representation of the seasonal distribution, thematic maps of chlorophyll-a concentration are presented for one representative date in May, June, August, and September. The dates were selected based on the quality of available satellite imagery and the characteristic values recorded during the analyzed period.

Date: 05.05.2024.

Figure 13. RGB satellite image of Lim Bay, 5 May 2024

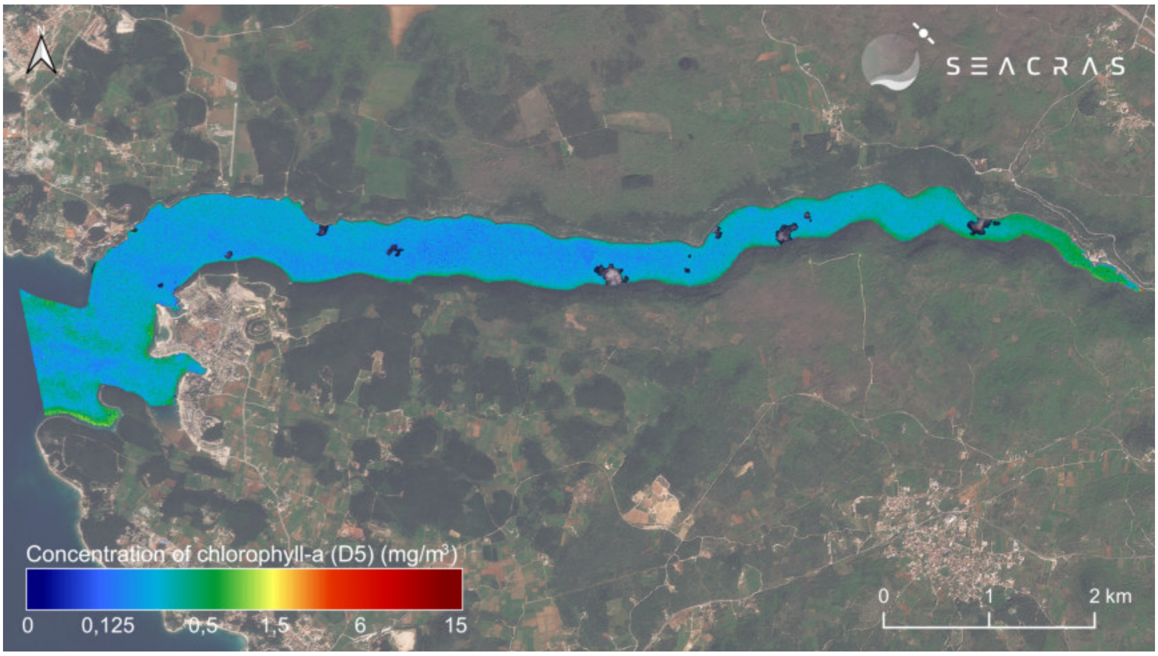

Figure 14. Thematic map derived from a processed satellite image showing chlorophyll-a concentration in Lim Bay, 5 May 2024

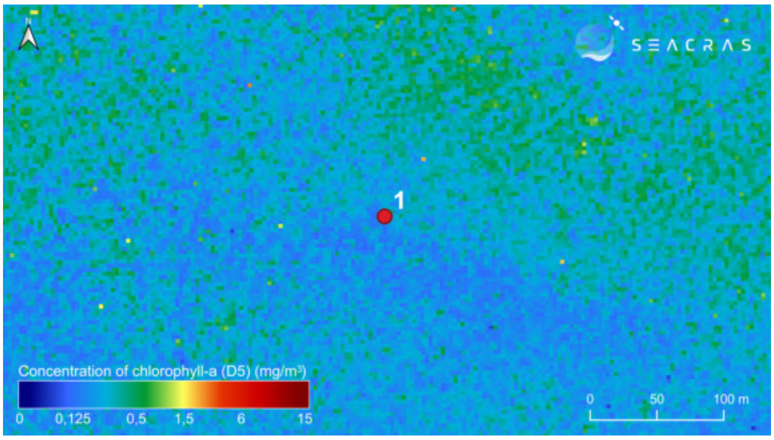

Figure 15. Thematic chlorophyll-a concentration map of Location 1, Lim Bay, from processed satellite imagery, 5 May 2024

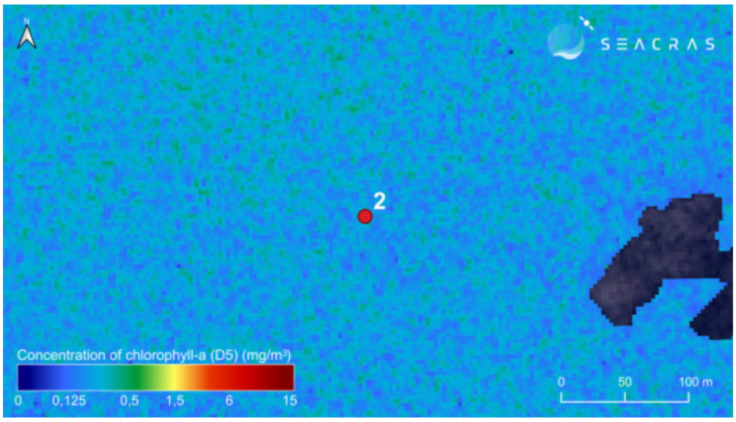

Figure 16. Thematic chlorophyll-a concentration map of Location 2, Lim Bay, from processed satellite imagery, 5 May 2024

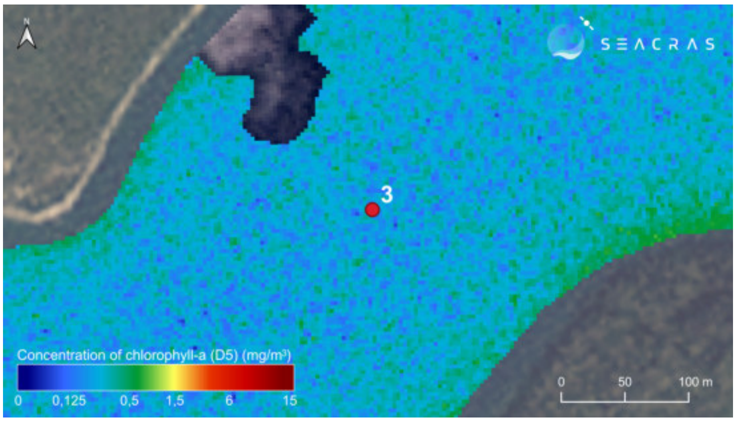

Figure 17. Thematic chlorophyll-a concentration map of Location 3, Lim Bay, from processed satellite imagery, 5 May 2024

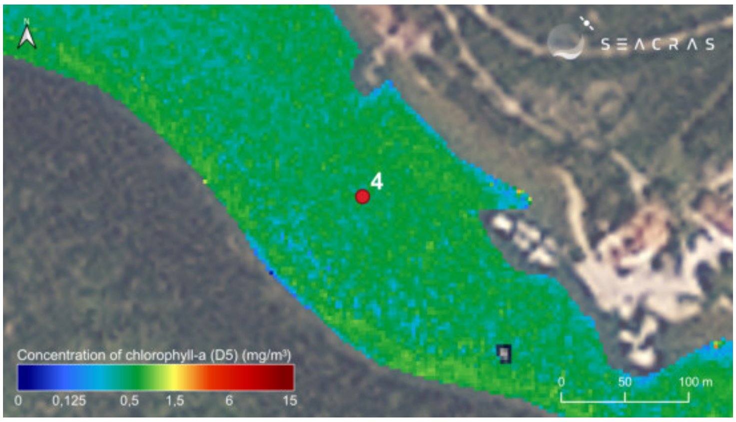

Figure 18. Thematic chlorophyll-a concentration map of Location 4, Lim Bay, from processed satellite imagery, 5 May 2024

Date: 30.06.2024.

Figure 19. RGB satellite image of Lim Bay, 30 June 2024

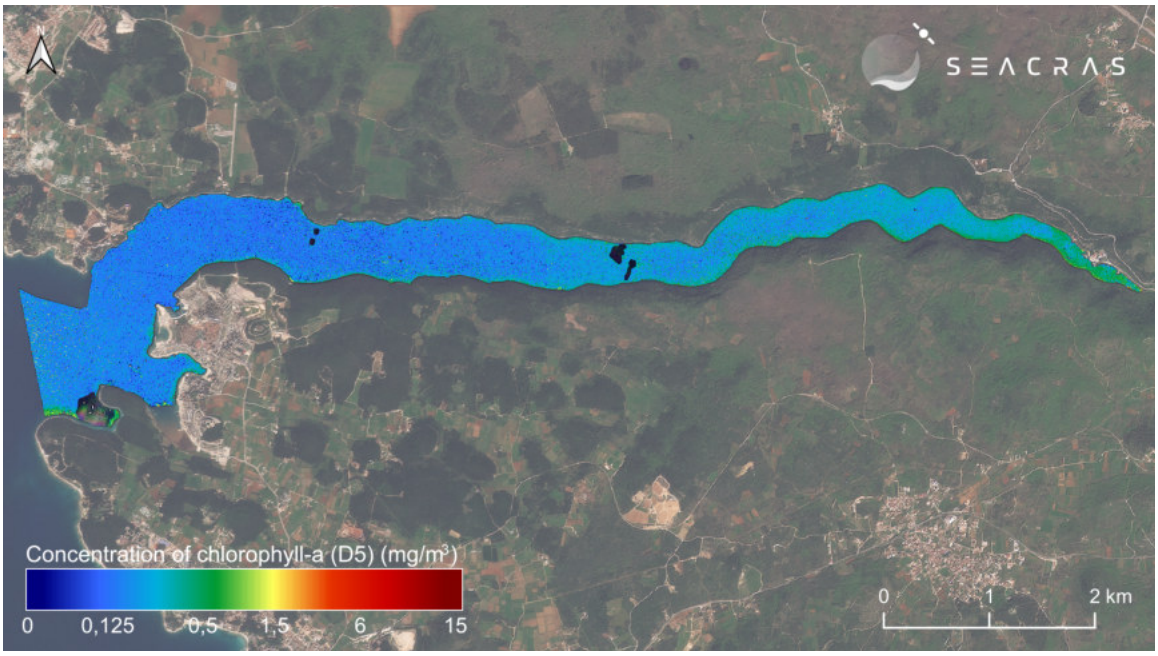

Figure 20. Thematic map derived from a processed satellite image showing chlorophyll-a concentration in Lim Bay, 30 June 2024

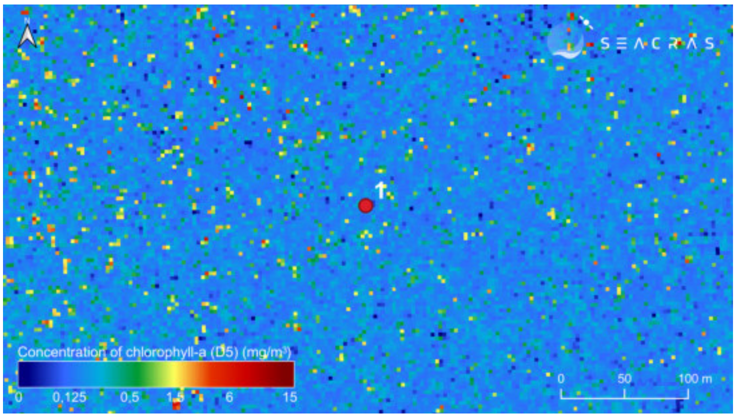

Figure 21. Thematic chlorophyll-a concentration map of Location 1, Lim Bay, from processed satellite imagery, 30 June 2024

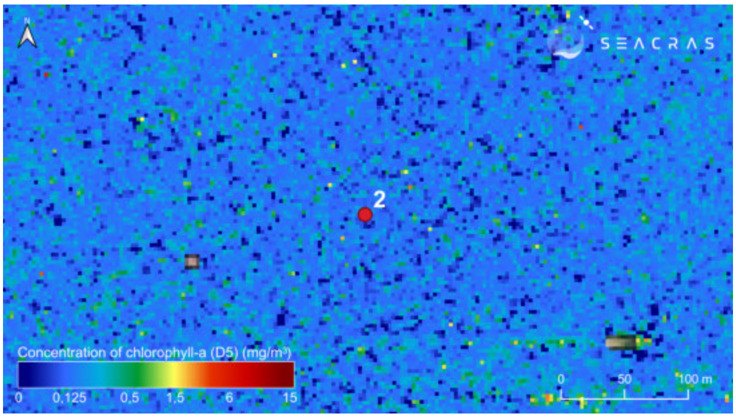

Figure 22. Thematic chlorophyll-a concentration map of Location 2, Lim Bay, from processed satellite imagery, 30 June 2024

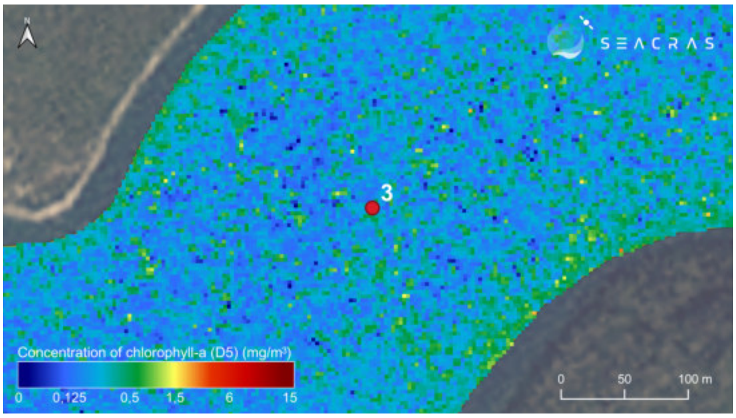

Figure 23. Thematic chlorophyll-a concentration map of Location 3, Lim Bay, from processed satellite imagery, 30 June 2024

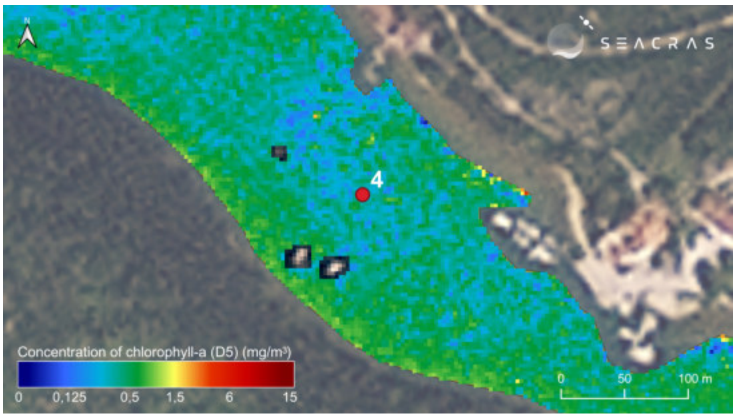

Figure 24. Thematic chlorophyll-a concentration map of Location 4, Lim Bay, from processed satellite imagery, 30 June 2024

Date: 27.07.2024.

Figure 25. RGB satellite image of Lim Bay, 27 July 2024

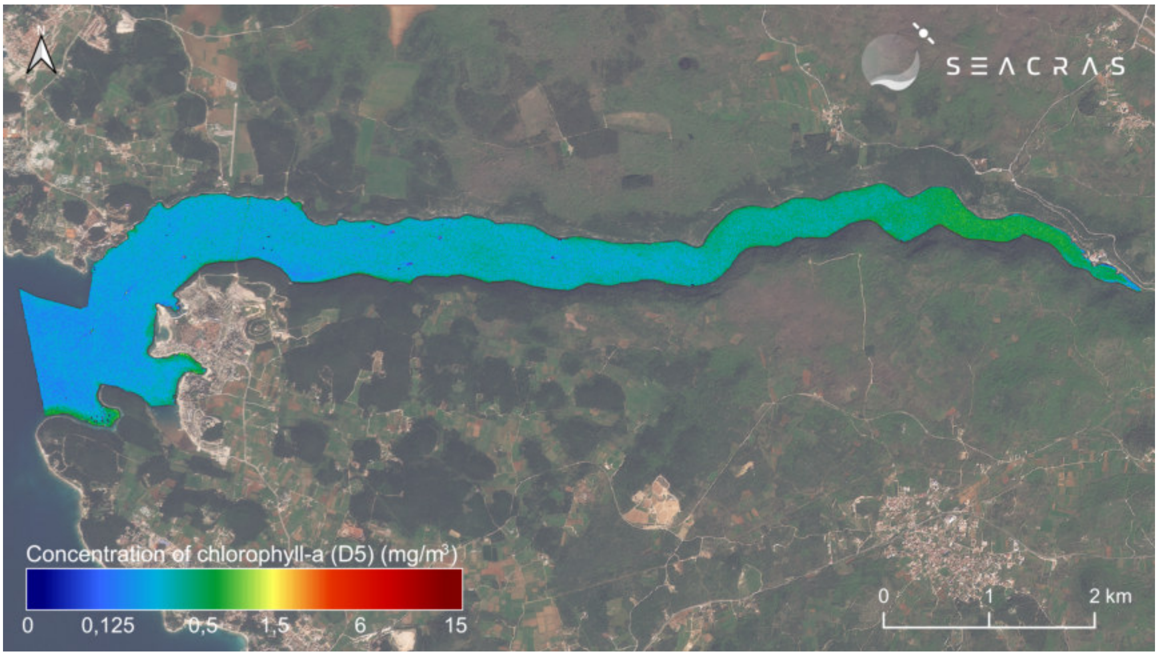

Figure 26. Thematic map derived from a processed satellite image showing chlorophyll-a concentration in Lim Bay, 27 July 2024

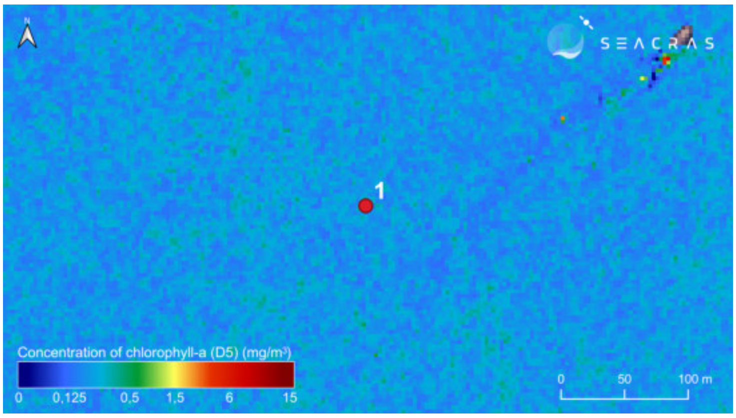

Figure 27. Thematic chlorophyll-a concentration map of Location 1, Lim Bay, from processed satellite imagery, 27 July 2024

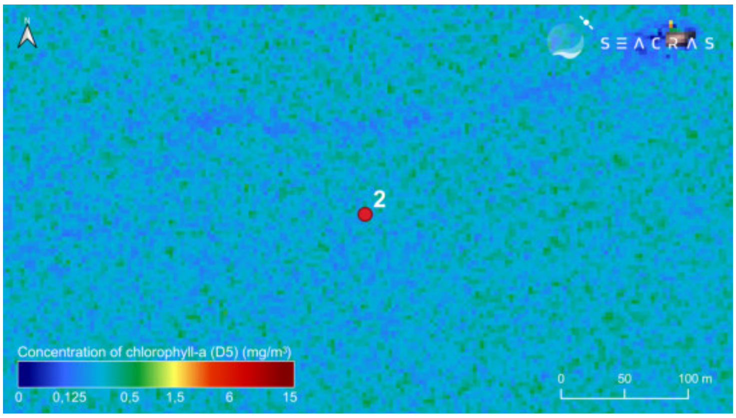

Figure 28. Thematic chlorophyll-a concentration map of Location 2, Lim Bay, from processed satellite imagery, 27 July 2024

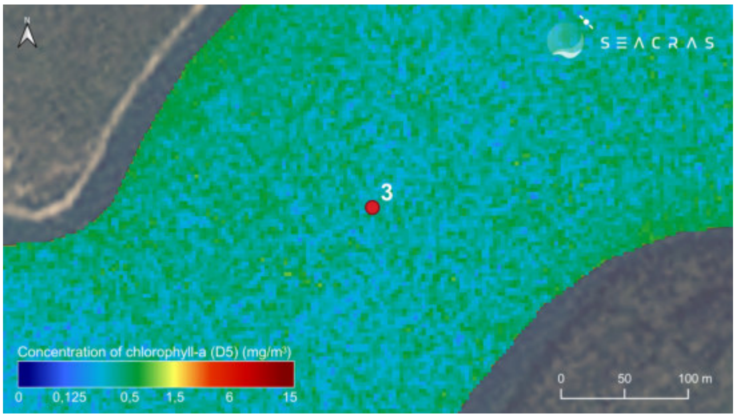

Figure 29. Thematic chlorophyll-a concentration map of Location 3, Lim Bay, from processed satellite imagery, 27 July 2024

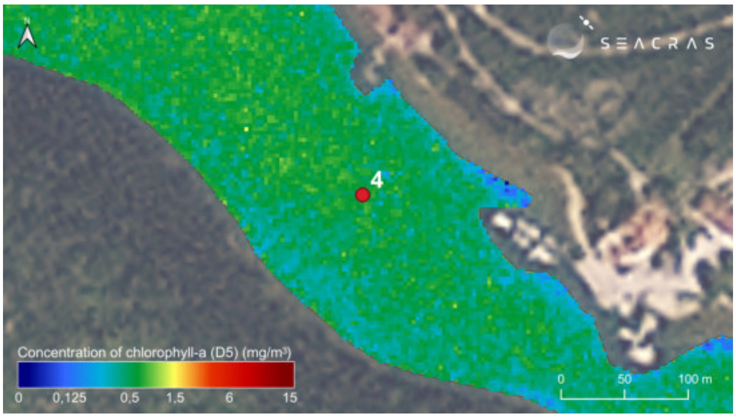

Figure 30. Thematic chlorophyll-a concentration map of Location 4, Lim Bay, from processed satellite imagery, 27 July 2024

Date: 14.08.2024.

Figure 31. RGB satellite image of Lim Bay, 14 August 2024

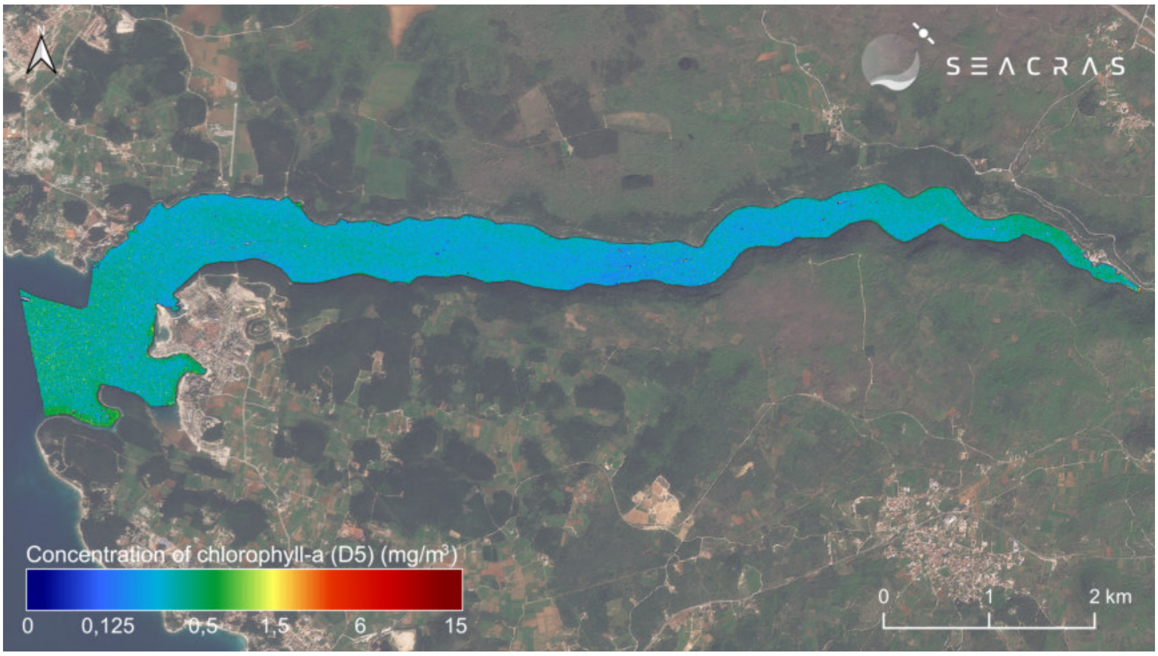

Figure 32. Thematic map derived from a processed satellite image showing chlorophyll-a concentration in Lim Bay, 14 August 2024

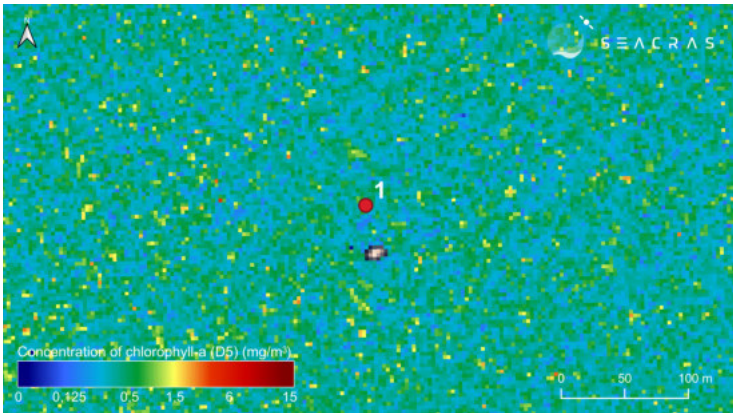

Figure 33. Thematic chlorophyll-a concentration map of Location 1, Lim Bay, from processed satellite imagery, 14 August 2024

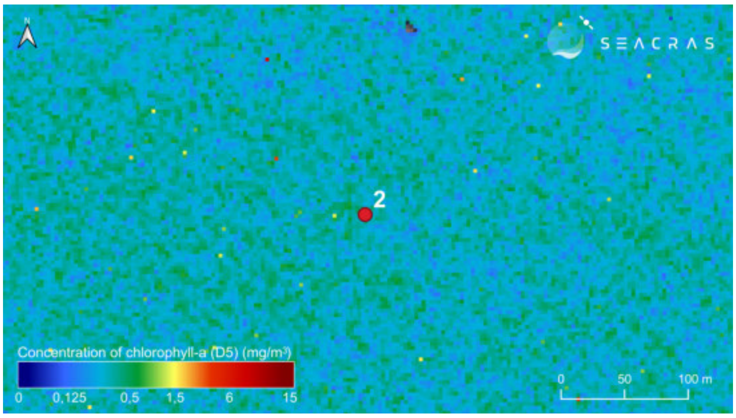

Figure 34. Thematic chlorophyll-a concentration map of Location 2, Lim Bay, from processed satellite imagery, 14 August 2024

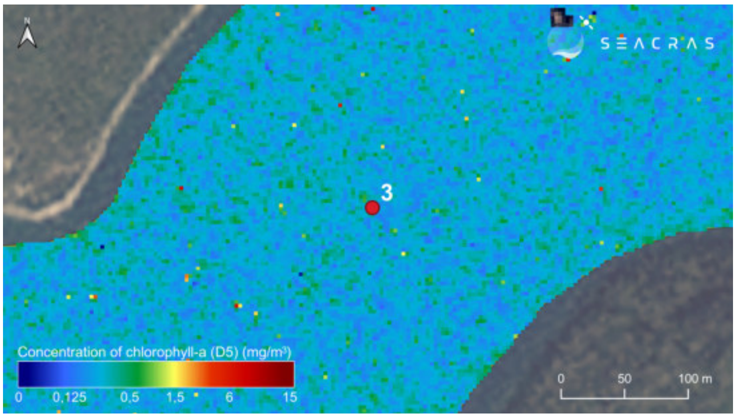

Figure 35. Thematic chlorophyll-a concentration map of Location 3, Lim Bay, from processed satellite imagery, 14 August 2024

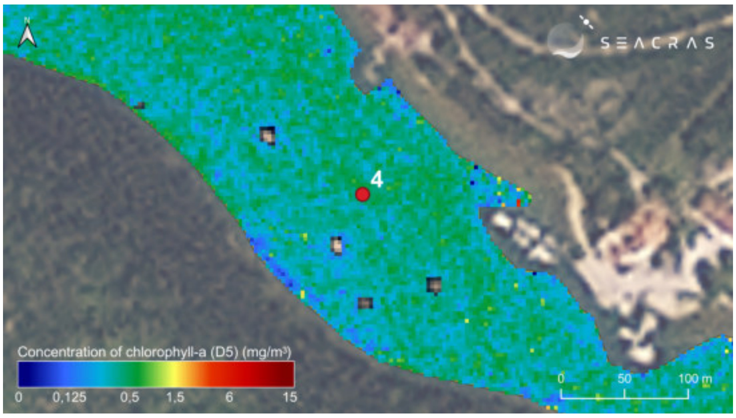

Figure 36. Thematic chlorophyll-a concentration map of Location 4, Lim Bay, from processed satellite imagery, 14 August 2024

Date: 21.9.2024.

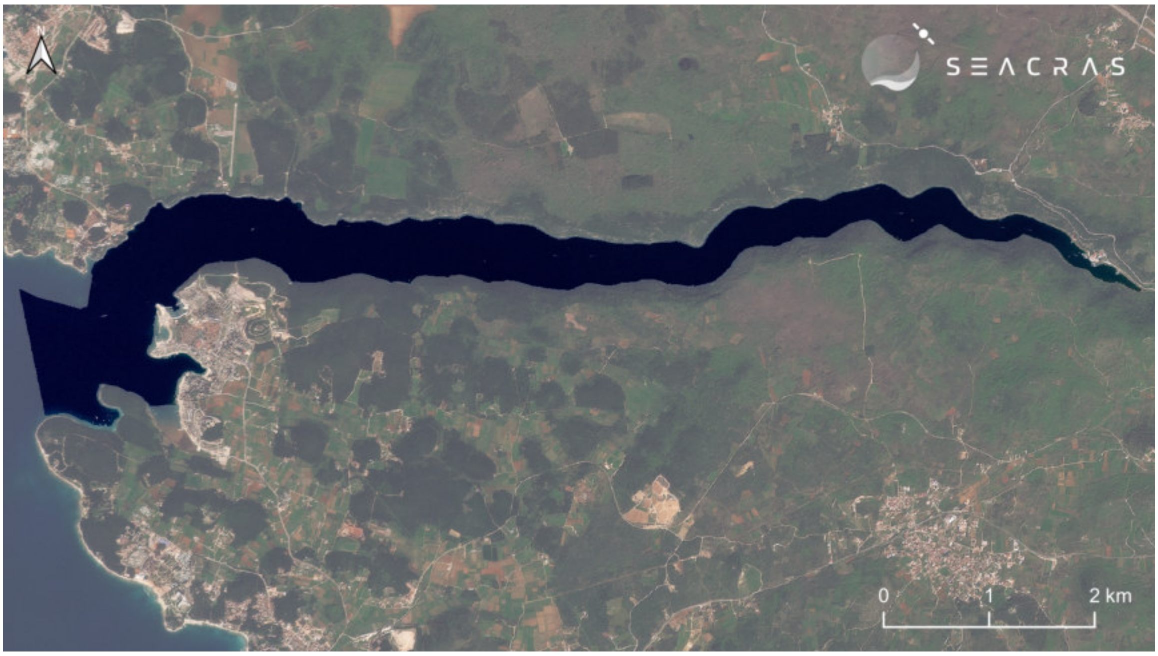

Figure 37. RGB satellite image of Lim Bay, 21 September 2024

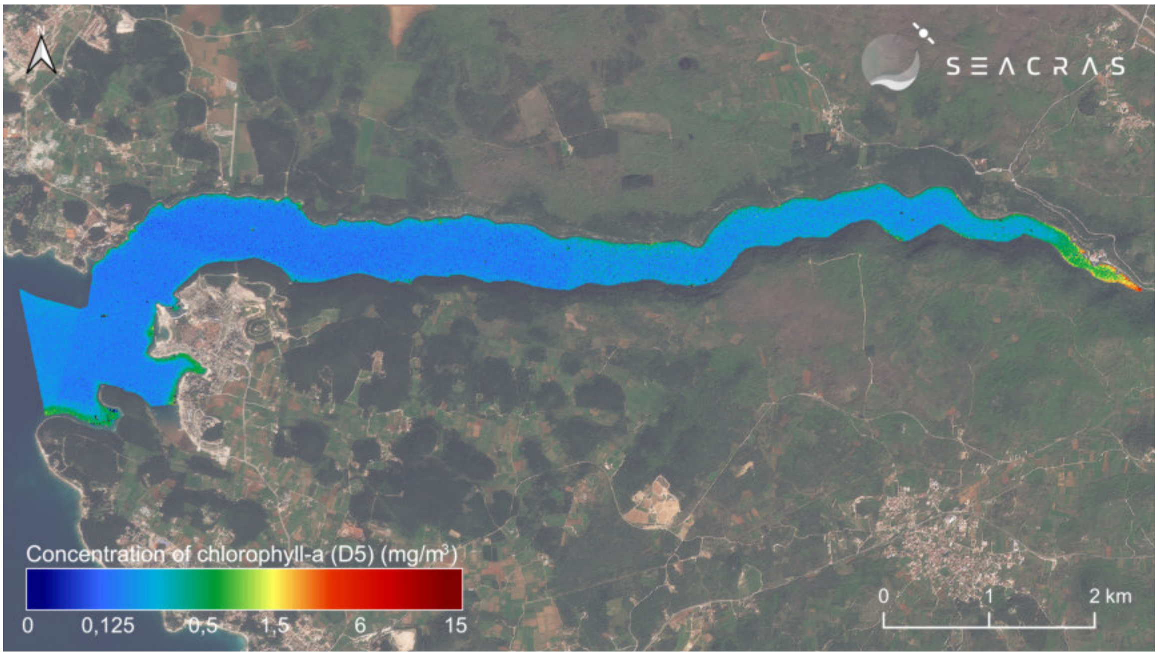

Figure 38. Thematic map derived from a processed satellite image showing chlorophyll-a concentration in Lim Bay, 21 September 2024

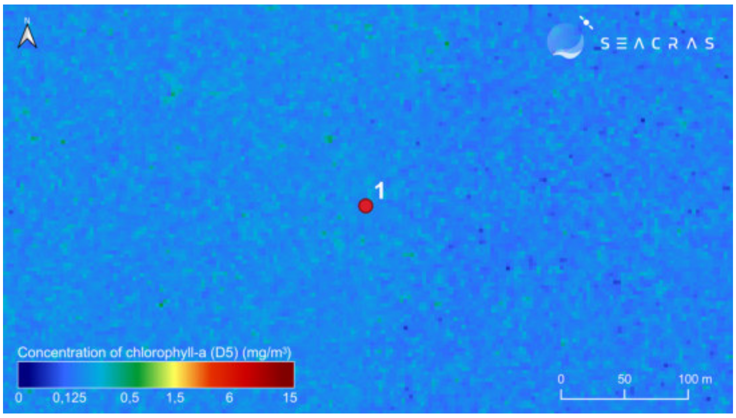

Figure 39. Thematic chlorophyll-a concentration map of Location 1, Lim Bay, from processed satellite imagery, 21 September 2024

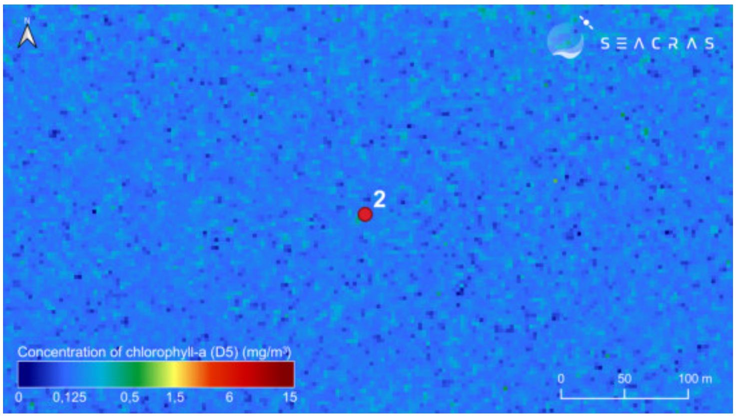

Figure 40. Thematic chlorophyll-a concentration map of Location 2, Lim Bay, from processed satellite imagery, 21 September 2024

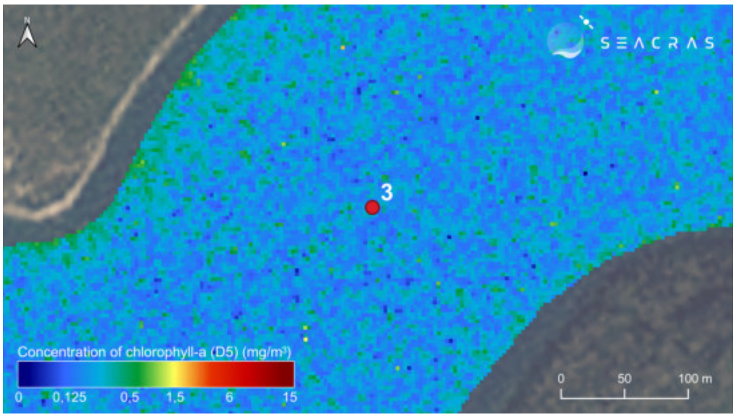

Figure 41. Thematic chlorophyll-a concentration map of Location 3, Lim Bay, from processed satellite imagery, 21 September 2024

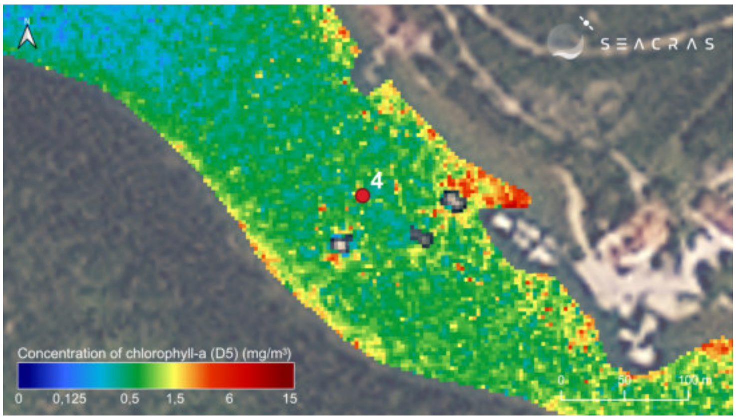

Figure 42. Thematic chlorophyll-a concentration map of Location 4, Lim Bay, from processed satellite imagery, 21 September 2024

Analysis of chlorophyll-a concentration during the period from May 1 to September 30, 2024, revealed pronounced seasonal and spatial variability within the Lim Bay. The highest values were recorded in the more enclosed parts of the waterbody (Locations 3 and 4), particularly during May and June, when meteorological conditions, primarily heavier rainfall—likely contributed to increased nutrient input.

Despite the expected gradient from open to enclosed areas, stations located closer to the open sea (Location 1) occasionally recorded elevated concentrations, even exceeding those in the inner stations. This phenomenon indicates the influence of local processes such as marine currents, short-term intrusions, or substance dispersion, further highlighting the complexity of eutrophication patterns in space.

The observed spatial dynamics underscore the need for frequent, spatially diverse monitoring, particularly in the enclosed parts of the bay where ecological changes are more pronounced, but also in the more open zones where episodic events may deviate from expected trends.

Monitoring of total suspended matter (Descriptor D7)

As part of the satellite monitoring program, an analysis of total suspended matter (TSM) concentrations was conducted as an indicator of changes in hydrographic conditions, corresponding to Descriptor D7. This parameter encompasses both organic and inorganic particles present in the water column, with elevated values potentially indicating the influence of anthropogenic activities, sediment resuspension, riverine inputs, or biological processes.

Table 3 presents the daily mean concentrations of total suspended matter for the four virtual monitoring stations on the days when satellite imagery met quality criteria and was included in the analysis. This overview provides insight into the spatial and seasonal dynamics of suspended matter from May to September 2024, accounting for varying degrees of enclosure within the study area.

Table 3. Concentration of total suspended matter (g/m^3) by virtual measurement stations for the analyzed dates in Lim Bay

Date	Location 1	Location 2	Location 3	Location 4
01.05.2024.	0,31	0,23	0,27	0,42
05.05.2024.	0,36	0,38	0,38	0,59
08.05.2024.	/*	0,33	0,32	/*
10.05.2024.	0,40	0,32	0,32	0,65
17.05.2024.	0,46	0,35	0,33	0,68
18.05.2024.	/	/	0,37	0,42
22.05.2024.	0,66	0,42	0,38	0,48
23.05.2024.	0,49	0,32	0,32	0,68
24.05.2024.	0,53	0,31	0,37	0,67

25.05.2024.	/*	0,32	0,33	0,61
26.05.2024.	0,34	0,32	0,28	0,82
28.05.2024.	0,28	0,21	/*	/*
03.06.2024.	0,31	0,26	0,35	0,63
12.06.2024.	/*	/*	0,37	0,99
15.06.2024.	0,51	0,49	0,37	0,69
23.06.2024.	0,32	0,29	0,23	0,71
30.06.2024.	0,24	0,19	0,24	0,44
05.07.2024.	0,30	0,29	0,44	0,81
06.07.2024.	/*	0,34	0,31	0,54
08.07.2024.	0,45	0,20	0,26	0,44
10.07.2024.	0,45	0,29	0,34	0,59
15.07.2024.	0,36	0,29	0,40	0,76
17.07.2024.	0,35	0,31	0,33	0,79
18.07.2024.	0,19	0,24	0,24	0,48
19.07.2024.	0,23	0,27	0,31	/*
21.07.2024.	0,36	0,24	0,23	0,49
22.07.2024.	/*	0,30	0,31	0,55
27.07.2024.	0,31	0,32	0,35	0,63
29.07.2024.	0,27	0,35	0,38	1,00
30.07.2024.	0,30	0,34	0,23	0,86
31.07.2024.	0,20	0,28	0,36	0,62
02.08.2024.	0,34	0,31	0,34	0,96
06.08.2024.	0,31	0,31	0,33	0,71
07.08.2024.	0,38	0,23	0,33	0,72
09.08.2024.	0,41	0,33	0,34	0,85
10.08.2024.	0,33	0,34	/*	/*
11.08.2024.	0,67	0,51	0,36	0,80
13.08.2024.	0,44	0,29	0,28	0,58
15.08.2024.	0,29	0,36	0,33	0,58
16.08.2024.	0,22	0,24	0,31	0,60

18.08.2024.	0,26	0,20	/*	/*
28.08.2024.	0,25	0,26	0,31	0,69
04.09.2024.	0,24	0,24	0,29	0,48
10.09.2024.	0,51	0,34	0,36	0,94
21.09.2024.	0,25	0,25	0,30	0,84
23.09.2024.	0,29	0,27	0,34	/*

*No data due to unfavorable atmospheric conditions over the observed area at the time of the satellite's pass.

The bar chart illustrating total suspended matter concentrations at the virtual monitoring stations (Figure 43) provides an overview of the spatial and temporal dynamics of this parameter during the period from May to September 2024. This representation facilitates comparison between different locations and helps identify periods of elevated concentrations.

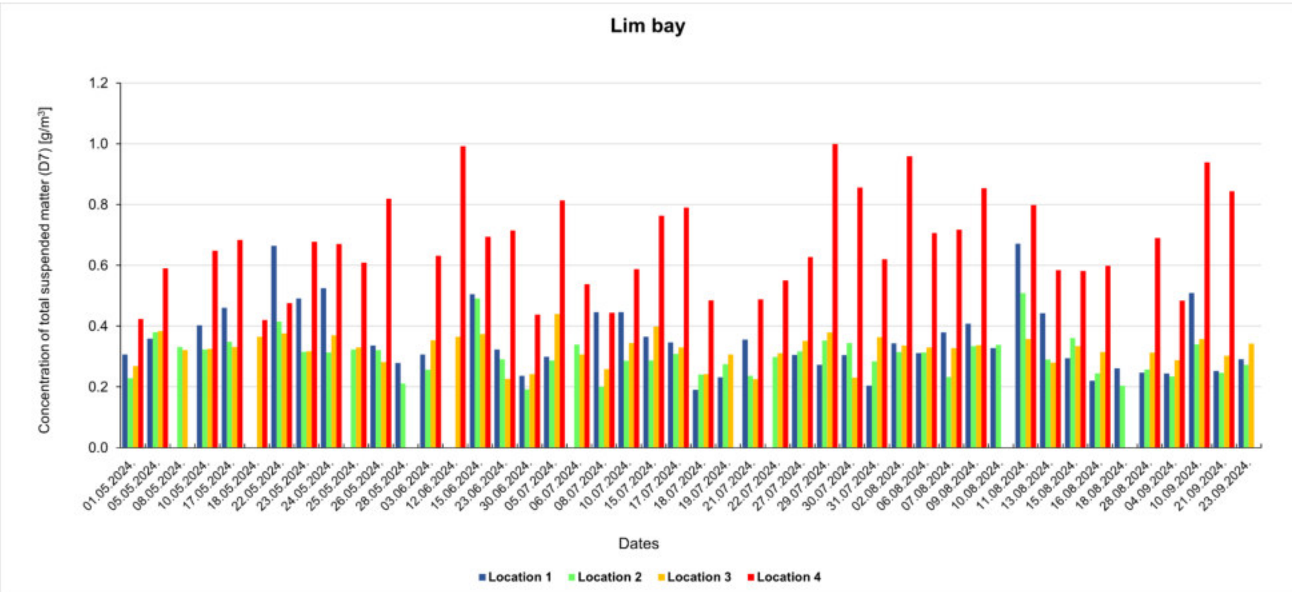

Figure 43. Graph of the spatial and temporal distribution of total suspended matter variation by virtual measurement stations (May – September 2024)

Detailed analysis of total suspended matter concentration by virtual station

The following bar charts present the total suspended matter (TSM) concentration for each individual virtual monitoring station, organized by month. This visualization provides a clearer insight into the temporal dynamics at each location, as well as spatial variations within the monitored waterbody.

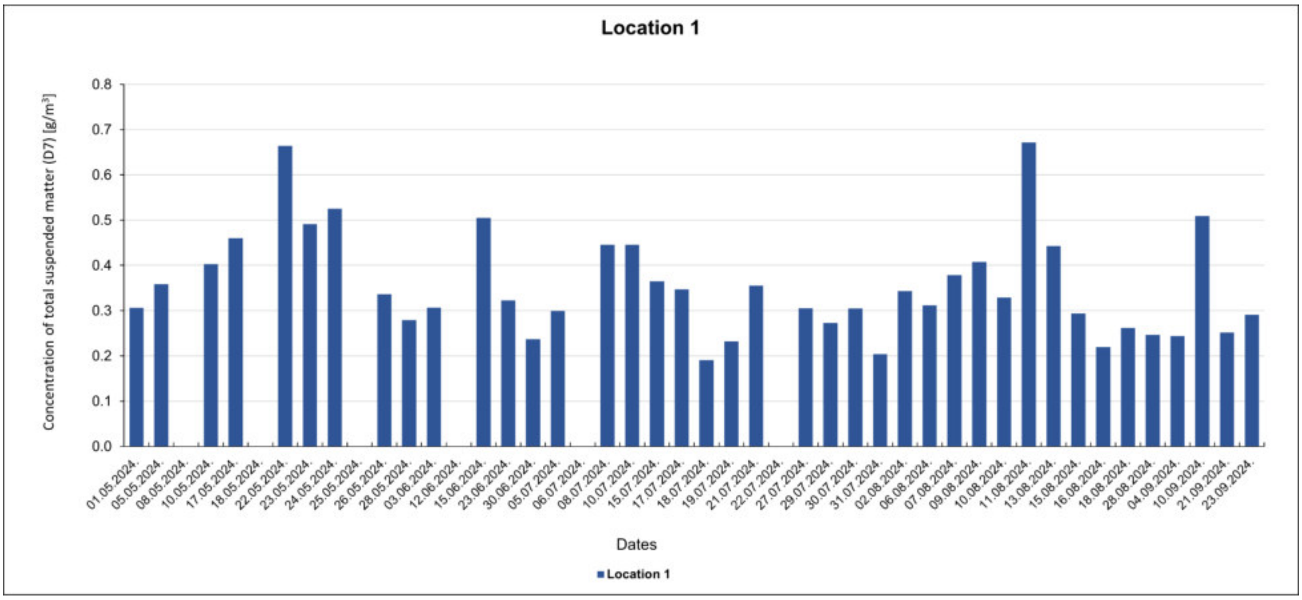

Figure 44. Graph of variation in total suspended matter concentration at Location 1 (May–September 2024)

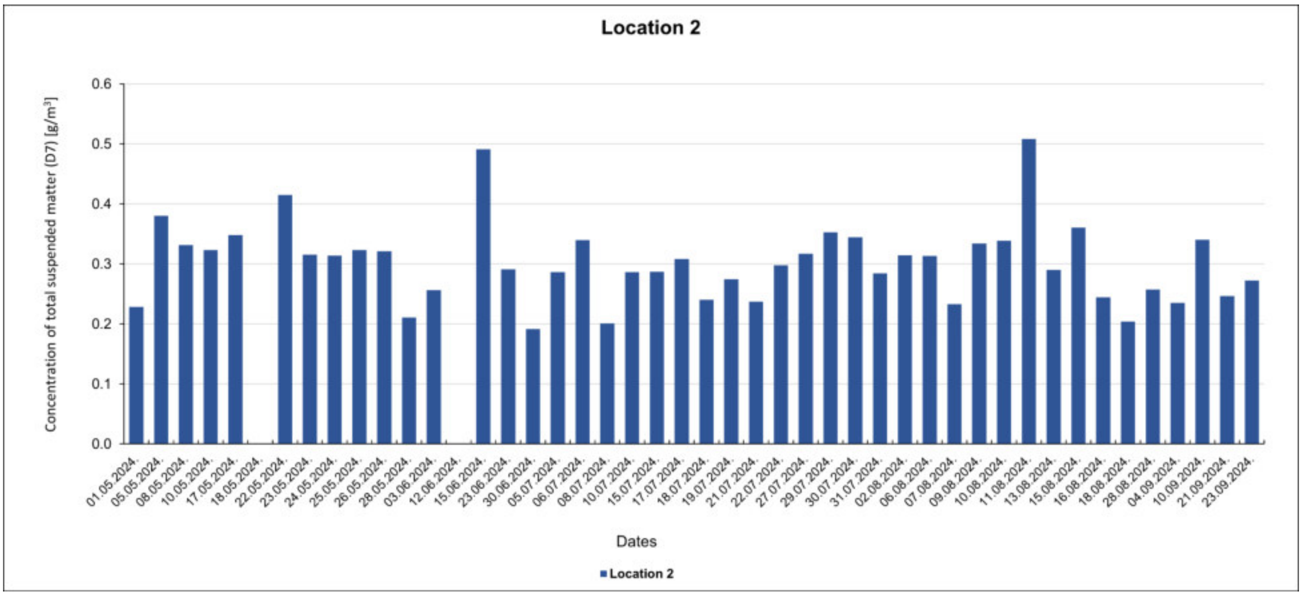

Figure 45. Graph of variation in total suspended matter concentration at Location 2 (May–September 2024)

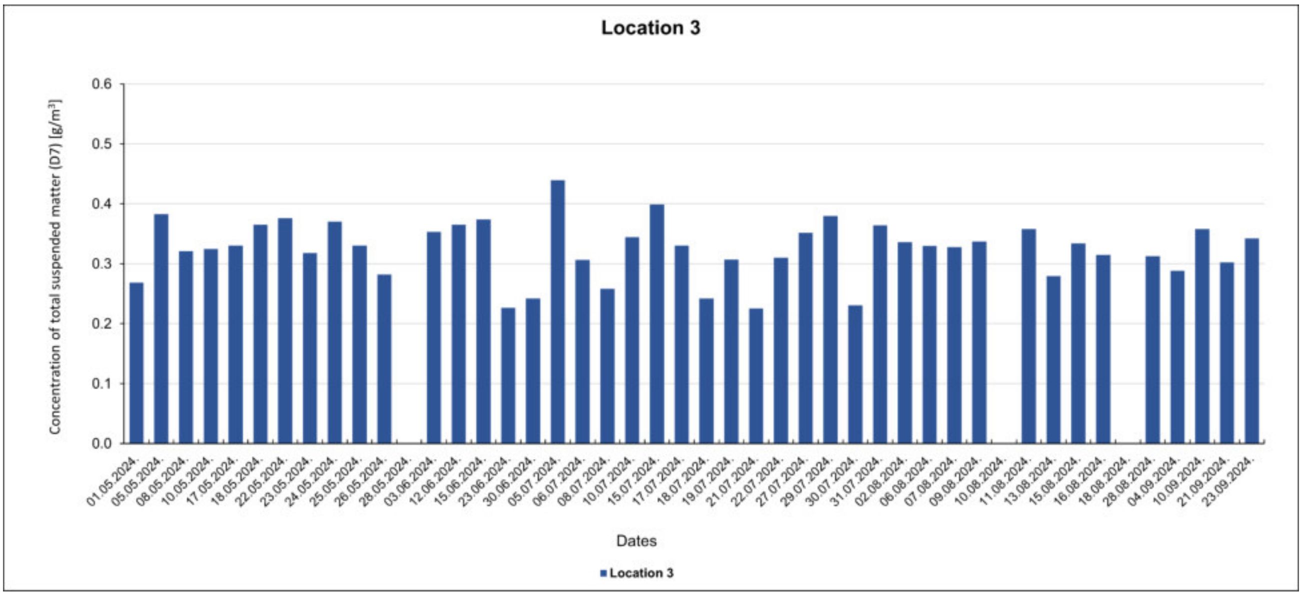

Figure 46. Graph of variation in total suspended matter concentration at Location 3 (May–September 2024)

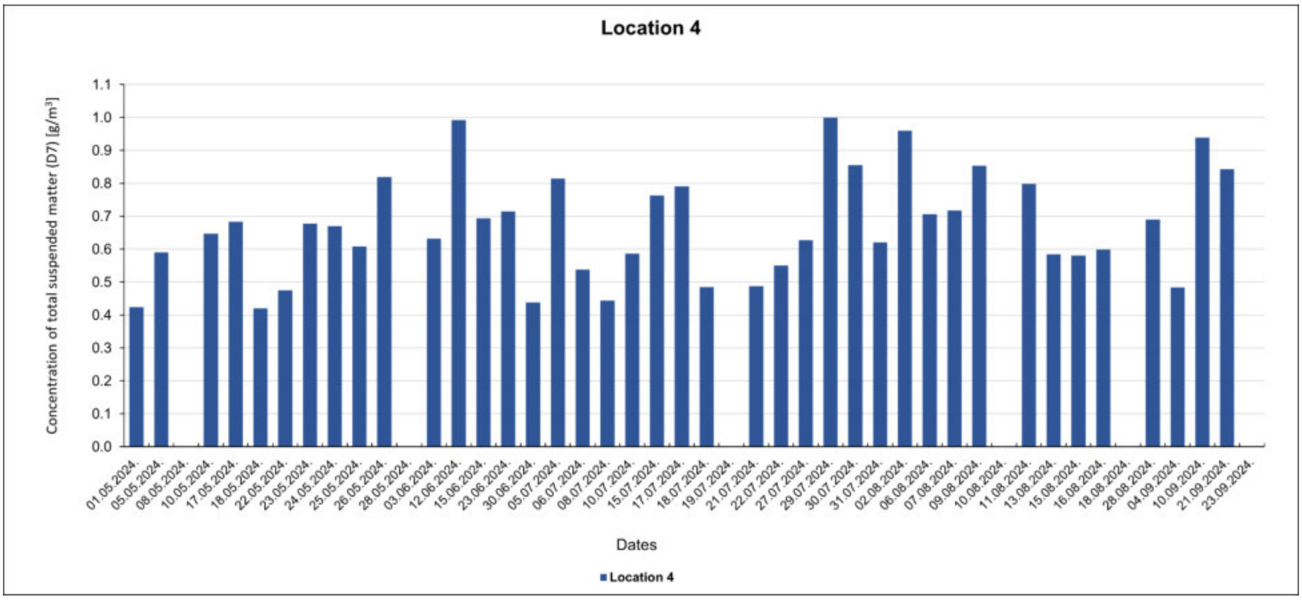

Figure 47. Graph of variation in total suspended matter concentration at Location 4 (May–September 2024)

Visualization of the spatial distribution of total suspended matter for selected dates

As a visual representation of seasonal distribution, thematic maps of total suspended matter concentration are presented for one representative date in May, June, August, and September. The selected dates were based on the quality of available satellite imagery and characteristic values observed during the analyzed period.

Date: 05.05.2024.

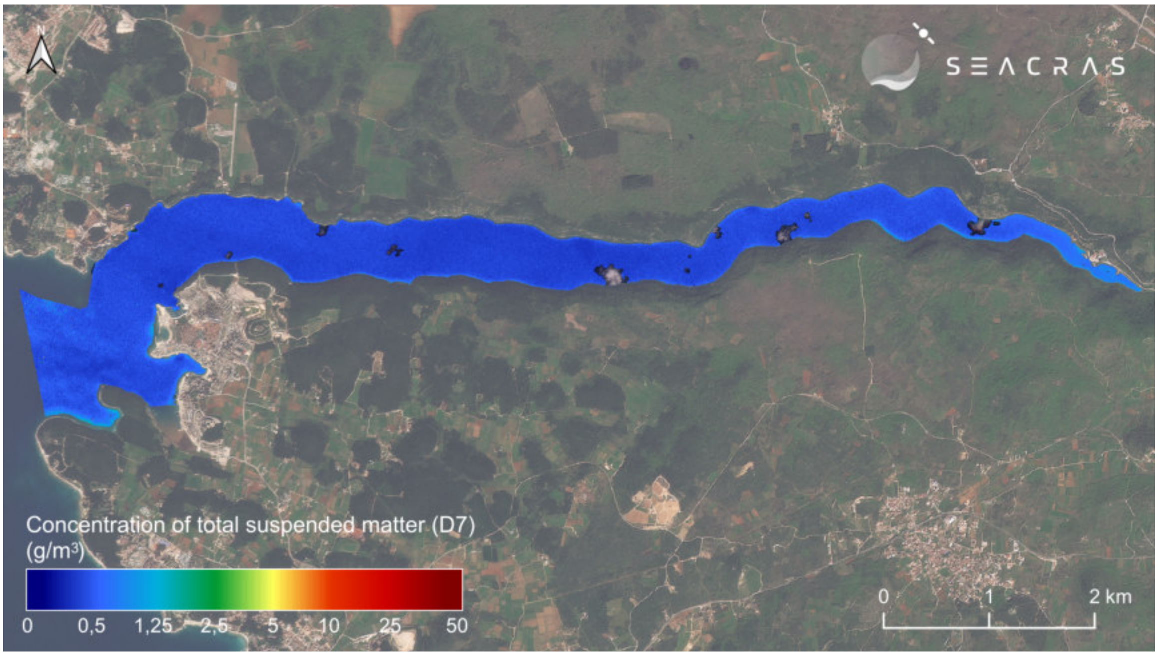

Figure 48. Thematic map derived from a processed satellite image showing concentration of total suspended matter in Lim Bay, 5 May 2024

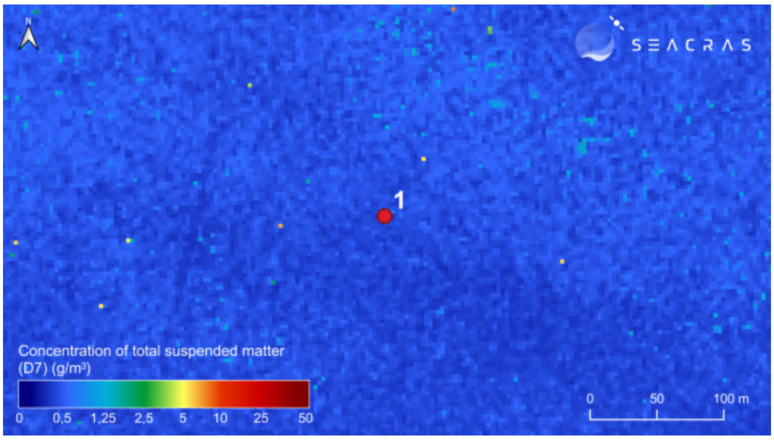

Figure 49. Thematic total suspended matter concentration map of Location 1, Lim Bay, from processed satellite imagery, 5 May 2024

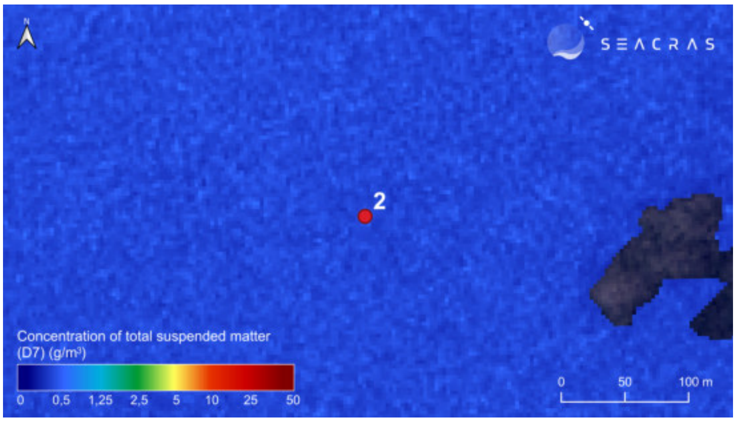

Figure 50. Thematic total suspended matter concentration map of Location 2, Lim Bay, from processed satellite imagery, 5 May 2024

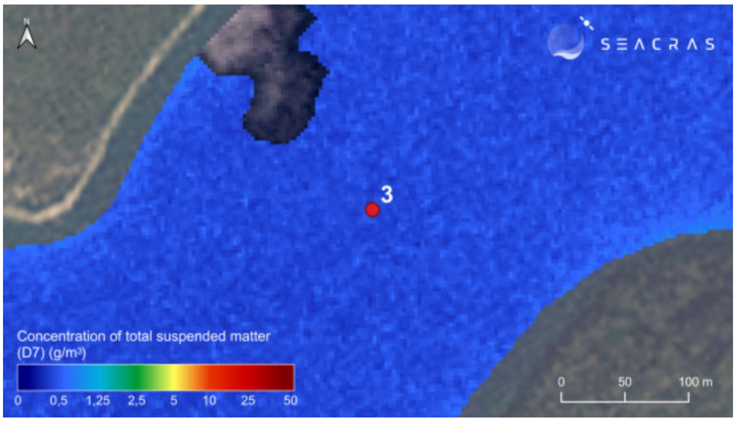

Figure 51. Thematic total suspended matter concentration map of Location 3, Lim Bay, from processed satellite imagery, 5 May 2024

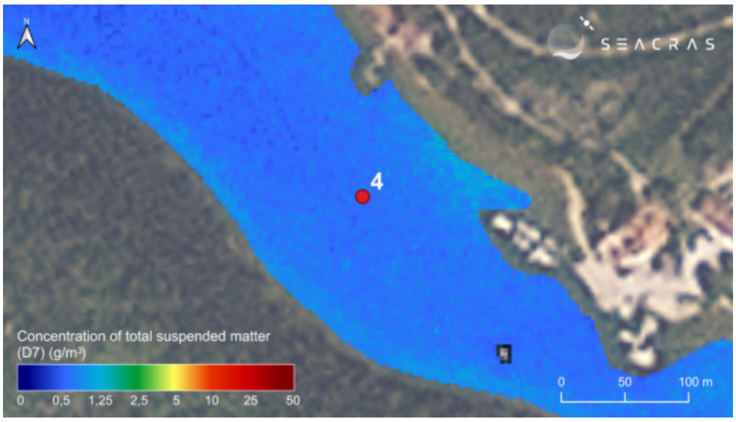

Figure 52. Thematic total suspended matter concentration map of Location 4, Lim Bay, from processed satellite imagery, 5 May 2024

Date: 30.06.2024.

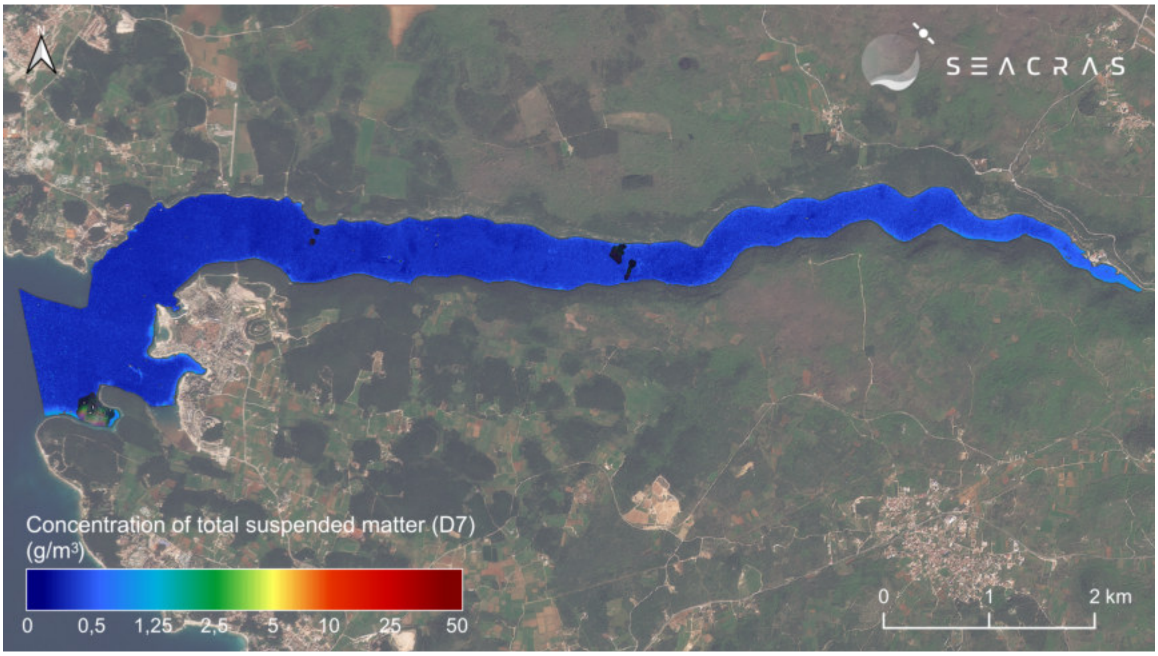

Figure 53. Thematic map derived from a processed satellite image showing concentration of total suspended matter in Lim Bay, 30 June 2024

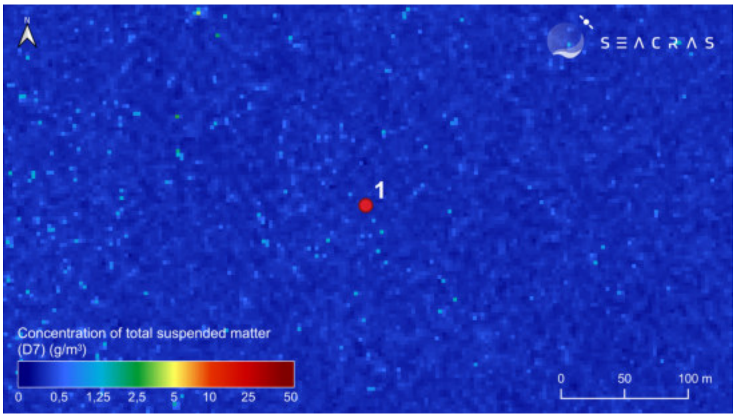

Figure 54. Thematic total suspended matter concentration map of Location 1, Lim Bay, from processed satellite imagery, 30 June 2024

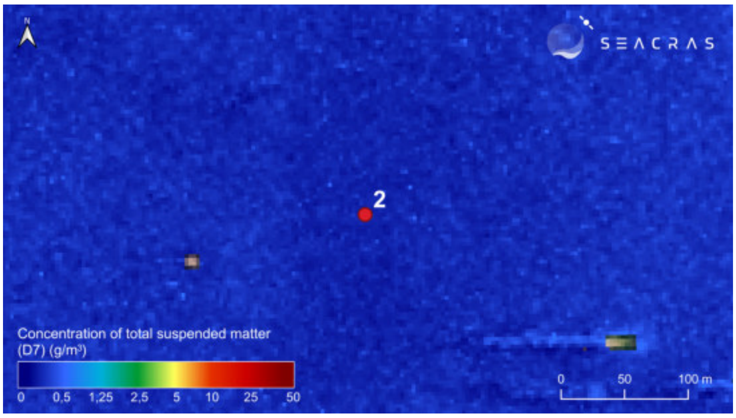

Figure 55. Thematic total suspended matter concentration map of Location 2, Lim Bay, from processed satellite imagery, 30 June 2024

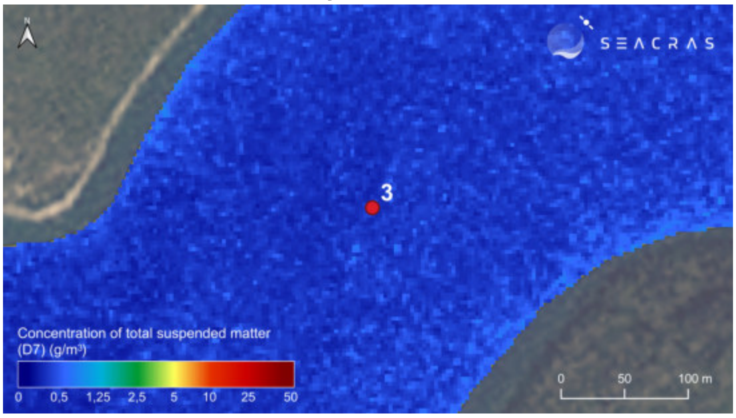

Figure 56. Thematic total suspended matter concentration map of Location 3, Lim Bay, from processed satellite imagery, 30 June 2024

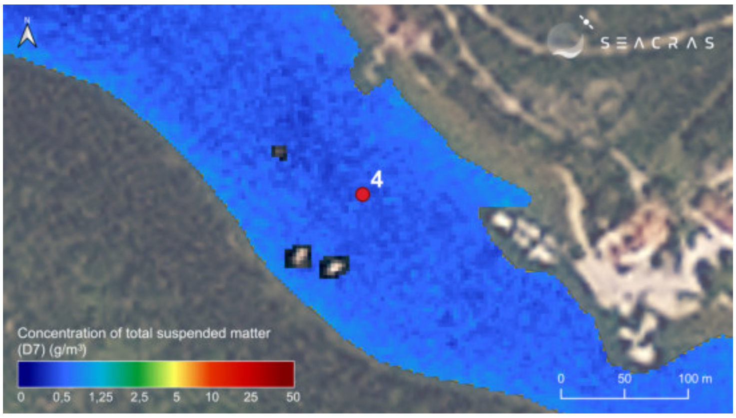

Figure 57. Thematic total suspended matter concentration map of Location 4, Lim Bay, from processed satellite imagery, 30 June 2024

Date: 27.07.2024.

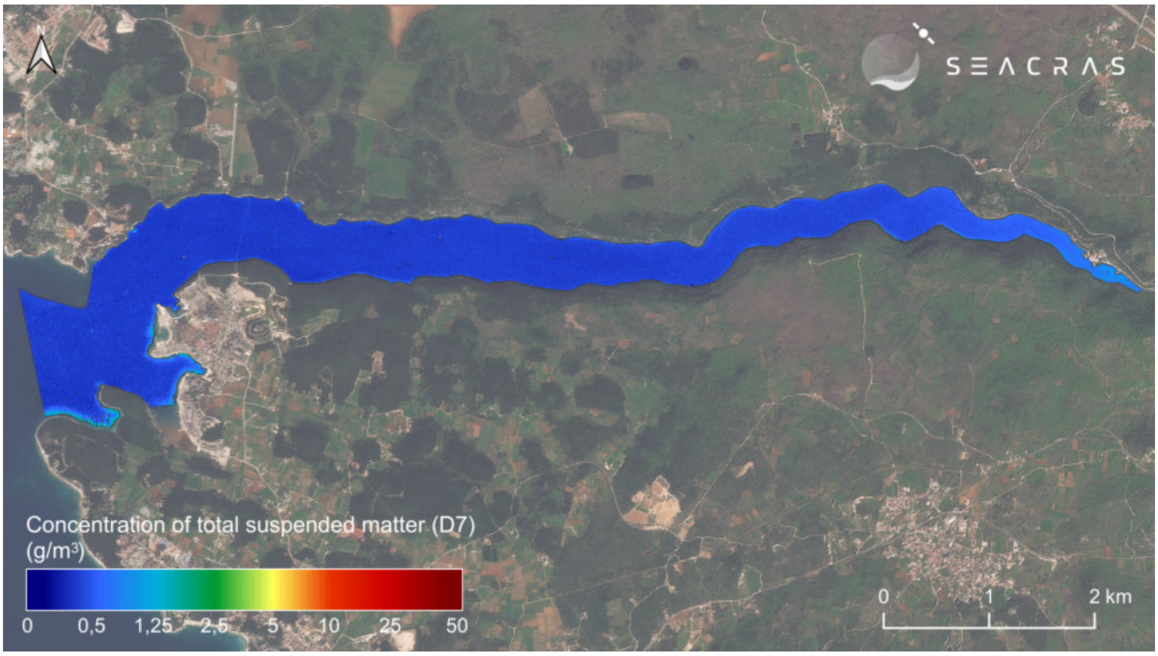

Figure 58. Thematic map derived from a processed satellite image showing concentration of total suspended matter in Lim Bay, 27 July 2024

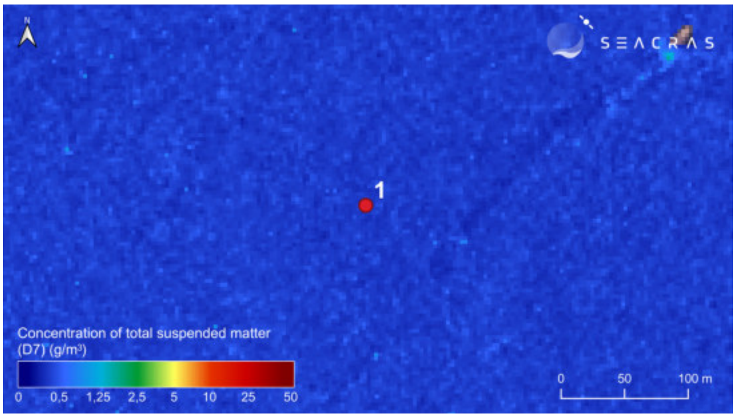

Figure 59. Thematic total suspended matter concentration map of Location 1, Lim Bay, from processed satellite imagery, 27 July 2024

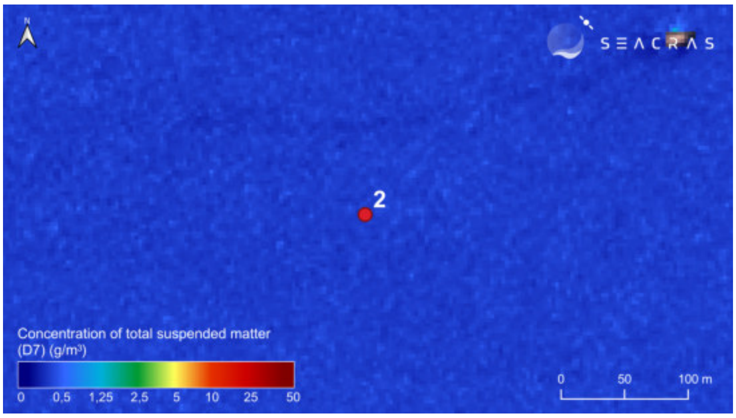

Figure 60. Thematic total suspended matter concentration map of Location 2, Lim Bay, from processed satellite imagery, 27 July 2024

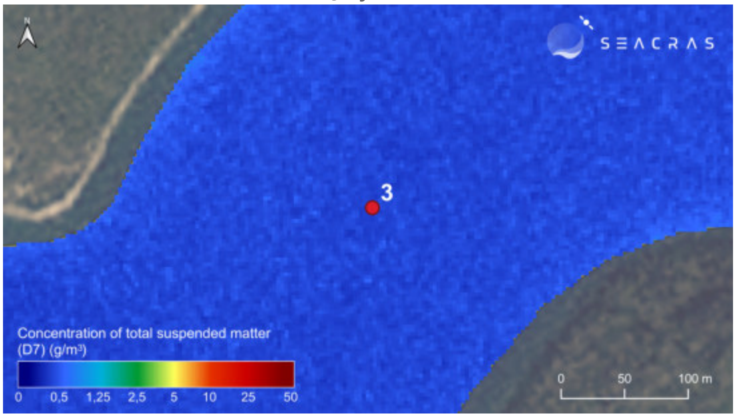

Figure 61. Thematic total suspended matter concentration map of Location 3, Lim Bay, from processed satellite imagery, 27 July 2024

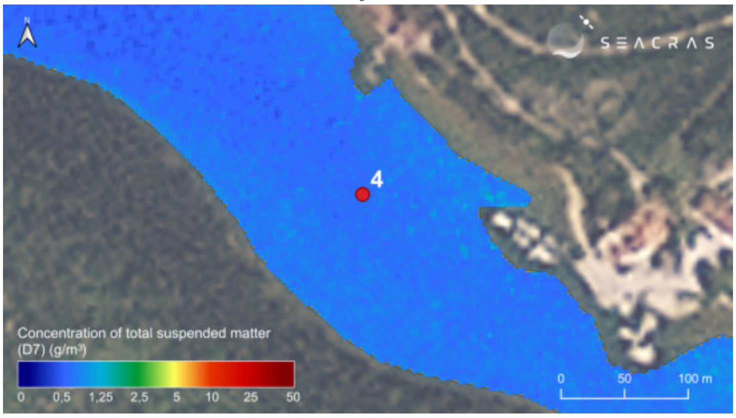

Figure 62. Thematic total suspended matter concentration map of Location 4, Lim Bay, from processed satellite imagery, 27 July 2024

Date: 14.08.2024.

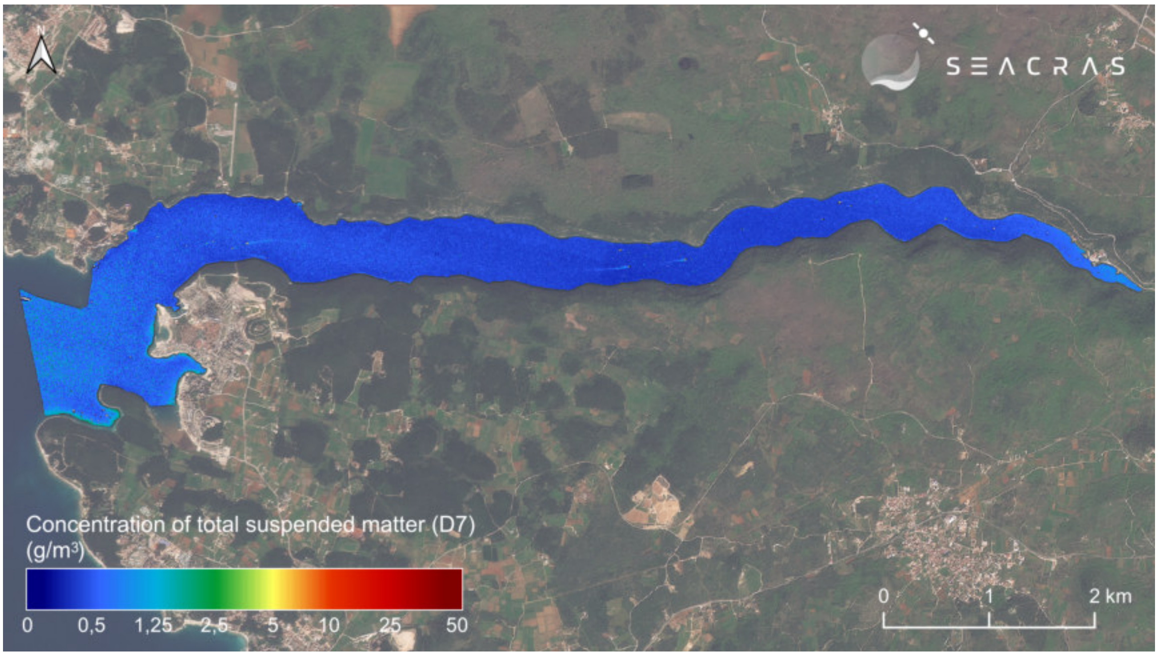

Figure 63. Thematic map derived from a processed satellite image showing concentration of total suspended matter in Lim Bay, 14 August 2024

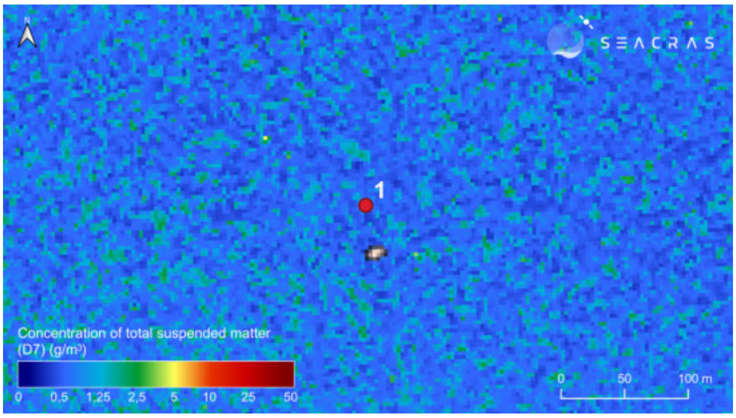

Figure 64. Thematic total suspended matter concentration map of Location 1, Lim Bay, from processed satellite imagery, 14 August 2024

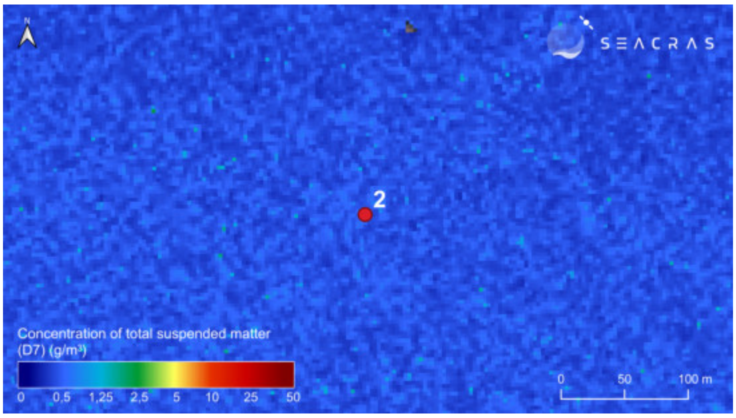

Figure 65. Thematic total suspended matter concentration map of Location 2, Lim Bay, from processed satellite imagery, 14 August 2024

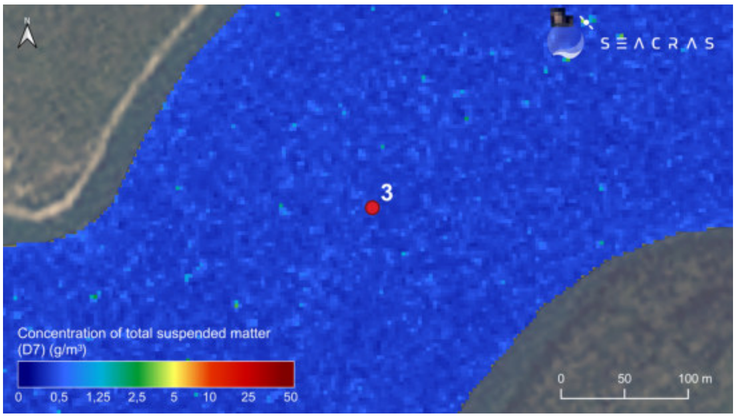

Figure 66. Thematic total suspended matter concentration map of Location 3, Lim Bay, from processed satellite imagery, 14 August 2024.

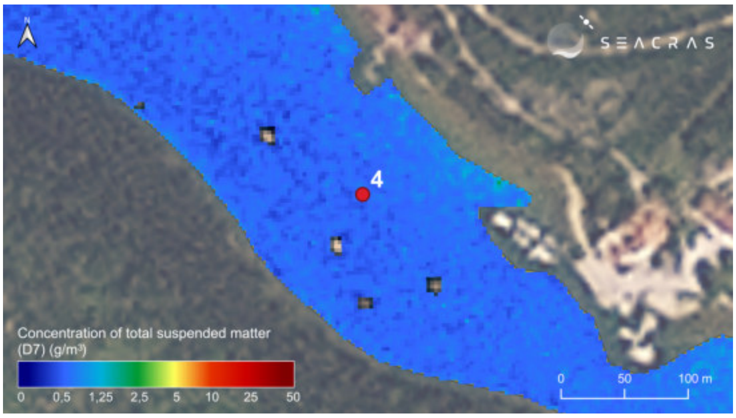

Figure 67. Thematic total suspended matter concentration map of Location 4, Lim Bay, from processed satellite imagery, 14 August 2024

Date: 21.9.2024.

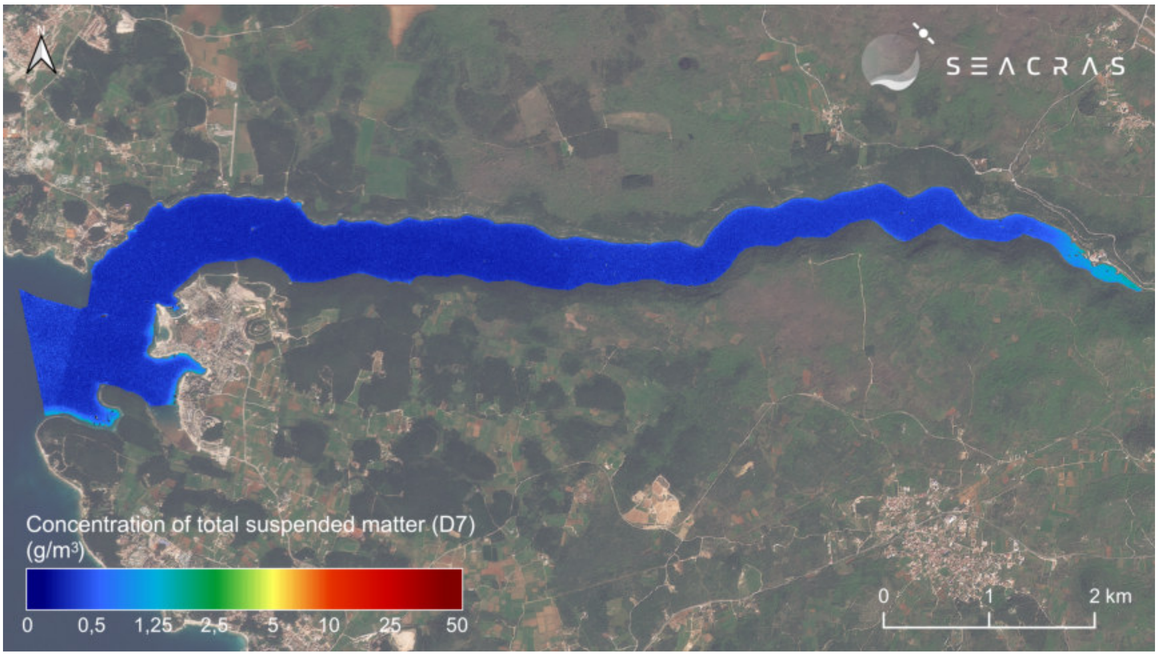

Figure 68. Thematic map derived from a processed satellite image showing concentration of total suspended matter in Lim Bay, 21 September 2024

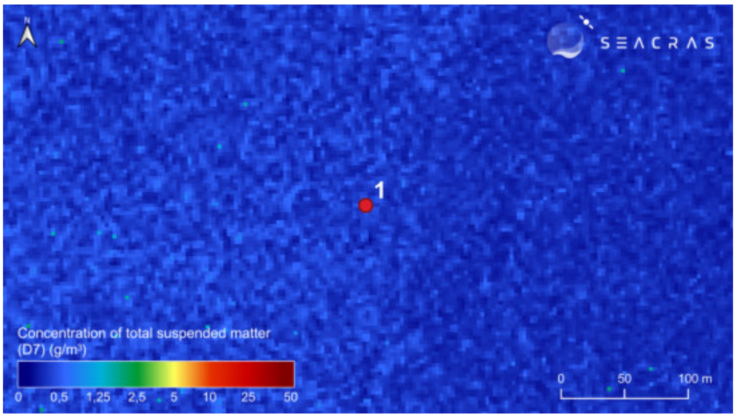

Figure 69. Thematic total suspended matter concentration map of Location 1, Lim Bay, from processed satellite imagery, 21 September 2024

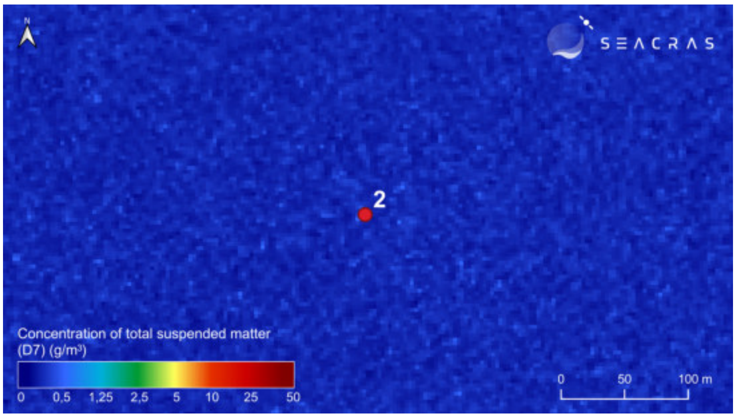

Figure 70. Thematic total suspended matter concentration map of Location 2, Lim Bay, from processed satellite imagery, 21 September 2024

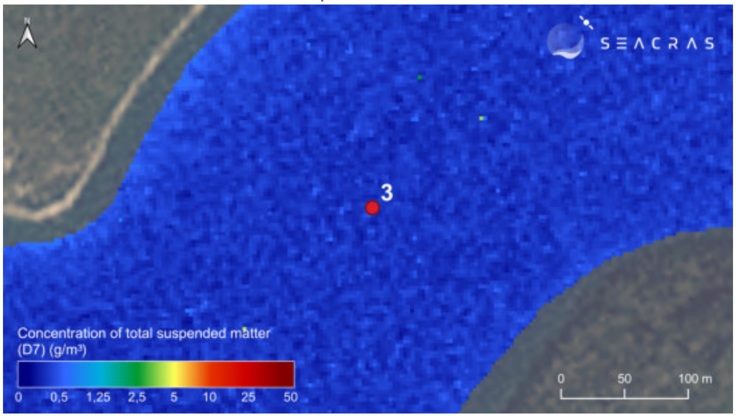

Figure 71. Thematic total suspended matter concentration map of Location 3, Lim Bay, from processed satellite imagery, 21 September 2024

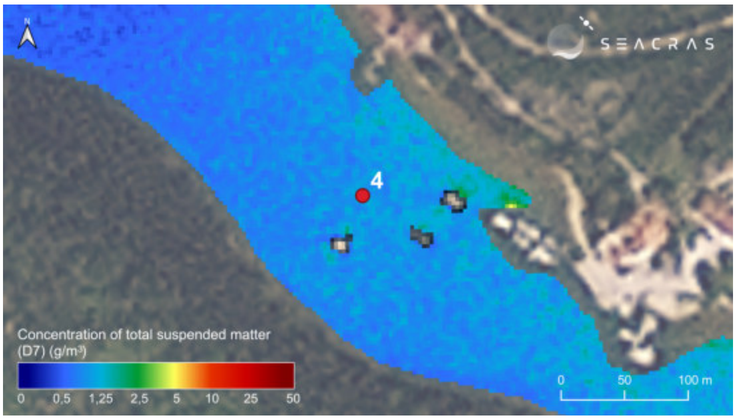

Figure 72. Thematic total suspended matter concentration map of Location 4, Lim Bay, from processed satellite imagery, 21 September 2024

Analysis of total suspended matter concentration from May to September 2024 showed pronounced differences between locations, as well as seasonal fluctuations linked to meteorological conditions.

The highest suspended matter values were recorded in the more enclosed part of the bay, particularly at Location 4, consistent with expectations due to limited water exchange, shallower depths, and potentially stronger influence from the land. Elevated values in May and June may result from rainfall episodes that increase input from coastal areas and resuspension of material in shallower zones. In July and September, values were lower and more stable, especially at more open locations.

It is noteworthy that, in some cases, even the more open stations (such as Location 1) recorded elevated values, indicating local processes such as wind-driven sediment resuspension, wave-induced turbulence, or inflow of organic matter from the open sea.

The spatial variability clearly highlights the influence of the bay's morphological characteristics, with enclosed areas accumulating higher amounts of suspended material.

Detection of marine mucilage presence

The occurrence of marine mucilage in the Lim Bay, recorded on August 9, 2024, was clearly detected in satellite imagery from that day, especially in the western part of the bay, in the area of Location 1 (Figure 73). That location, situated closest to the open sea, showed visible floating aggregates characteristic of mucilage. This is consistent with field observations by the Ruđer Bošković Institute, which documented multiple episodes of this phenomenon in the northern Adriatic during the same period (Source: https://doi.org/10.1016/j.ecss.2025.109222).

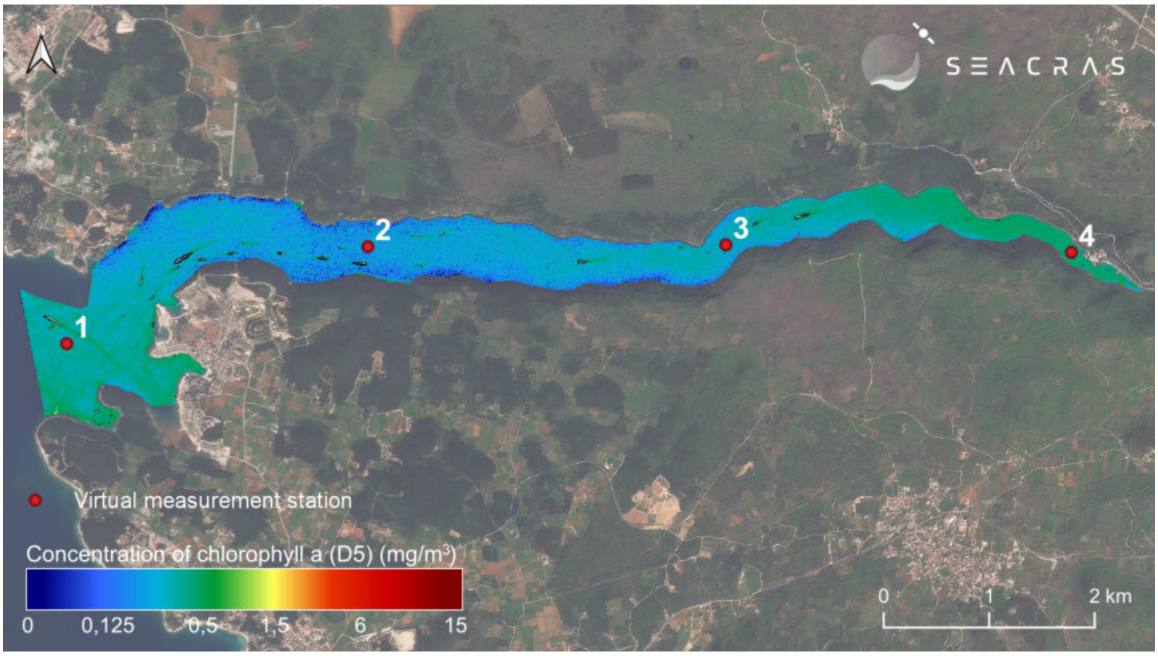

Figure 73. Thematic map of chlorophyll-a concentration and positions of virtual measurement stations in Lim Bay, derived from processed satellite imagery, 9 August 2024

Satellite data confirms that on August 9th, an elevated concentration of chlorophyll-a was recorded specifically at Location 1. While the values were not the highest throughout the entire observation period, their increase relative to previous days, as well as to other more open locations, suggests enhanced biological activity. This further confirms the connection between the appearance of mucilage and periods of marine blooms.

In addition to chlorophyll-a, the concentration of total suspended matter was also elevated at the same location. This may indicate the presence of organic material and the remains of plankton masses, but also a direct detection of mucilage aggregates in the surface layer of the sea. Concurrently, in the more enclosed parts of the bay (Locations 3 and 4), suspended matter values were lower than usual, which further emphasizes the localized nature of this event at the mouth of the bay.

Given the visually confirmed appearance of mucilage on August 9, 2024, at the western edge of the Lim Bay, an additional microlocation analysis was conducted to quantify in detail the intensity and spatial distribution of the aggregates. The analysis was based on very high spatial resolution imagery and included five additional reference points (virtual measurement stations) within the aggregation area (Figure 74).

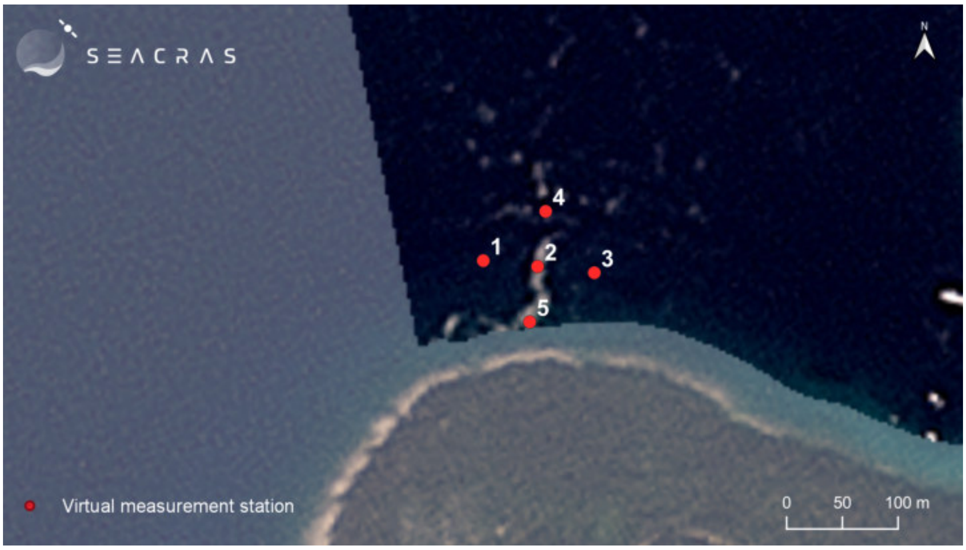

Figure 74. Locations of reference measurement points within the area affected by the mucilage phenomenon on the RGB composite of the satellite image, August 9, 2024.

The satellite RGB display (Figure 75) clearly confirms the visual appearance of mucilage in the form of white, fibrous structures in the surface layer of the sea.

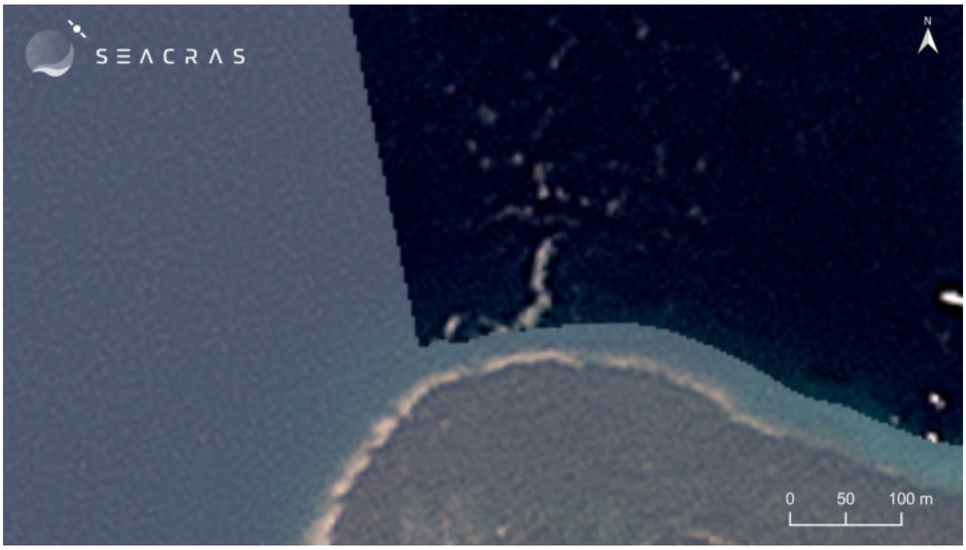

Figure 75. Satellite RGB composite of the area affected by the mucilage phenomenon, August 9, 2024.

Thematic map of aggregate intensity (Figure 76) further quantifies the spatial distribution of the aggregation, while a thematic map of chlorophyll-a concentration (Figure 77) in the same area shows the presence of elevated values, particularly around point 5.

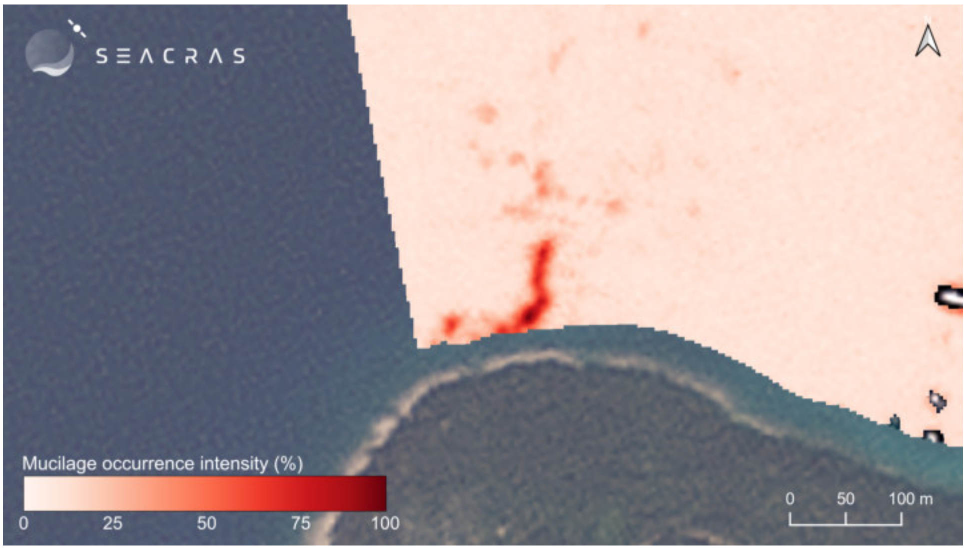

Figure 76. Thematic map of the intensity of aggregate occurrence within the area affected by the mucilage phenomenon, August 9, 2024

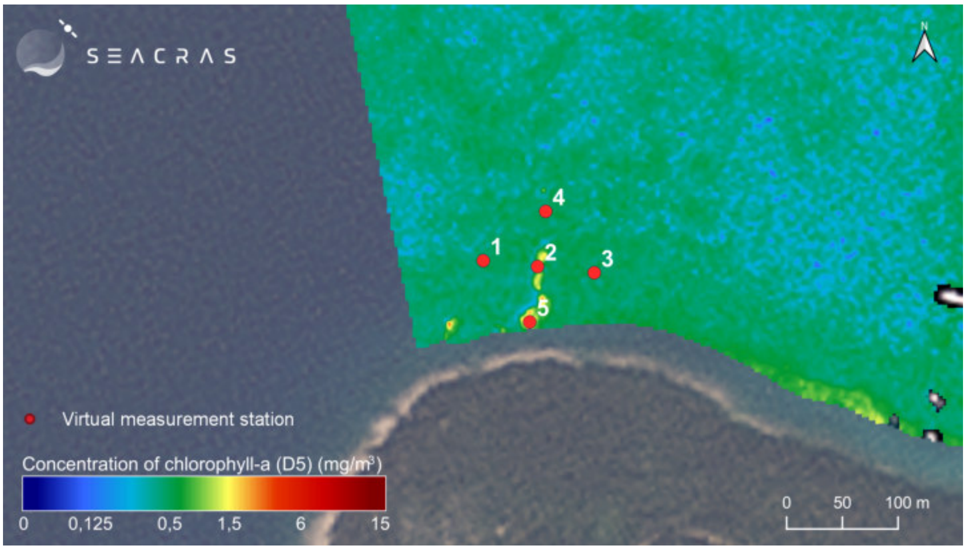

Figure 77. Thematic map of chlorophyll-a concentration in the area of mucilage occurrence, August 9, 2024.

The graphical representation of chlorophyll-a concentrations at the microlocations (Figure 78) indicates a significantly higher value at location 5 compared to the other points. This may suggest localized biological activity as one of the possible causes for the appearance of mucilage.

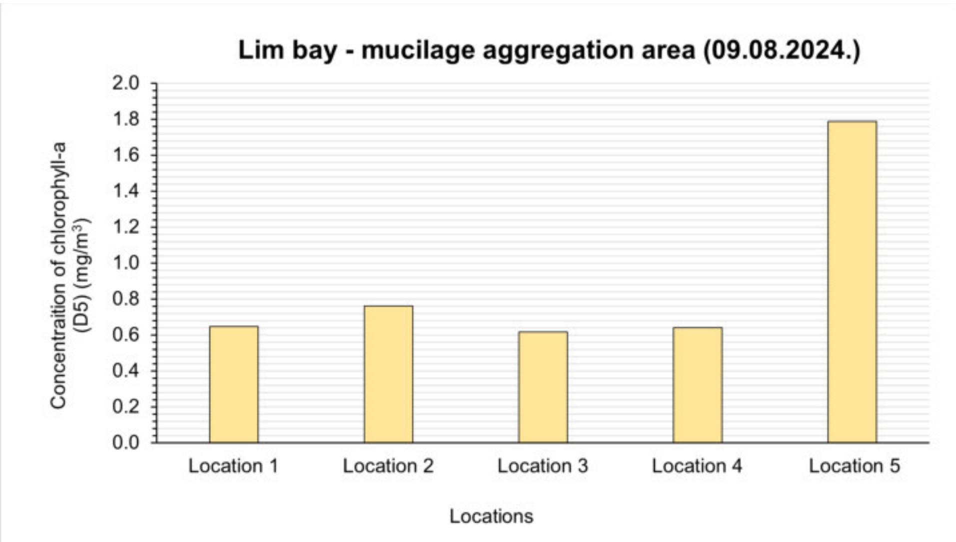

Figure 78. Graph of chlorophyll-a concentration values at microlocations within the area of mucilage occurrence, August 9, 2024.

A comparison with the regular stations within the bay (Figure 79) confirms that the concentrations in the affected area were among the highest that day, although they were not extremely high at the level of the entire bay.

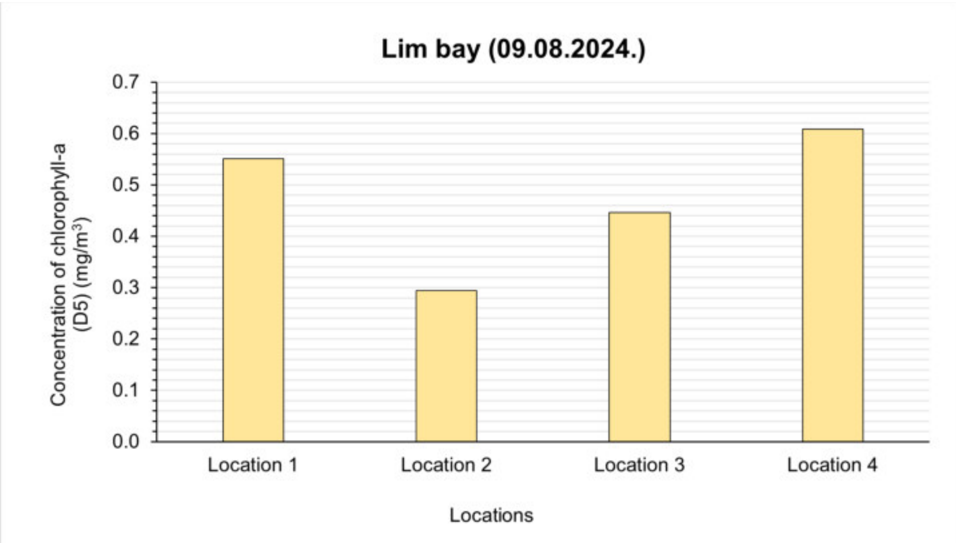

Slika 79. Koncentracija klorofila-a na redovnim virtualnim postajama (Lokacija 1 - 4) unutar Limskog zaljeva, 09. kolovoza 2024.

It is important to note that Location 1, being the most exposed to the influence of the open sea, is susceptible to the transport of biological material from the wider northern Adriatic region. Satellite imagery of the broader region (Figure 80), recorded on August 7, 2024, indicated enhanced eutrophication processes. This further supports the hypothesis that the conditions for mucilage development were triggered by regional environmental impulses.

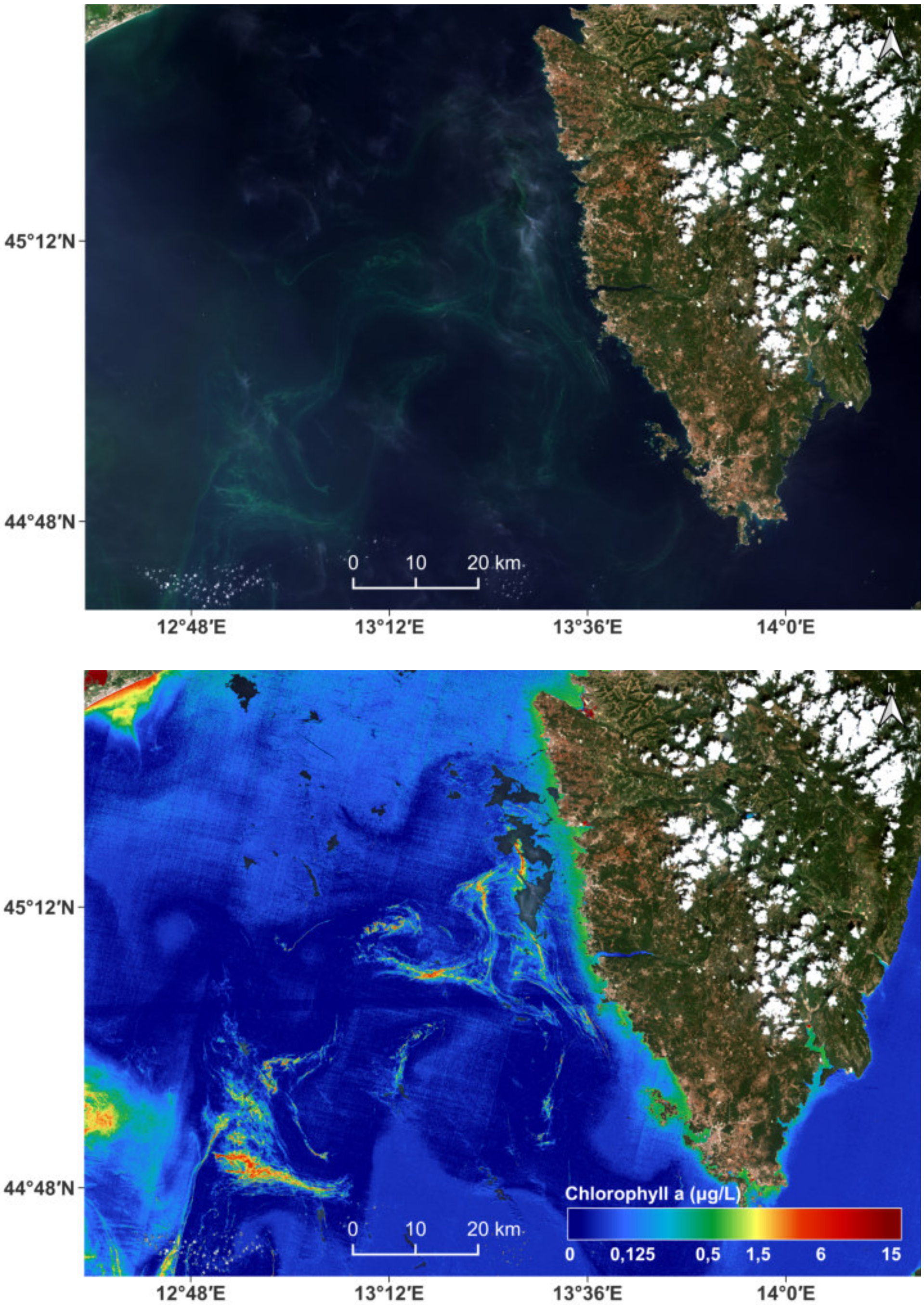

Figure 80. Satellite view of the northern Adriatic, 7 August 2024. Top: RGB composite; Bottom: Thematic map of satellite-derived chlorophyll-a concentration

The distribution and dynamics of mucilaginous aggregates in the Lim Bay show a clearly limited horizontal transport, which unequivocally points to the strong influence of specific local geomorphological and oceanographic conditions. The aggregates formed primarily in the transition zone between the open sea and the bay system, without significant spreading towards the more enclosed parts of the water body.

This localization can be explained by a combination of several factors. First, the geomorphological enclosure of the Lim Bay, characteristic of canyon systems, naturally limits the exchange of water masses with the open sea. Additionally, the weak hydrodynamics and absence of strong currents within the bay prevent the transport of aggregates towards the interior, meaning the aggregates remain concentrated at their point of origin.

Furthermore, the formation of the mucilage was preceded by locally favorable conditions that were particularly pronounced in the transition zone. In the days leading up to the recorded mucilage event on August 9th, weather conditions were exceptionally stable—with elevated sea temperatures and low wind speed. Such conditions are conducive to the formation of a vertical stratification of the water column, a prerequisite for the development and surface accumulation of mucilage aggregates.

Therefore, the combination of the bay's geomorphological characteristics, high sea temperatures, calm weather, and pronounced stratification limited the appearance of the mucilage, without further spatial spreading toward the interior of the bay.

Plastic waste detection - descriptor D10

As part of the satellite monitoring, an analysis of floating marine litter was conducted using high and very high spatial resolution imagery. The objective was to detect and differentiate floating objects such as plastics, mucilage, and vessels, using advanced algorithms for spectral data processing.

Vessels were clearly distinguished thanks to the application of an internally developed (in-house) vessel detection algorithm, which enabled the reliable identification of their positions and sizes in the satellite imagery. Furthermore, the presence of mucilaginous aggregates was visually and spectrally recognizable, particularly in the western part of Lim Bay, where the aggregates formed clearly distinguishable surface structures.

The detection of floating plastic resulted in several positive signals, but their reliability was limited due to frequent "false positive" results—i.e., signal mixing with other objects like vessels, buoys, shadows, or smaller surface structures. The spectral distinction of plastic under such conditions remains limited, especially in geomorphologically complex systems like the Lim Bay.

In addition, the current dynamics within the bay—defined by weak hydrodynamics and geomorphological enclosure—preclude any significant horizontal transport of material from the open sea towards the interior. As also demonstrated with the mucilage event, no migration of floating objects from external areas was observed, which further supports the hypothesis that the detected litter has a local origin.

Based on these findings, it can be concluded that the majority of floating litter in Lim Bay originates from internal sources, within the boundaries of the protected area itself. In this context, local human activities, particularly nautical traffic and recreation, represent likely sources of input. An additional analysis of the coastal zone revealed small amounts of plastic waste, consisting mainly of tourist items such as air mattresses and plastic objects. This finding may reflect a genuinely low presence of plastic during the observation period.

False-positive signals of plastic objects of static and dynamic nature

Figure 81. Highlighted locations of false-positive signals in the Lim bay, August 29, 2024

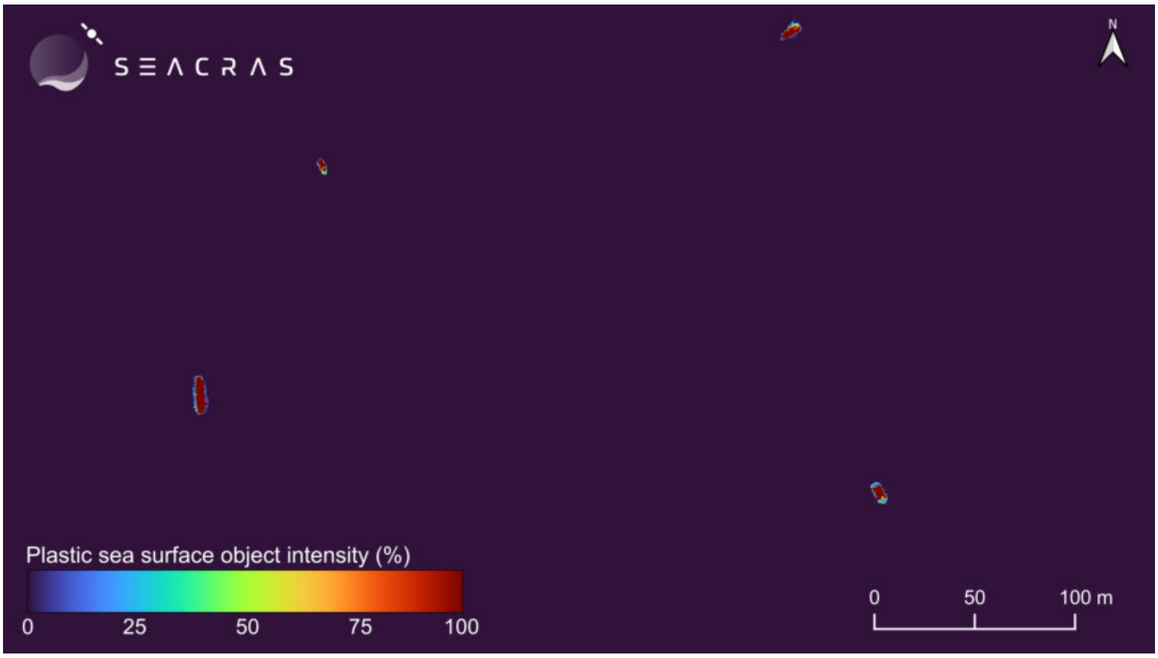

Figure 82. Displaying sea surface plastic intensity on highlighted location 1, August 29, 2024

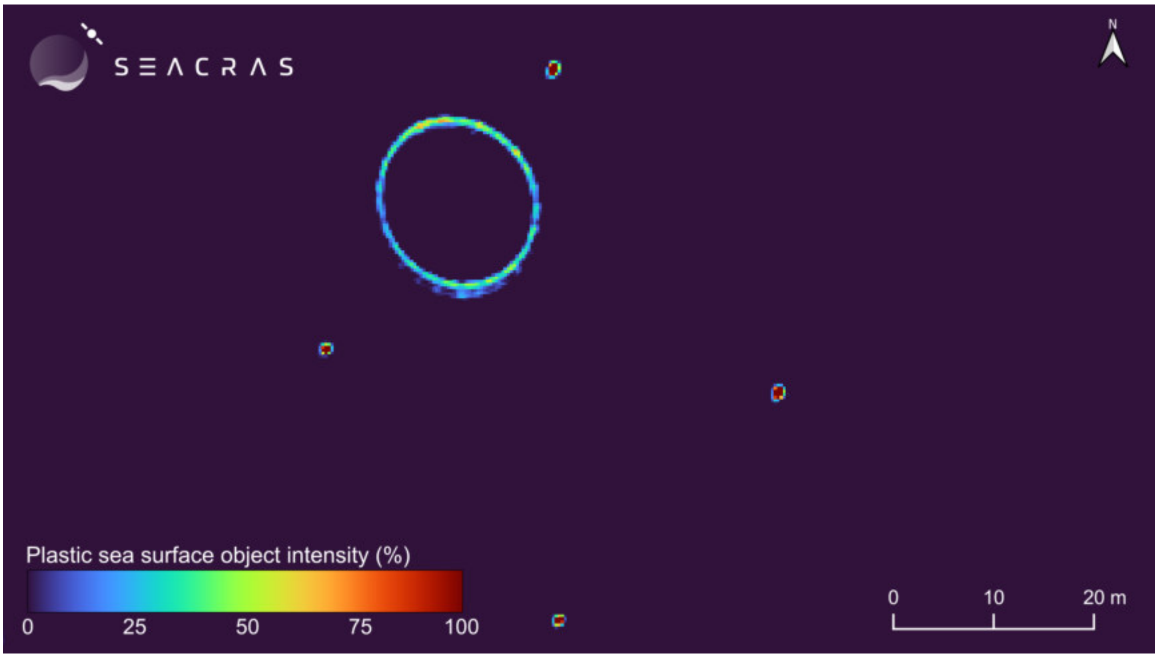

Figure 83. Displaying sea surface plastic intensity on highlighted location 2, August 29, 2024

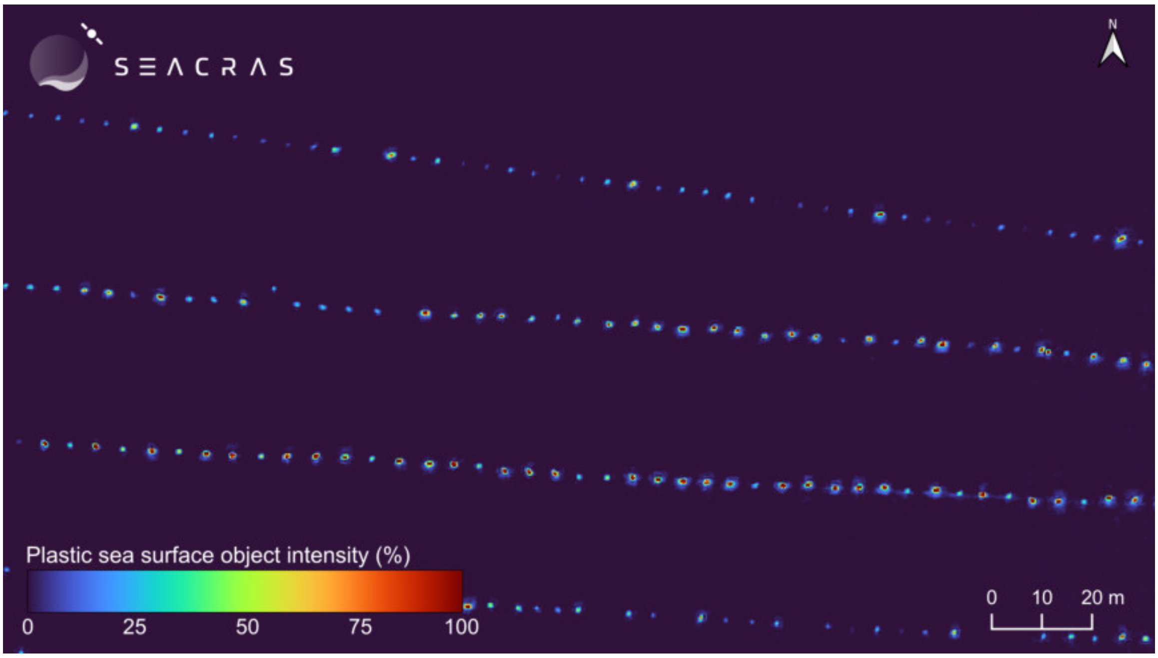

Figure 84. Displaying sea surface plastic intensity on highlighted location 3, August 29, 2024

Examples of such false positive detections are shown at the highlighted locations (Figure 81), where objects are visible whose spectral analysis indicates plastic as the material (Figures 82–84). The size of these objects ranges from 30 cm to 25 m.

These objects represent false positive detection signals in the remote sensing of plastic pollution in the Lim Bay. Although they are static sources of microplastic pollution due to systematic material degradation, they also serve as potential dynamic sources of macro- and microplastic pollution.

Risk assessment and spatial distribution of plastic pollution in the marine ecosystem of Lim Bay

Based on the analysis of mucilage migration incidents in the Lim Bay area, it was concluded that the propagation of floating objects (including floating plastic) toward the deeper parts of the bay was prevented in most cases, even under varying meteorological conditions.

Accordingly, a higher-order analysis was conducted to identify potential internal sources of macroplastic pollution. This analysis considered pollution resulting from anchoring and navigation, as well as the use of existing infrastructure and facilities within the bay, including anchorages, roadways, access paths, and tourist amenities. In addition, natural and hydrodynamic factors were included in the analysis, such as dominant wind direction, sea depth, types of marine habitats, and the openness of the bay.

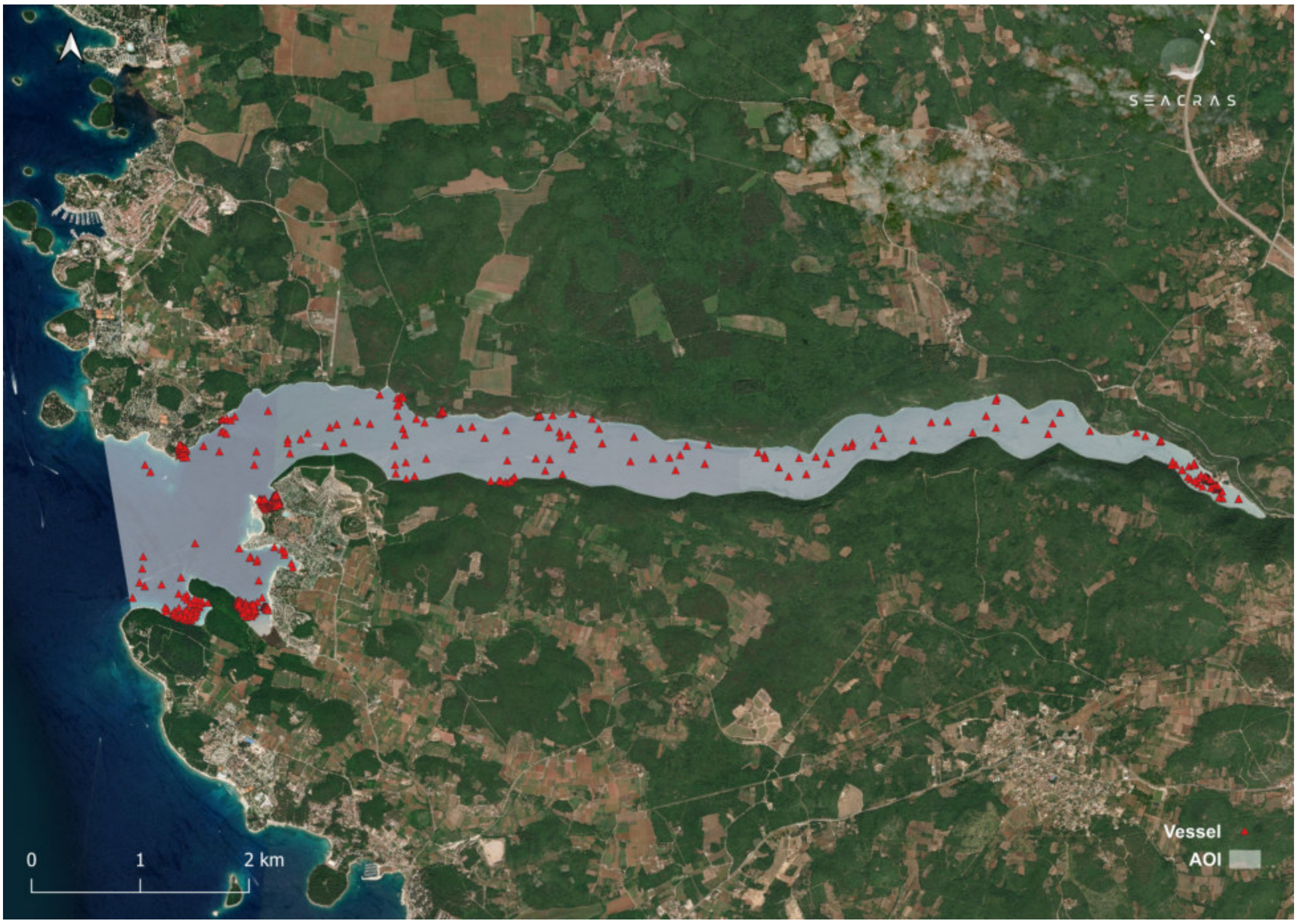

Figure 85. Vessel detection in the Lim Bay (01.05.2024. - 30.09.2024.).

By detecting vessels through extremely high-resolution imagery, zones of high vessel incidence were determined. Specifically, these included key vessel anchoring zones, vessel navigation routes, and vessel mooring zones. These indicators, combined with other parameters, represent one of the main factors for determining the likelihood of plastic pollution risk.

According to the map shown, the following hotspots of detected vessels are visible: Križ Bay, Soline Bay, Fujaga Bay, Vrh Lima, and Valalta marina. In addition to these, there are several other locations with a lower but not negligible incidence of vessels, such as Larij Bay or smaller mooring areas within the bay. In anchoring zones like Križ Bay, dozens of vessels anchor during the summer season. On a surface area of approximately 0.076 km^2, this represents significant pressure on the marine environment and a greater likelihood of plastic pollution risk. The locations of Soline, Valalta, and Vrh Lima are sites with an extremely high incidence of moored vessels, which also represent locations with a high likelihood of plastic pollution risk.

Figure 86. Existing infrastructure at the Lim Bay in 2024..

Figure 86 shows the existing infrastructure located along Lim Bay. The map displays all the beaches along the bay's coast, mooring points, hospitality and accommodation facilities, shops, and roadways that connect the coast to the mainland.

All of these spatial features represent zones of potentially high human frequency, which translates to an increased likelihood of the input, transport, and accumulation of plastic in the water. The spatial distribution of these features indicates more developed infrastructure at the very entrance to Lim Bay, on the northern and southern coasts, and at the very end of the bay, i.e., Vrh Lima. This distribution is also largely consistent with the spatial distribution of detected vessels.

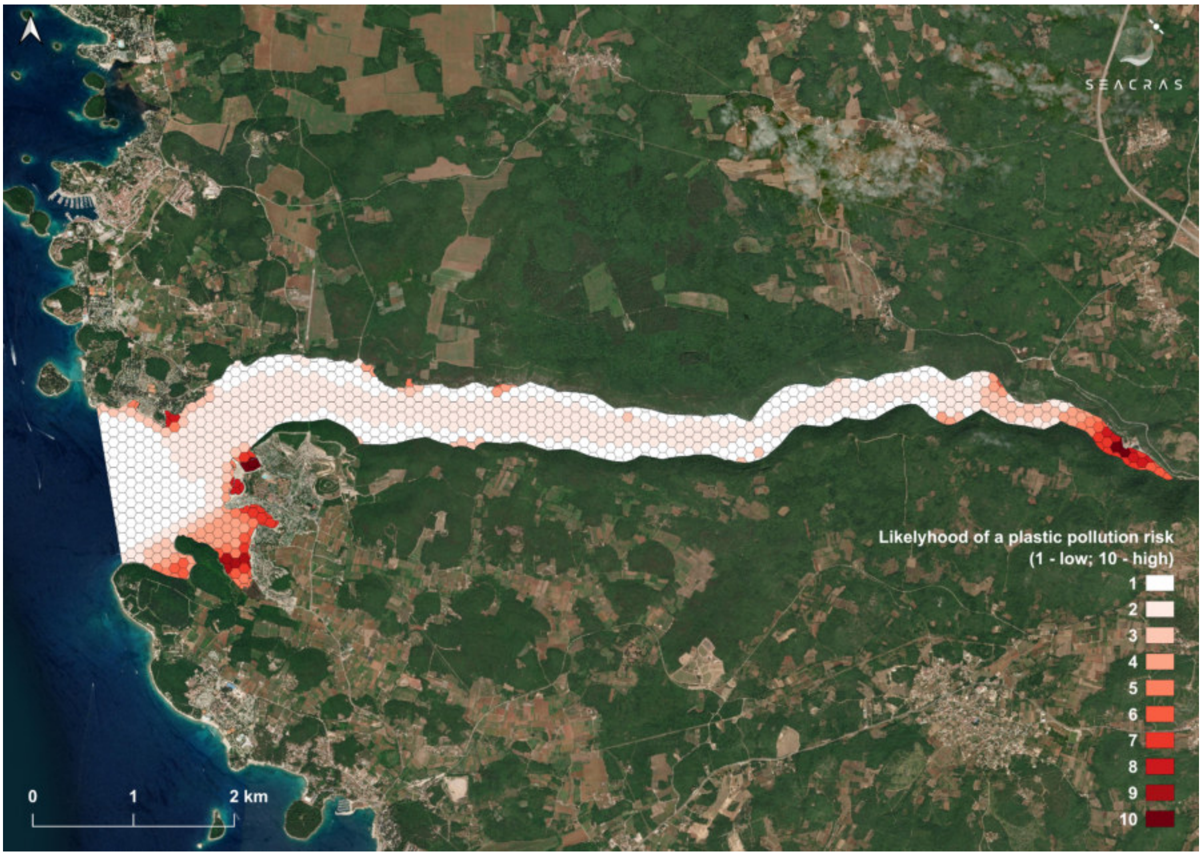

Figure 87. Spatial distribution of the likelihood of the plastic pollution risk in the Lim Bay in 2024.

The probability and spatial variability of plastic pollution risk zones in the Lim Bay area were calculated. The results of this higher-order analysis are shown in Figure 87.

The findings reveal significant spatial variability in the likelihood of pollution risk. The highest likelihood of plastic pollution risk is located at the very entrance of the Lim Channel and at its easternmost point. In contrast, a lower or medium likelihood of risk exists along the channel within smaller coves and navigation routes. The high likelihood of pollution is potentially caused by the migration of floating litter from the Adriatic Sea, which is localized exclusively at the bay entrance and within nearby coves due to hydrodynamic factors. Additionally, along the coast of the westernmost part of the bay, before it narrows, there is added pressure from maritime traffic and tourist activities, which are most prominent there.

Particularly vulnerable locations include Valalta marina, which has over 100 moored vessels daily during the summer season, and where water flow is extremely low due to the cove's enclosed nature. The Vrh Lima area also has a similar likelihood of plastic pollution risk because of a high incidence of both anchored and moored vessels. The presence of tourist facilities and roadways also encourages an additional influx of people from the mainland. Furthermore, the weak water movement at the very end of the bay is an additional factor in retaining plastic at that location.

Zones with a medium likelihood of risk are primarily a consequence of vessel navigation, lower-intensity anchoring in some coves, and access to the sea at certain points via access paths.

Based on the analysis, a series of measures for both recovery and prevention are proposed to address plastic pollution in the Lim Bay:

- Recovery Measures: These include improved control and monitoring of areas with an increased likelihood of pollution risk. The proposal also includes conducting cleanup activities for the affected areas, based on the intensity and frequency of the pollution's occurrence.
- Prevention Measures: These encompass proactive activities aimed at bay visitors, particularly in the context of maritime operations such as navigation, to reduce the input of pollutants.

Limitations of Sentinel-2 and Landsat-8 data for plastic detection

The results of this study suggest that using medium spatial resolution satellite imagery from sources like Sentinel-2 and Landsat-8 is not a reliable method for either the detection or quantification of floating litter in water bodies, nor for its documentation in the coastal area of Lim Bay. This same conclusion applies to most of the Adriatic Sea, except in rare cases where large accumulations of floating litter occur under the significant influence of meteorological conditions.

Furthermore, the low revisit frequency of these satellites over the Lim Bay area and the Adriatic in general further complicates the detection of floating plastic.

Conclusion

Satellite Monitoring of Lim Bay: Summary of Findings

The satellite monitoring of Lim Bay, conducted from May to September 2024, enabled a detailed analysis of the sea's condition by tracking key **biochemical descriptors**: chlorophyll-a concentration (D5), Total Suspended Matter (TSM) (D7), and marine litter (D10). Using multiple satellite systems with high and very high **spatial resolution**, a high temporal and spatial coverage was ensured. This allowed for the recognition of seasonal patterns and local anomalies in the ecosystem of a semi-enclosed coastal canyon like Lim Bay.

Biochemical Descriptors (D5 and D7)

The analysis of chlorophyll-a concentration showed a seasonal pattern of increase during the spring-summer period, with the highest values found in the more enclosed parts of the bay (Locations 3 and 4), particularly during May and June. These results point to the influence of nutrient input under conditions of occasional rainfall, as well as potential accumulation due to weaker circulation in the enclosed parts of the water body. **Spatial variability** was pronounced, with the lowest concentrations recorded in the more open sections (Location 1).

The concentration of **Total Suspended Matter (TSM)** showed similar spatial patterns, with elevated values in the more enclosed parts of the water body, but with more pronounced fluctuations tied to individual weather events and episodes of enhanced biological activity. High TSM values on certain days correlated with an increase in chlorophyll-a, indicating an interrelationship between these two environmental indicators.

The Mucilage Event

A significant event was recorded on August 9, 2024, when surface **mucilage aggregates** were clearly observed in satellite imagery in the western part of Lim Bay, at the transition zone between the open sea and the bay system. A **microlocation analysis** conducted at five additional reference points showed elevated chlorophyll-a values and the presence of aggregates with a pronounced **spatial localization**. A comparison with broader satellite imagery of the Adriatic (e.g., August 7, 2024) indicated enhanced **eutrophication** processes in the region, supporting the hypothesis of regional environmental impulses as potential triggers.

However, the **geomorphological enclosure** of Lim Bay, weak **hydrodynamics**, and local stratification of the water column led to a limited **horizontal distribution** of the aggregates, the mucilage remained spatially confined to the outer, more open part of the bay. This finding confirms the crucial role of local conditions in determining the spatial dynamics of this phenomenon.

Waste Detection (D10)

The monitoring of descriptor D10 was conducted using specialized algorithms for the detection of floating objects. The goal was to differentiate between plastics, mucilage, and vessels. Vessels were successfully detected using an **in-house algorithm**, and mucilage aggregates were confirmed both visually and spectrally. The detection of floating plastic was limited by frequent **false positive signals**, among which were confirmed plastic objects ranging from 30 cm to 25 m in size. While these are considered static sources, they can be sources of both macro- and microplastic. Small quantities of plastic litter, such as tourist paraphernalia, were observed in coastal areas. This may reflect genuinely low plastic volumes during the observation period or decreased detection efficiency of satellite tools in complex coastal environments.

Plastic Pollution Risk Assessment

The **likelihood and spatial variability of plastic pollution risk zones** in the Lim Bay area were calculated. The results of the **higher-order analysis** are presented in Figure 87. The results show exceptional **spatial variability** in the likelihood of pollution. The highest likelihood of plastic pollution risk is at the very entrance of the Lim Channel and at its easternmost point. Along the channel, within smaller coves and navigation routes, there is a lower or medium likelihood of risk.

Potential causes for the high likelihood of pollution are the **migration of floating litter** from the Adriatic Sea, which is localized exclusively at the bay entrance and in nearby coves as a result of **hydrodynamic factors**. Additionally, the westernmost part of the bay, before its narrowing, experiences additional pressure from **maritime traffic** and tourist activities, which are most prominent in that area. Particularly vulnerable locations include Valalta marina, which has over 100 moored vessels daily during the summer, and where water flow is extremely low due to the cove's enclosure. The Vrh Lima area also has a similar likelihood of plastic pollution risk due to a high incidence of both anchored and moored vessels. The existence of tourist facilities and roadways also contributes to an additional influx of people from the mainland. A weak water movement at the very end of the bay is another factor in retaining plastic at that location.

Zones with a medium likelihood of risk are mainly a consequence of vessel navigation, lower-intensity anchoring in some coves, and access to the sea at certain points via access paths.

Proposed Measures

A proposal for recovery measures includes improved **control and monitoring** of areas with an increased likelihood of pollution risk. The proposal for prevention measures encompasses **proactive activities** aimed at bay visitors, particularly in the context of maritime operations such as navigation. The proposal for recovery also includes cleanup activities for the areas based on the **intensity and frequency** of pollution occurrence.

Literature

Biermann, L., Clewley, D., Martinez-Vicente, V. *et al.* Finding Plastic Patches in Coastal Waters using Optical Satellite Data. *Sci Rep* 10, 5364 (2020). https://doi.org/10.1038/s41598-020-62298-z

Muhammad Waqas, Man Sing Wong, Alessandro Stocchino, Sawaid Abbas, Sidrah Hafeez, Rui Zhu, Marine plastic pollution detection and identification by using remote sensing-meta analysis, Marine Pollution Bulletin, Volume 197, 2023, 115746, ISSN 0025-326X, https://doi.org/10.1016/j.marpolbul.2023.115746.

Bijeesh Kozhikkodan Veettil, Nguyen Hong Quan, Leon T. Hauser, Dong Doan Van, Ngo Xuan Quang, Coastal and marine plastic litter monitoring using remote sensing: A review, Estuarine, Coastal and Shelf Science, Volume 279, 2022, 108160, ISSN 0272-7714, https://doi.org/10.1016/j.ecss.2022.108160.

Duplančić Leder, T. (2024) "Optical Remote Sensing Methods for Floating Marine Debris Detection – Review and Bibliography Analysis", Transactions on Maritime Science. Split, Croatia, 13(2). doi: 10.7225/toms.v13.n02.005.

Ivica Vilibić, Elena Terzić, Iva Vrdoljak, Iva Dominović Novković, Martin Vodopivec, Irena Ciglenečki, Tamara Djakovac, Bojan Hamer, Extraordinary mucilage event in the northern Adriatic in 2024—a glimpse into the future climate?, Estuarine, Coastal and Shelf Science, Volume 317, 2025, 109222, ISSN 0272-7714, https://doi.org/10.1016/j.ecss.2025.109222.

Data storage note:

SEA CRAS d.o.o. stores all processed data on the detection and monitoring of vessels at mooring and anchoring sites, as well as the corresponding imagery, on its servers for a period of one year from the end of the monitoring. During this period, you may request access to all processed data, which can be provided in appropriate formats.